AN EXPERIMENTAL STUDY ON HIGHER ORDER WAVES AND HYDRODYNAMIC LOADING ON VERTICAL SURFACE PIERCING CYLINDERS

KRISHNAPRASAD THIAGARAJAN, B. Tech.

ISBN 0-315-54995-5

Canada

AN EXPERIMENTAL STUDY ON HIGHER ORDER WAVES AND HYDRODYNAMIC LOADING ON VERTICAL SURFACE PIERCING CYLINDERS

©KRISHNAPRASAD THIAGARAJAN, B.Tech

A thesis submitted to the School of Graduate Studies
in partial fulfillment of the degree of Master of Engineering

Faculty of Engineering and Applied Sciences
Memorial University of Newfoundland
February 1989

St.John's Newfoundland

Abstract

Estimation of second order wave loading on offshore structures has attracted recent attention in research. This thesis presents the results of an experimental study carried out to quantify second order wave forces on a vertical cylinder in a wave tank. The initial part of this thesis is directed towards formulating and analyzing the wave field present in the laboratory. These results formed part of the input for further studies on wave forces. Due to the physical limitations of the wave tank, it was found that several waves coexist with the progressive wave of interest in the tank. An analysis procedure was developed using a Fast Fourier Transform technique and a least squares curve fitting method to separate the wave of interest from the side effects and identify its principal parameters. Several side effects were quantified in the process. Wave forces on a vertical cylinder to second order were theoretically formulated from a literature survey. Analysis of the measured wave forces in the wave tank involved using a fast fourier transform to identify the first and second order force components. Towards the end of the study, it was found that the proposed formulations for the total wave field in the tank and the wave forces on a cylinder were adequate. There exist many phenomena in a wave tank whose effects on measurements requires further research. It is emphasized that systematic experimental studies of higher order waves form an important part of offshore research development.

To my parents
whose footsteps formed my ladder

Acknowledgements

The need for second order experimental studies in the present trend of research was first pointed to me by my research supervisor Professor R.E. Baddour of the Faculty of Engineering, MUN. I am extremely grateful to him for the encouragement, active supervision and cooperation he offered to me during this study.

This research was financially supported by a graduate research fellowship from the School of graduate studies at Memorial University. My thanks are due to the Dean of Graduate Studies and his staff for their help and support. I am indebted in gratitude to the offices of the Dean and Associate Dean of Engineering for coordinating my activities during the period of study towards an efficient outcome.

The cooperation extended to me during the experiments by the wave tank crew and the staff of the structures lab are remembered at this opportunity. I appreciate the help offered to me by the staff of the CCAE in preparing this document.

One final kudos to all Newfoundlanders, their hospitality and warmth for making my stay memorable at St.John's.

K.T.

Contents

1 Introduction 1

I Wave Propagation: Theory and Experiments 5

2 Background and Literature Review 6

3 Theoretical Development 15
- 3.1 The boundary value problem 15
- 3.2 Second order Stokes theory 18
- 3.3 Theories for piston type wave maker 22
- 3.4 The total wave field 26

4 Experimental setup and procedure 30

5 Discussion of results 41
- 5.1 First order results 43
- 5.2 Second order results 46
- 5.3 Conclusions 49

II Wave Forces: Theoretical Formulation and Experiments 64

6 Background and Literature review 65

7 Theoretical development 71
- 7.1 Force equation in a real flow 71
- 7.2 Inertia forces on a cylinder 75
- 7.3 Drag forces on a cylinder 80

8 Experiments and Analysis 85

9 Discussion of results 93

10 Concluding remarks 114

List of References 118

Appendices

A ANALYS - Source code 122

B The Fast Fourier Transform 128

C Description of the subroutine LSSIN 131

D Harmonic components of $u|u|$ 136

List of Figures

2.1 Range of validity of various wave theories 14
3.1 Representative diagram of a two - dimensional progressive wave 29
3.2 Representative diagram of two - dimensional wave generation by a piston type wave maker 29
4.1 Configuration of the piston type wave maker 39
4.2 Beach configuration 39
4.3 Information flow chart for wave experiments 40
4.4 Wave probe calibration diagram; Date Feb 12 40
4.5 First order analysis flow chart for wave experiments 41
5.1 Sample wave form graphs: f = 1.0Hz, $H/gT^2 = 0.001$; Location zero (20m away from the wave board mean position) 52
5.2 Sample wave form graphs: f = 1.0Hz, $H/gT^2 = 0.001$; Location one (0.2m from location zero) 52
5.3 Sample wave form graphs: f = 1.0Hz, $H/gT^2 = 0.001$; Location two (0.4m from location zero) 53
5.4 Sample wave form graphs: f = 1.0Hz, $H/gT^2 = 0.001$; Location three (0.6m from location zero) 53
5.5 Sample wave form graphs: f = 1.0Hz, $H/gT^2 = 0.001$; Location four (0.8m from location zero) 54
5.6 First order amplitude fit: f = 1.0Hz, $H/gT^2 = 0.001$ 55
5.7 Second order amplitude fit: f = 1.0Hz, $H/gT^2 = 0.001$ . . 55
5.8 Relative depth: theory vs experiment 56
5.9 Wave maker amplitude ratio vs kh 56
5.10 First order reflection coefficient vs kh 57
5.11 First order reflected wave phase angle vs kh 57
5.12 Stokes amplitude ratio vs kh; H/gT^2=0.0007 58

5.13 Stokes amplitude ratio vs kh; H/gT^2=0.001 58
5.14 Stokes amplitude ratio vs kh; H/gT^2=0.003 59
5.15 Stokes amplitude ratio vs kh; H/gT^2=0.005 59
5.16 Free wave number ratio vs kh 60
5.17 Free wave amplitude ratio vs kh 61
5.18 Free wave phase angle vs kh 62
5.19 Second order reflection coefficient vs κh 62
5.20 Second order reflected wave phase angle vs κh 63
7.1 Representative diagram of the wave flume with the wave generator, beach and coordinate system 84
8.1 Configuration of the test cylinder in the wave tank 90
8.2 Configuration of the force transducer 91
8.3 Calibration chart for the force transducer 91
8.4 Schematic diagram of wave force analysis 92
9.1 Sample wave force graph: Run 01, D = 0.0725m, f = 0.9Hz, H/gT^2 = 0.003, KC = 2.12 103
9.2 Sample wave force graph: Run 22, D = 0.0479m, f = 0.4Hz, H/gT^2 = 0.005, KC = 26.56 103
9.3 Wave force spectrum for run 01, D = 0.0725m 104
9.4 Wave force spectrum for run 22, D = 0.0479m 104
9.5 Inertia coefficient (C_m) vs Keulegan Carpenter number (KC) 105
9.6 Drag coefficient (C_d) vs Keulegan Carpenter number (KC) 106
9.7 Ratio of second to first order inertia forces versus Sarpkaya's parameter (β) 107
9.8 Ratio of second to first order drag forces versus Sarpkaya's parameter (β) 107
9.9 Comparison between calculated and measured second order inertia force at low steepness (H/gT^2 = 0.0007, 0.001) . . . 108
9.10 Comparison between calculated and measured second order inertia force at high steepness (H/gT^2 = 0.003, 0.005) . . . 108
9.11 Comparison between calculated and measured second order drag force at low steepness (H/gT^2 = 0.0007, 0.001) 109
9.12 Comparison between calculated and measured second order drag force at high steepness (H/gT^2 = 0.003, 0.005) 109
9.13 Comparison between measured and calculated second order inertia force function vs kh; H/gT^2 = 0.003; D = 0.0479m . 110

9.14 Comparison between measured and calculated second order inertia force function vs kh; $H/gT^2 = 0.005$; $D = 0.0479$m . 111
9.15 Comparison between measured and calculated second order inertia force function vs kh; $H/gT^2 = 0.003$; $D = 0.0725$m . 112
9.16 Comparison between measured and calculated second order inertia force function vs kh; $H/gT^2 = 0.005$; $D = 0.0725$m . 113
C.1 Flow chart for the subroutine LSSIN 135
D.1 Cosine functions at $f_2 = 0.2f_1$ 140
D.2 Harmonic components of $f|f|$; $f_2 = 0.1f_1$ 141
D.3 Harmonic components of $f|f|$; $f_2 = 0.2f_1$ 142

List of Tables

4.1 System 570 specifications 36
4.2 Record of wave probe calibration constants 37
5.1 Parameters of experimental runs 51
7.1 Formulation of the second order inertia force function $f(kh)$ 84
9.1 Experimental wave forces and related parameters 101

List of Symbols

The following notations are used in this thesis:

a_1	First order amplitude of the incident wave
a_2	Second order amplitude of the incident wave
a_{22}	Free wave amplitude
a_R	First order reflected wave amplitude
a_{22R}	Second order reflected wave amplitude
C_d	Coefficient of drag force
C_m	Coefficient of inertia force
D	Diameter of cylinder
f	first order wave frequency
f	Elementary wave force on a cylinder
F	Total wave force on a cylinder
F_d	Total drag force on a cylinder
F_m	Total inertia force on a cylinder
g	Acceleration due to gravity
h	Still water depth
H	First order incident wave height
k	First order wave number of the incident wave
KC	Keulegan - Carpenter number
Re	Reynold's number of flow
S	Stroke length of the wave generator
t	Time axis
T	First order period of the incident wave
u	Horizontal component of water particle velocity
w	Vertical component of water particle velocity
(x, z)	Two - dimensional Coordinate system
α	Phase difference between reflected wave and incident wave
β	Sarpkaya's period parameter

Symbols (contd.)

γ	Phase difference between second order reflected wave and incident wave
δ	Phase difference between free wave and incident wave
η	Free surface displacement
κ	Free wave number
λ	First order wave length
ξ	Wave generator displacement
ρ	Mass density of water
ϕ	Irrotational flow velocity potential
ω	First order angular frequency of the incident wave

Chapter 1

Introduction

Estimation of fluid loading is an intermediate step in an offshore structural design. The final result is usually the response of or the stresses induced in the structure. On the aspect of wave loading, presence of random seas and a spectrum of wave heights and lengths calls for a probabilistic estimate of the design wave conditions. The forces arising due to the design wave are modelled by empirical or semi-empirical formulae, where the waves and wave forces are generally considered linear in nature.

Apart from design wave conditions, low probability extreme wave conditions occur, which are important for the design of structural foundations and also design against structural overloading. Modelling of extreme or steep waves was done using a nonlinear wave theory, but the loading was nevertheless estimated by the same empirical formulae. Though it appeared conceptually erroneous, lack of availability of better force models made this an engineering practice. With a factor of safety of 30% included

in the design, most offshore structures survived beyond their stipulated lifetime. Search for better force models in the recent past has led to well-developed theories for wave forces on offshore structures. Development in theoretical and analytical studies has been substantiated by very few experimental studies.

Simulating real seas in a laboratory is inherently complicated by the variability and randomness of the seas and, by the scaling barrier which exists between the viscous flow conditions prevailing in reality and those attained in the laboratory. Empirical corrections are employed for this flow difference and experimental results are extrapolated for design. Apart from these fundamental problems, several side effects arise in a wave tank which can affect the results of experiments. Many of these effects are usually considered negligible during a first order wave force estimation, because of their relatively small magnitude. At the second order of analysis, two major problem areas are:

1. Second order effects due to the equipments used (generator, beach etc.) have to be quantified and this area of research is still not well developed.

2. Many side effects neglected previously might be significant because second order measurements are small quantities.

The present study began with a survey of literature for any new developments in the two areas listed above. Modelling of the wave field formed

a pre-requisite for a study of wave forces on offshore structures. Regular waves with relative depth of $0.137 < h/\lambda < 0.971$ and wave steepness of $0.0044 < H/\lambda < 0.0474$ were considered in the experiments. First and second order wave fields in a wave tank were formulated and the amplitudes of various wave components were estimated using a fast fourier transform and a least squares analysis. Several second order effects were quantified. The forces on a vertical cylindrical pile was considered in the second part of the experiments. Second order wave forces were formulated based on a literature survey. Experiments were conducted for two cylinder diameters with the diffraction parameter (D/λ) varying over 0.0066 to 0.0704. Results were fitted into the formulated model and analysed.

Shortcomings of the study were analysed in the light of available results found in the literature for systematic second order experimental studies. It was expected that the present research would serve towards the following:

- Formulate a strategy for separating first and second order effects in a laboratory and wherever possible, identify the individual components.
- Highlight on difficulties and provide suggestions for future second order experimental studies.

This thesis has been organised into two parts. The first part explains the wave form experiments, the literature review and theories that formed the basis for the procedure of experiments and for the discussion of results. The second part is composed of the wave force formulation backed

by the literature review. Experiments and analysis of results are followed by discussions and conclusions. Additional details are presented in four appendices following the last chapter on general conclusions and suggestions for future research.

Part I

Wave Propagation: Theory and Experiments

Chapter 2

Background and Literature Review

Waves generated in a laboratory are contaminated by several waves created due to the physical limitations involved in the apparatus used. These waves together form a combined wave field whose characteristics vary down the flume. To eliminate these side effects, one can either procure more accurate and refined apparatus or separate the side effects from the total wave field. The latter route can be implemented by the following three steps:

1. Anticipating the significant side effects, create a model of the total wave field.

2. Measure the total wave field, which would involve measuring the variation of wave characteristics down the flume.

3. Fit the measured values into the developed model, quantify the side effects and also explain the discrepancies if any.

This part of the thesis presents a literature survey and the theoretical background required for creating a model of the wave field upto second order. The experiments carried out at the MUN wave tank facility to measure the total wave field are then explained followed by a discussion of the results of fitting the measured values into the developed model.

Most of the research in wave hydrodynamics originally began with a pure progressive wave. The progressive wave theories are solutions to the boundary value problem of a gravity wave travelling in an ideal fluid domain, subject to certain initial and boundary conditions. Each theory is distinct in its range of applicability in terms of water depth, wave steepness etc. The classical wave theory of Stokes (1847) involved the perturbation approach. In this method, solutions to an order of accuracy are obtained by using the results of the preceding order. The first order solution in wave steepness is obtained by formulating the problem with linearized boundary conditions viz., the linear wave theory. The solution upto the second order in wave steepness is obtained by a more precise definition of the problem and utilizing the first order solution, (Stokes, 1847; see also Dean and Dalrymple, 1984.) For a sinusoidal free surface, this theory predicts that the velocity potential would be sinusoidal with time and horizontal distance and would decay hyperbolically with depth. Further developments of the theory has been in extending the solution upto higher orders, Skjelbreia and Hendrickson

(1960). Stokes formalism was found to be more applicable in deep waters thus creating a necessity for shallow water wave theories. The shallow water wave theory developed by Korteweg and DeVries (1895) expresses the wave profile in terms of a Jacobian elliptic integral 'cn'. The Stream function theory by Dean (1965) is based on a numerical iteration technique to get the best fit to the boundary conditions. Further details on these and other theories can be found in Dean and Dalrymple (1984), Sarpkaya and Isaacson (1981) and the Shore Protection Manual (1984).

Chakrabarti (1980b) conducted a series of experiments over a wide range of water depths and wave steepnesses in an effort to evaluate the relative validity of various theories. While the linear theory and third order Stokes theory gave better fits to the measured wave lengths, the irregular stream function theory gave a better fit to the measured wave profiles. Dean (1974) was involved in establishing a basis for selection of a wave theory, given a set of wave conditions. Analytical studies revealed that deep water waves were well represented by higher order Stokes theories, shallow water waves by the first order cnoidal theory and the stream function theory provided an overall good validity. The stream function theory also showed good correlation with published data, thus Dean (1974) concluded that stream function theory was best suited for design purposes.

The range of applicability of various theories has been well discussed in the Shore Protection Manual (1984). Fig. (2.1) reproduced from the

manual is a plot of two parameters, the depth parameter h/gT^2 and the steepness parameter H/gT^2. The applicability of Stokes theory is restricted by the so-called Ursell parameter (cf. 3.2). Be ond an Ursell value of 26, the theoretical Stokes form develops a secondary wave crest due to the largeness of the second order term compared to the first order term thus restricting the application of this theory to transitional and deep waters.

Laboratory generation of progressive waves is different as opposed to the pure progressive wave problem because of the vicinity of the generating surface. No flow across the generating surface is an additional condition the flow has to satisfy in this problem. Havelock (1929) was concerned with the problem of forced waves due to a sinusoidally oscillating forcing surface, the piston type generator. His solution, based on linear wave theory showed an additional term in the velocity potential which decayed exponentially with distance from the wave generator. Ursell et al. (1960) have obtained expressions for the amplitude ratio of both piston and paddle type generators. Results of experiments seemed to correspond well with the theoretical results. However for steeper waves, the theory was found to over-predict the results by as much as 10%. Experiments on plunger type wave makers conducted by Ellix and Arumugam (1984) and also Ellix (1984) showed that the existing theory overestimated by as much as 20 %. Poor correla-

tion at lower frequencies was attributed to leakage around the wedge type plunger. Chen (1978) has done experiments at the MUN wave tank facility to verify the linear wave generator theory for the piston type generator installed in the tank. Two water depths of 3.0 ft and 4.5 ft in wave conditions $0.059 < h/\lambda < 0.6977$ and $0.0012 < H/\lambda < 0.1$ were considered. The results showed a heavy scatter to the order of 50%. The explanations given were too general and did not serve to explain fully as to why the generator did not follow the linear generator theory even in the linear wave ranges. In this context, later work by Muggeridge and Murray (1981) showed that the same generator followed the linear theory for a wide range of experimental conditions, $0.058 < h/\lambda < 0.548$ and $0.0012 < H/\lambda < 0.1$ at a constant water depth of 1 m. The apparent discrepancies among these two researchers' results were inexplicable.

Second order wave generator theories have been proposed following Stokes second order theory by some researchers, (Fontanet, 1961; Madsen, 1970 1971; Daugaard, 1972; Flick and Guza 1980) but none has been widely accepted. Solving for the generator boundary condition at the second order, these theories indicated the generation of a second harmonic free wave at twice the wave frequency. This wave was considered parasitic as it travelled over the second order incident wave. Expressions for the free wave amplitude were varied among these theories. Detailed discussions on the second order wave generator theories are done in section 3.3 of this thesis.

Experimental work based on these theories have been reported. Buhr Hansen and Svendsen (1974) have analysed the beating phenomenon between second order incident wave and the free wave generated by the wave maker. Experiments have been carried out to measure the amplitude of the free wave at various wave steepnesses and relative depths. Record was taken from a wave probe travelling down the flume and a band pass filter was used to remove the first order signal from the output. Results for the free wave amplitude were in partial agreement with theories of Madsen, Fontanet and Daugaard. One important outcome of Buhr Hansen and Svendsen's work was that the authors were successful in reducing the free wave amplitude by a non sinusoidal motion to the generator, based on the fact that the free wave was a linear wave with respect to its amplitude, as had been suggested by Madsen (1971). Ellix and Arumugam (1984) and also Ellix (1984) were concerned with the second order generator theory for a plunger type generator. From a wave probe placed at distinct locations down the flume, records were taken and analysed using a Fast Fourier Transform (FFT) and a least squares curve fitting technique. The authors showed that the free wave amplitude was as much as three to four times the second order Stokes wave amplitude. No theoretical comparisons were made because no theories were available for plunger type wave makers.

Waves generated at one end of a wave tank has to be absorbed by an energy dissipating beach at the other end. All beaches absorb most of the energy and reflect the rest. Beach reflection is an intriguing area of research and to date no theories are available to estimate the reflected wave amplitude and its dependency on various incident wave parameters. Each wave tank has to be calibrated to estimate the amount of reflection from the beach. This is often represented by the reflection coefficient which is a ratio of the amplitudes of the reflected wave and the incident wave. Goda and Suzuki (1976) have presented a technique for estimating the incident and reflected wave heights from two time records taken simultaneously from two wave probes located at less than a wavelength apart. Experiments were done both for regular and irregular waves. The effects of location and distance between probes were discussed. Ellix and Arumugam (1984) and also Ellix (1984) as part of their experiments have estimated the first order reflection coefficient of the beach in their wave flume to be about 5% or less. However, the reflection coefficient at second order was as high as 40-50%, which was puzzling to the authors. Chen (1978) has used seven wave probes spaced 2ft apart to measure the beat pattern due to reflected and incident waves. He noted that the reflection coefficient at the MUN wave tank facility was in the order of 10% at 3ft and 4.5ft water depths.

Waves travelling in the vicinity of stationary surfaces experience loss of

energy due to friction at these surfaces. This is called wave attenuation. Attenuation of two - dimensional waves in a channel of finite width was first treated by Biésel (1949) and later by Hunt (1952). They defined an attenuation coefficient which was composed of two components, one due to bottom friction and another due to side wall friction. Chen (1978) as part of his experiments found that the attenuation factors at the MUN wave tank were in the order of 10^{-5} thus causing negligible reduction to the wave amplitudes.

The above literature survey was focussed on understanding the wave fields existing in a laboratory. Second order Stokes theory was found suitable for the experiments as most of the second order generator theories were valid in that range. Following any one particular generator theory was not possible. But certain common results of these theories were used. Beach reflection was an inevitable part of these experiments. It was proposed to split the reflection effects into first and second order. Other side effects in the tank were generally considered small and neglected.

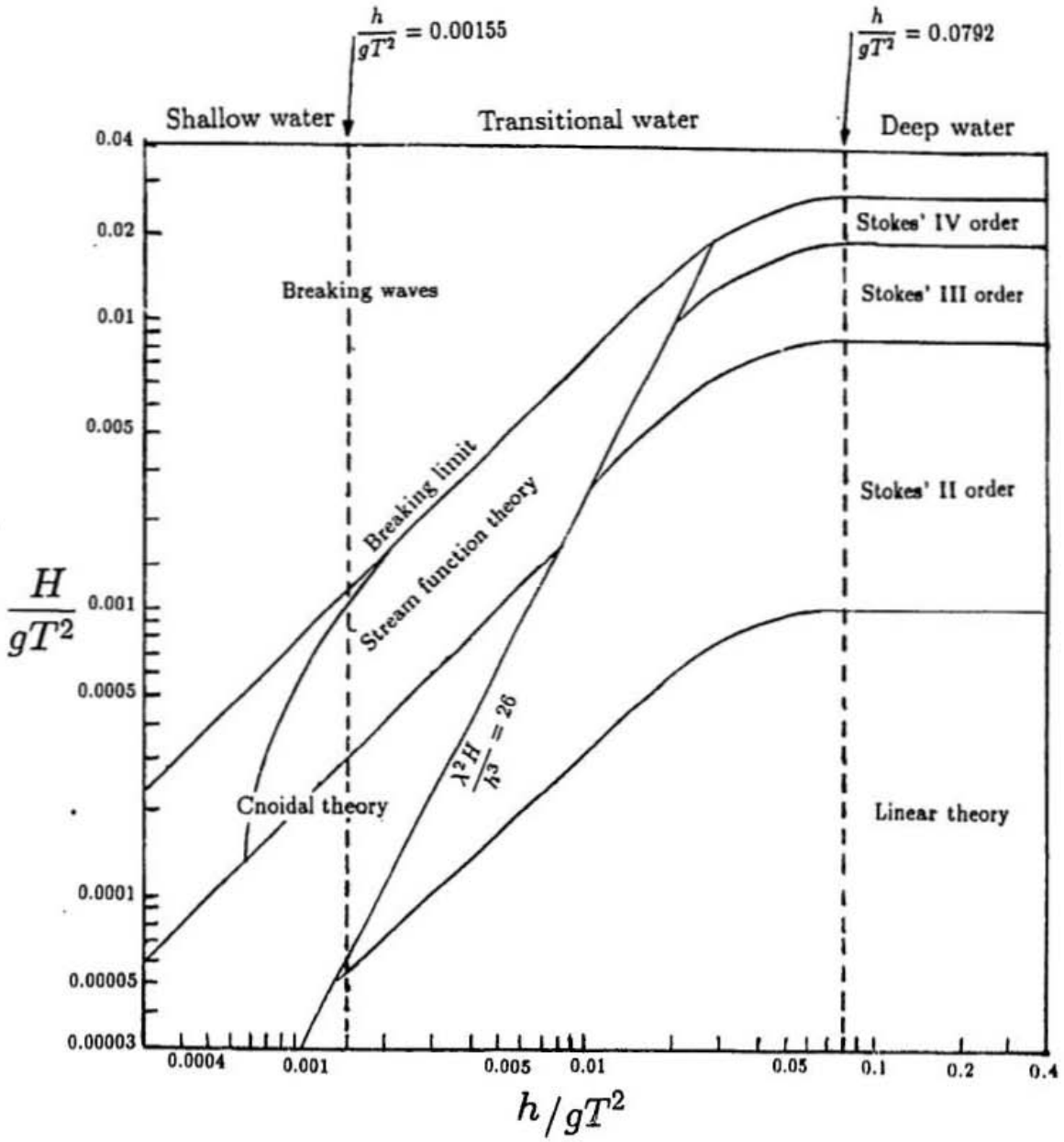

Figure 2.1 Range of validity of various wave theories (Shore protection manual, 1984)

Chapter 3

Theoretical Development

All waves and associated phenomena can be obtained as solutions to a basic boundary value problem with general boundary and/or initial conditions. Wave and wave generator theories are solutions to this problem, with the appropriate boundary conditions applied. We begin this chapter by presenting the fundamental problem. Second order Stokes theory is introduced as a solution to this problem. First and second order generator theories are successively discussed. The chapter concludes with a second order formulation for the total wave field in a laboratory.

3.1 The boundary value problem

The boundary value problem of interest is a two-dimensional gravity wave travelling on the free surface of a fluid (water), involving the following assumptions:

- The fluid (water) is incompressible and inviscid

- Zero surface tension
- The flow is irrotational and acyclic
- No underlying current exists
- Waves are of permanent form
- The pressure is constant and assumed to be equal to zero on the free surface
- Gravity is the only body force
- The bottom is smooth and horizontal.

The representative diagram of the flow with the chosen axes are shown in Fig. (3.1). The origin of the coordinate axes is on the free surface, with positive x in the direction of wave propagation and positive z pointing upwards. The water depth is denoted by h.

Assuming the validity of the above assumptions (Lamb, 1932; Wehausen and Laitone, 1960), the velocity of flow can be considered to be the gradient of a scalar namely the velocity potential $\phi(x, z, t)$. This potential satisfies the two-dimensional Laplace equation

$$\frac{\partial^2 \phi}{\partial x^2} + \frac{\partial^2 \phi}{\partial z^2} = 0 \tag{3.1}$$

in the fluid domain. The boundary conditions applicable over this domain are (Dean and Dalrymple, 1984; Sarpkaya and Isaacson, 1981)

1. No flow across any solid boundary (S_b)

$$\vec{n} \cdot \vec{v} + \frac{\partial \phi}{\partial n} = 0 \quad \text{on } S_b \tag{3.2}$$

where $\vec{n}$ is the unit vector normal to the solid surface, $\vec{v}$ is the velocity of the boundary and $\partial\phi/\partial n$ is the velocity component of the flow normal to the body.

2. The spatial periodicity is the requirement that the potential at any location x repeats itself at $x + \lambda$, where λ is the wavelength. Thus

$$\phi(x, z, t) = \phi(x + \lambda, z, t) \tag{3.3}$$

3. Periodicity with respect to time means

$$\phi(x, z, t) = \phi(x, z, t + T) \tag{3.4}$$

where T is the wave period.

4. The kinematic free surface boundary condition states that the water particle once in the free surface continue to remain with the surface. This means that

$$\frac{\partial \phi}{\partial z} - \frac{\partial \eta}{\partial t} = \frac{\partial \phi}{\partial x} \frac{\partial \eta}{\partial x} \tag{3.5}$$

must be satisfied on the free surface represented by $z = \eta(x, t)$ which is not known *à priori* and where η is a function of x and t only.

5. The dynamic free surface boundary condition arises from the law of conservation of momentum, utilizing the fact that the pressure is

constant at the surface. This leads to

$$\frac{\partial \phi}{\partial t} + \frac{1}{2}\left[\left(\frac{\partial \phi}{\partial x}\right)^2 + \left(\frac{\partial \phi}{\partial z}\right)^2\right] + g\eta = f(t) \qquad (3.6)$$

to be satisfied on $z = \eta(x,t)$. $f(t)$ is a function of time only and which is usually included in ϕ, (Sarpkaya and Isaacson, 1981)

6. A radiation condition implying that the wave system generated by a body is an outgoing one.

Since the free surface is an impermeable boundary, the kinematic free surface condition can be included in the no flow condition, Eq. (3.2). For easy computation, the kinematic and dynamic free surface conditions are usually combined to give a single free surface boundary condition, (Sarpkaya and Isaacson, 1981).

3.2 Second order Stokes theory

Progressive wave theories are solutions to the boundary value problem with the bottom as the only impermeable surface. The representative diagram of the coordinate system is given in Fig. (3.1). One of the classical methods used to solve the two-dimensional progressive wave problem is the perturbation approach where the variables of flow are developed as a power series of a perturbation parameter. Following Stokes (1847), this perturbation parameter (ϵ) is the wave steepness. Accordingly, ϕ and η are written as

$$\phi = \epsilon\phi_1 + \epsilon^2\phi_2 + \cdots \qquad (3.7)$$

$$\eta = \epsilon\eta_1 + \epsilon^2\eta_2 + \cdots \tag{3.8}$$

for some functions $\phi_i(x,z,t), i = 1,2,\cdots$ and $\eta_i(x,t), i = 1,2,\cdots$. The free surface boundary conditions contain non-linear terms which are evaluated at a variable limit, $z = \eta$. In order to be applicable at $z = 0$, they are expanded in the form of a Taylor's series about $z = 0$. Say given

$$f(z) = 0 \qquad \text{on } z = \eta,$$

Taylor's expansion of $f(z)$ about $z = 0$ implies that for small η we can write

$$f(z) + \eta\frac{\partial f}{\partial z} + \cdots = 0 \qquad \text{on } z = 0$$

Substituting the above expansions in the fundamental equations of flow, and collecting terms of order ϵ, the first order problem is described by

$$\frac{\partial^2\phi_1}{\partial x^2} + \frac{\partial^2\phi_1}{\partial z^2} = 0 \tag{3.9}$$

$$\frac{\partial\phi}{\partial z} = 0 \qquad \text{on } z = -h \tag{3.10}$$

$$\frac{\partial^2\phi_1}{\partial t^2} + g\frac{\partial\phi_1}{\partial z} = 0 \qquad \text{on } z = 0 \tag{3.11}$$

$$\eta_1 = -\frac{1}{g}\left(\frac{\partial\phi_1}{\partial t}\right) \qquad \text{on } z = 0 \tag{3.12}$$

Eq. (3.10) is the no flow condition for the progressive wave, the flat bottom being the only solid boundary in the vicinity of the flow.

Collecting the terms of order ϵ^2, the second order problem is described by

$$\frac{\partial^2 \phi_2}{\partial x^2} + \frac{\partial^2 \phi_2}{\partial z^2} = 0 \tag{3.13}$$

$$\frac{\partial \phi_2}{\partial z} = 0 \qquad \text{on } z = -h \tag{3.14}$$

$$\begin{aligned} \frac{\partial^2 \phi_2}{\partial t^2} + g\frac{\partial \phi_2}{\partial z} &= -\eta_1 \frac{\partial}{\partial z}\left[\frac{\partial^2 \phi_1}{\partial t^2} + g\frac{\partial \phi_1}{\partial z}\right] \\ &\quad -\frac{\partial}{\partial t}\left[\left(\frac{\partial \phi_1}{\partial x}\right)^2 + \left(\frac{\partial \phi_1}{\partial z}\right)^2\right] \qquad \text{on } z = 0 \end{aligned} \tag{3.15}$$

$$\begin{aligned} \eta_2 &= -\frac{1}{g}\left[\frac{\partial \phi_2}{\partial t} + \eta_1 \frac{\partial^2 \phi_1}{\partial z\, \partial t}\right. \\ &\quad \left. + \frac{1}{2}\left\{\left(\frac{\partial \phi_1}{\partial x}\right)^2 + \left(\frac{\partial \phi_1}{\partial z}\right)^2\right\}\right] \qquad \text{on } z = 0 \end{aligned} \tag{3.16}$$

Expressions for the velocity potential and the free surface to second order of a progressive wave propagating in the positive x-direction are obtained by solving the above problems. Assuming a sinusoidal free surface, they are given in dimensional forms by, (Sarpkaya and Isaacson, 1981; Dean and Dalrymple, 1984; Stokes, 1847)

$$\begin{aligned} \phi &= \frac{Hg}{2\omega}\frac{\cosh\, k(h+z)}{\cosh kh}\sin\,(kx - \omega t) + \\ &\quad + \frac{3}{8}\left(\frac{H}{2}\right)^2 \omega \frac{\cosh 2k(h+z)}{\sinh^4\, kh}\sin\, 2(kx - \omega t) \end{aligned} \tag{3.17}$$

$$\eta = \frac{H}{2}\cos(kx-\omega t) + \left(\frac{H}{2}\right)^2 \frac{k}{4}\frac{\cosh kh(2+\cosh 2kh)}{\sinh^3 kh}\cos 2(kx-\omega t) \quad (3.18)$$

where H, the wave height is twice the first order amplitude a_1 and h is the water depth. k the first order wave number is equal to $2\pi/\lambda$, where λ is the first order wave length. ω is the angular velocity of the wave and is related to the first order wave period (T) as $2\pi/T$. The linear dispersion relationship holds good upto the second order and is given by

$$\omega^2 = gk\tanh kh \quad (3.19)$$

Results of Stokes theory upto first order coincides with the classical linear theory (Dean and Dalrymple, 1984). The second order terms are functions of H^2 and are usually one order of magnitude less than the first order terms. Limitations regarding the validity of this theory arises due to:

1. Convergence of the power series used

2. Development of a secondary wave crest in shallow waters.

It can be shown (Dean and Dalrymple, 1984) that an Ursell parameter defined by

$$Ur = \frac{\lambda^2 H}{h^3}$$

determines the range of validity of Stokes theory. In order to satisfy the above mentioned considerations, it is required that (Dean and Dalrymple, 1984)

$$Ur < \frac{8}{3}\pi^2 \simeq 26 \tag{3.20}$$

The straight line with $Ur = 26$ is shown in Fig. (2.1) and limits the applicability of this theory to transitional and deep water ranges.

3.3 Theories for piston type wave maker

A piston type wave maker is a vertical flap that translates normal to its surface. Activated hydraulically or pneumatically, the wave maker displaces water while in motion causing waves. For the boundary value problem of two-dimensional wave generation, Eqs. (3.1) - (3.6) hold good. The no flow condition has to be satisfied at the bottom, Eqs. (3.10) and (3.14) and on the generator surface. If the equation of motion of the generator is given by

$$\xi(t) = \xi_0 \sin \omega t \tag{3.21}$$

the no-flow condition on the generator surface takes the form

$$\omega \xi_0 \cos \omega t - \frac{\partial \phi}{\partial x} = 0 \qquad \text{on } x = \xi \tag{3.22}$$

$S = 2\xi_0$ is the so-called stroke length of the wave maker. The representative diagram for the two dimensional wave generation problem is given in Fig. (3.2).

A linear solution to the above problem upto first order was proposed as a combination of a single progresive wave and an infinite number of standing waves, (Havelock, 1929; see also Ursell et al, 1960). According to this theory, the velocity potential is given as:

$$\phi = b_0 \cosh k(h+z)\sin(kx-\omega t) + \tag{3.23}$$

$$+ \cos\omega t \sum_{n=1}^{\infty} b_n e^{-k_n x} \cos k_n(h+z) \tag{3.24}$$

where the wave numbers k and k_n satisfy the relationships

$$\omega^2 = gk \tanh kh \tag{3.25}$$

$$\omega^2 = gk_n \tan k_n h \tag{3.26}$$

The amplitudes b_0 and b_n are obtained as:

$$b_0 = \frac{\int_{-h}^{0} \xi_0 \omega \cosh k(h+z)dz}{k\int_{-h}^{0} \cosh^2 k(h+z)dz} \tag{3.27}$$

$$b_n = \frac{\int_{-h}^{0} \xi_0 \omega \cos k_n(h+z)dz}{k_n\int_{-h}^{0} \cos^2 k_n(h+z)dz} \tag{3.28}$$

The relation between the height of the progressive wave and b_0 is obtained by evaluating the free surface elevation far from the generator surface as

$$\frac{b_0\omega}{g}\cosh kh = \frac{H}{2}$$

The ratio of the wave height to stroke length for the piston type generator was given by Ursell et al (1960) as:

$$\frac{a_1}{\xi_0} = \frac{\tanh kh}{n_1} \tag{3.29}$$

where n_1 is the ratio of group speed to celerity of the progressive wave given as

$$n_1 = \frac{1}{2}\left[1 + \frac{2kh}{\sinh 2kh}\right]$$

The exponential amplitude standing waves decay rapidly with distance from the wave maker. It has been shown that within two or three water depths away from the generating surface, most of the standing wave terms are negligible, (Ursell et al, 1960; Dean and Dalrymple, 1984).

Second order theories for the wave generation problem have been proposed, but none has been accepted widely. A theory by Fontanet,(1961) is applicable to piston-type wave makers, but was found to be cumbersome. Madsen, (1970,1971) employed an expansion similar to the Stokes perturbation technique to develop a simple theory for piston type wave makers. The author has used a perturbation expansion for the piston motion in the form,

$$\xi = \epsilon\xi_1 + \epsilon^2\xi_2 + \cdots \tag{3.30}$$

where ξ_1 and ξ_2 represented the first and second order piston motions respectively. The first order solution of this theory is similar to the classical solution discussed previously. In second order, this theory reveals, similar to Fontanet (1961), the existence of a second harmonic free wave in addition to the Stokes second order progressive wave. The amplitude of the free wave is given by this theory as

$$a_{22} = \frac{1}{2}\left(\frac{H}{2}\right)^2 \frac{1}{h\tanh kh}\left(\frac{3}{4\sinh^2 kh} - \frac{n_1}{2}\right)\frac{\tanh \kappa h}{n_2} \tag{3.31}$$

where n_2 is analogous to n_1 of Eq. (3.29) and is given by

$$n_2 = \frac{1}{2}\left[1 + \frac{2\kappa h}{\sinh 2\kappa h}\right] \tag{3.32}$$

κ is the wave number of the free wave and satisfies the dispersion relation (Madsen, 1970; 1971)

$$4\omega^2 = g\kappa \tanh \kappa h \tag{3.33}$$

Limitations on the applicability of Madsen's theory follows the usual limitations of second order Stokes theory. A drawback of Madsen's theory is that the value of a_{22} rapidly drops to zero with increasing kh because of the negative term in the expression.

The theory by Flick and Guza,(1980) was developed to include a variety of wave maker configurations. This theory resorts to a more exact solution by including the lowest order standing waves into the second order solution. The amplitude of the free wave is given as

$$a_{22} = \frac{2\omega}{g} \cosh \kappa h (B_o^2 + D_o^2)^{0.5}$$

where B_o and D_o are integrals over depth of certain algebraically complicated functions.

A few results common to all these theories, which have been assumed in the course of the present work are as follows:

- The second order wave field consists of a Second order Stokes progressive wave and a second harmonic free wave.

- The free wave behaves like a linear wave and travels at twice the first order frequency. It satisfies the dispersion relation given by Eq. (3.33).

- The standing waves are virtually negligible a few water depths away from the generator.

3.4 The total wave field

The total wave field in the laboratory was expected to consist apart from the desired progressive wave, contributions due to reflections from the beach and due to free wave effects. Effects of the beach were not theoretically quantified, but it was expected that a wave arising due to the reflection of the incident wave will be present in the tank. This wave would be of the same frequency as the incident wave and travel in a direction opposite to it. Yet another reflected wave of similar qualities was found to arise due to the reflection of the free wave. [1] The total wave field in a wave flume was thus assumed as a linear superposition of the following waves

- First order Stokes wave with amplitude a_1 and wave number k

- Second order Stokes wave with amplitude a_2 and wave number $2k$

- Second order free wave with amplitude a_{22} and wave number κ

[1] It was initially assumed that this reflected wave would be negligible. During the course of experiments, a beat pattern corresponding to this wave was found superimposed over other beat patterns. Hence a re-formulation had to be effected.

- First order reflected wave with amplitude a_R and wave number k
- Second order reflected wave with amplitude a_{22R} and wave number κ.

This is represented mathematically as,

$$\begin{aligned}\eta_{\text{total}} &= a_1 \cos(kx - \omega t) + a_2 \cos 2(kx - \omega t) + \\ &+ a_{22} \cos(\kappa x - 2\omega t + \delta) + a_R \cos(kx + \omega t + \alpha) + \\ &+ a_{22R} \cos(\kappa x + 2\omega t + \gamma) \qquad (3.34)\end{aligned}$$

where α, δ, γ are the phases of the corresponding waves with respect to the first order Stokes wave. Rewriting the total wave field as:

$$\eta_{\text{total}} = \eta_1 \cos(\omega t + \theta_1) + \eta_2 \cos(2\omega t + \theta_2)$$

we obtain the following expressions.

$$\eta_1^2 = a_1^2 + a_R^2 + 2a_1 a_R \cos(2kx + \alpha) \qquad (3.35)$$

$$\begin{aligned}\eta_2^2 &= a_2^2 + a_{22}^2 + a_{22R}^2 + 2a_2 a_{22} \cos((\kappa - 2k)x + \delta) + \\ &+ 2a_2 a_{22R} \cos((\kappa + 2k)x + \gamma) + 2a_{22} a_{22R} \cos(2\kappa x + \gamma + \delta) \qquad (3.36)\end{aligned}$$

$$\theta_1 = \arctan\left[\frac{a_1 \sin kx - a_R \sin(kx+\alpha)}{a_1 \cos kx + a_R \cos(kx+\alpha)}\right] \tag{3.37}$$

$$\theta_2 = \arctan\left[\frac{a_2 \sin 2kx + a_{22} \sin(\kappa x+\delta) - a_{22R} \sin(\kappa x+\gamma)}{a_2 \cos 2kx + a_{22} \cos(\kappa x+\delta) + a_{22R} \cos(\kappa x+\gamma)}\right] \tag{3.38}$$

Both the first and second order amplitudes, η_1 and η_2 can be seen to be functions of the horizontal distance, x down the flume. This is referred to as the beat pattern arising due to a superposition of two or more waves.

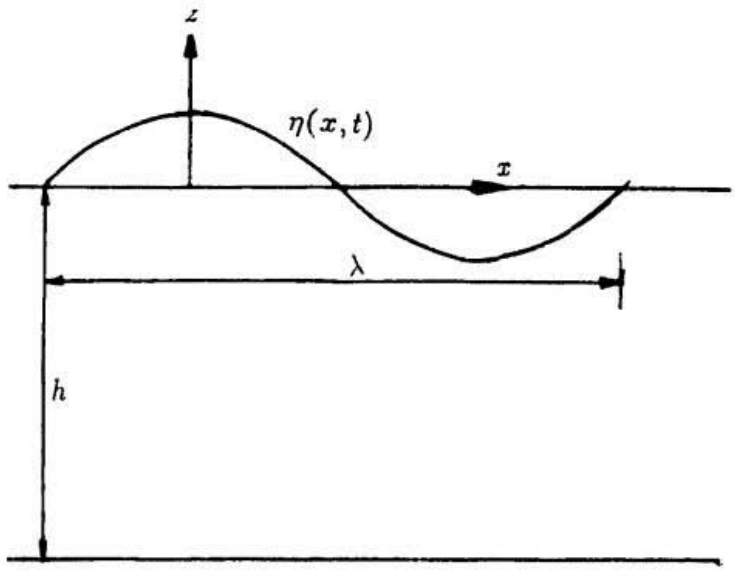

Figure 3.1 Representative diagram of a two-dimensional progressive wave.

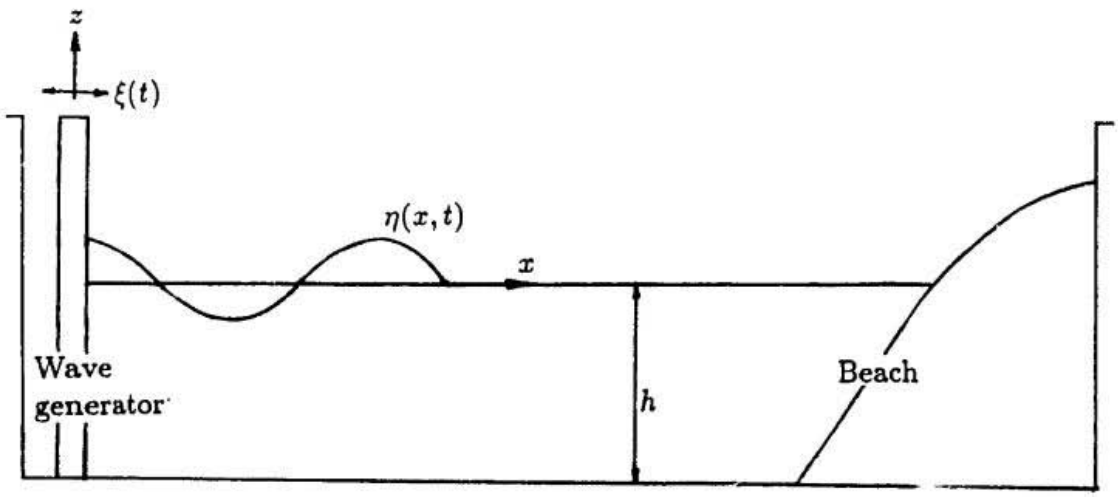

Figure 3.2 Representative diagram of two-dimensional wave generation by a piston type wave maker.

Chapter 4

Experimental setup and procedure

The wave tank located at the Faculty of Engineering, MUN is a steel reinforced structure with inner dimensions of 58.27m × 4.57m × 3.04m. One of the side walls is glass panelled at various depths for viewing purposes. A piston type wave generator is installed at one end of the tank as shown in Fig. (4.1). The generator is driven by a hydraulic actuator with a capability of 48.8KN force over a 0.25m stroke. Electronic control for the waveboard is provided from a control room through an MTS closed loop servo-controlled system with error detection and compensation applied through a LVDT feedback loop. The board has a maximum span of 0.58m and is expected to respond well to command signals in a frequency range of 0.35Hz - 1.3Hz. Both the frequency and span can be set manually by means of counters which have an accuracy upto the second decimal. The waveboard has a watertight

teflon seal along its sides and bottom and no leakage behind the board had been observed or reported to date. Wave filter plates affixed to the front of the board serve to reduce the cross oscillations in the tank.

At the other end of the tank is located a parabolic beach. The beach is constructed out of three modules as shown in Fig. (4.2). The basic structure is steel, topped by wooden grids and three layers of net to absorb energy efficiently. A gap of one foot between the beach and the bottom of tank allows a free flow of water under the beach for maintenance purposes. A towing carriage runs on rails parallel to the length of the tank. The carriage control system emits 10,000 pulses for every 1.0m travelled. The horizontal distance moved by the carriage can be estimated by tracking the number of pulses emitted using a frequency counter installed for this purpose.

A schematic diagram of the setup used for these experiments is shown in Fig. (4.3). A resistance type wave probe was used during the experiments to measure instantaneous wave surface elevations. This probe operated on the principle that variation of the conductivity of the wires would linearly depend on the level of water in between them, provided the ambient temperature remained constant. The wave monitor hosted an amplifier and a Wheatstone network. The probe was connected to the Wheatstone bridge in the monitor. Since the variations in the bridge voltage due to variations in the probe resistance were small, it was necessary for the signal to be

amplified. The amplified signal was then recorded on magnetic tapes by an 8 channel FM recorder.

On-line data processing was not preferred for the present study as there was a need to store analog data for re-analysis purposes. Digitisation of the analog data was performed using a work station data acquisition and control device called Keithley System 570. Specifications of this system are shown in Table (4.1). The required input parameters for the digitisation program were: name of the output file, sampling rate, length of record and the number of channels of input. The length of record was usually two cycles and the sampling rate was determined based on the requirement of 64 samples per wave period.[1] Commands were issued through a desktop computer and the data stored as files in the VAX/VMS 8530 computer through the Remote access facility (RAF) available on the VAX/VMS system.

Calibration tests for the wave probe were conducted before the experiments to evaluate the relation between the water level and the resistance of the probe. These tests were conducted by manually raising and lowering the probe and noting the corresponding outputs from the wave monitor. Since the probes were sensitive to temperature fluctuations, it was necessary to calibrate the probes every day of the experiments. A record of the calibration constants thus estimated is shown in Table (4.2) for all the days when experiments were conducted. Fig. (4.4) shows the calibration data

[1] For efficient functioning of the FFT algorithm, it was required that the total samples be a power of 2. It was decided that 64 samples per wave period would be optimal for the present purpose.

for a particular day and a least squares straight line through the data. The slope of the line gave the value of the calibration constant.

The problem at hand was to estimate the individual wave parameters, given the total wave field. The approach adopted in the present study was to obtain wave surface data at discrete locations down the tank. From these time signals, the frequency components at first and second order were analysed. Curves corresponding to Eqs. (3.35) and (3.36) were fitted to these components and, the amplitudes of interest were discerned. The experimental procedure for this approach was:

- Set the frequency and span of the wave generator.
- Select number of locations and distance between them.
- Allow sufficient time for the wave field in the tank to attain steady state.
- Place the probe at the first location, record data over three cycles.
- Move on to the next location.
- Clear all locations, prepare for next run.

The data thus obtained was recorded, digitised and stored sequentially as computer files. Each file was coded by a four digit number, the first two

digits indicating the run number and the last two showed the location from which the data was taken. The number and distance between locations depended on the wave lengths of the beat patterns present. It was ensured that atleast five locations were present within the smallest beat wave length. The first location (designated as location zero) was fixed at 20m away from the mean position of the generator.

Analysis of the data was performed by a program called ANALYS, developed for this purpose. A flow chart of this program is shown in Fig. (4.5) and the source code is provided in Appendix A. Inputs to the program were the sampled data at every location and the parameters characterising the run like the frequency, distance between locations, number of locations, interval within which the wave numbers of beat patterns lie etc. Conversion of the sampled data into the frequency domain was performed by a fast fourier transform subroutine called F2TRF of the IMSL/MATH library available within the VAX/VMS system. This program utilised the data for one wave cycle and evaluated the amplitudes of various cosine and sine components of the data. Amplitudes of first and second order were thus obtained at every location. Appendix B explains the working of a standard fast fourier transform. A subroutine LSSIN was used to fit a least squares sine curves to these amplitudes, with the wave number being an unknown. Basically it performed the following operations:

- From the variation of amplitudes down the flume, LSSIN identified the wave number of the beat patterns within a user-specified interval by an optimization procedure to minimise the least squared error in the fitted curve.

- At the optimal wave number a curve was fitted and the amplitudes and mean values of the beats were evaluated.

- From these values, the amplitudes of individual waves were estimated using Eqs. (3.35) and (3.36).

Appendix C explains the working of the subroutine LSSIN. In the equation for the total first order amplitude (3.35), there existed only one beat pattern. So the working of the program was straight forward. In the second order equation (3.36) however, there existed three beat patterns. The procedure followed in ANALYS in this case was to fit a curve to the predominant pattern (the curve with number $\kappa - 2k$). This was then subtracted from the amplitudes to obtain data for the remaining patterns. To minimise distortions caused due to the subtraction, the amplitudes were interpolated using splines to get a smooth curve. Subtraction of the fitted curve from the interpolated curve was then effective. The data available after subtraction was fitted with the next predominant curve.

Essentially the available data was fitted into the formulated model to evaluate the desired quantities. These were then compared with available theories to check the validity of the model.

Table 4.1 System 570 Specifications

General		
Supplied software	:	SOFT500 extensions to BASICA
Host computer configuration	:	IBM pc, XT, AT COMPAC pc, COMPAC Deskpro 286 with atleast 256K bytes of RAM
Standard channel capacity		
Analog input	:	32 single-ended or 16 differential
Analog output	:	2
Digital input	:	16
Digital output	:	16
Power requirements	:	5V at 2amp max. from host computer.
Analog input		
Instrumentation amplifier	:	X1, X10, X100, switch selectable
Programmable gain amplifier	:	X1, X2, X5, X10, software selectable
A/D converter full scale ranges	:	±10V, ±5V, ±2.5V, 0 to 10V, 0 to 5V, switch selectable
Resolution	:	12 bits (1 part in 4096)
Max. sample rate	:	31.4K samples per sec.
Digital Output		
Channel capacity	:	16 non-isolated
Output range	:	TTL compatible, low true
Drive capability	:	10 TTL loads, 20mA sink @ 0.5V
Accessories and options		
AIM6	:	Strain gage and RTD analog input module
DaDiSP I	:	Data Acquisition and Signal Processing software package
DaDiSP II	:	Extended Digital Signal Processing software package

Table 4.2 Record of wave probe calibration factors

Date of Experiment	Calibration Factor V/m
Feb 12	5.99
Feb 15	6.30
Feb 16	6.41
Mar 02	6.29
Mar 03	6.06
Mar 04	6.13
Mar 07	6.82
Mar 08	7.06
Mar 09	6.98

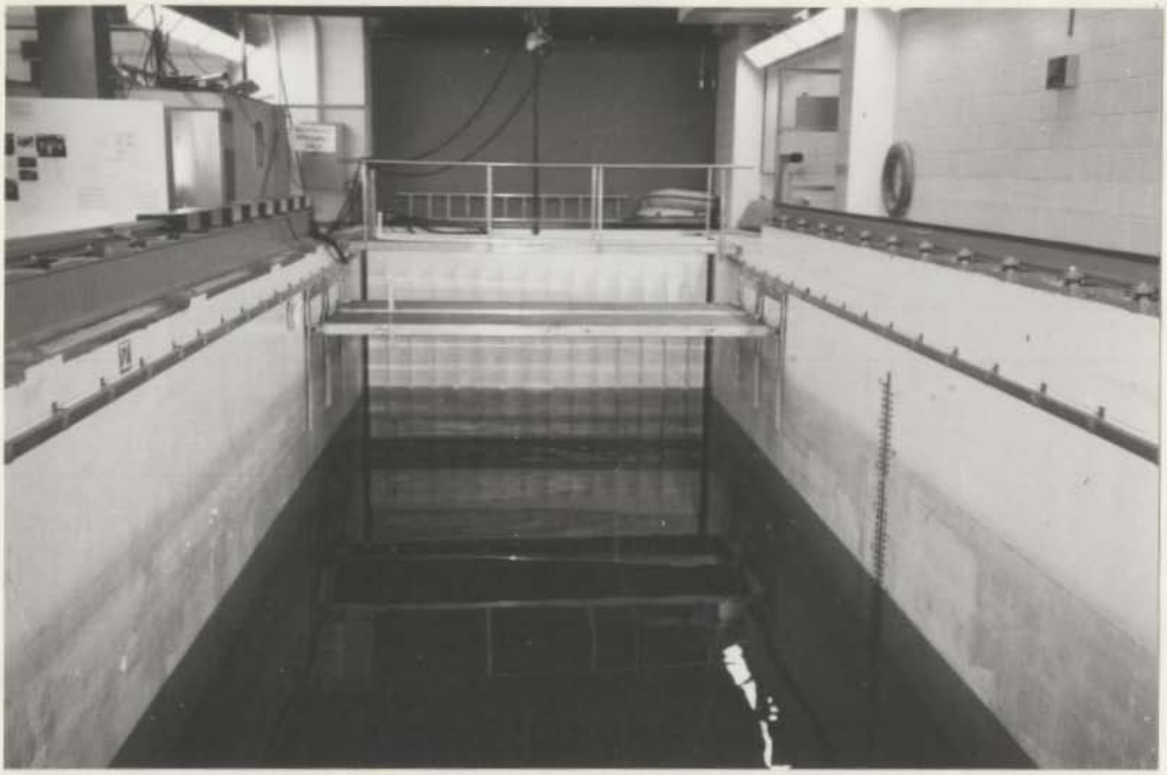

Figure (4.1) Configuration of the piston type wave maker

Figure (4.2) Beach configuration

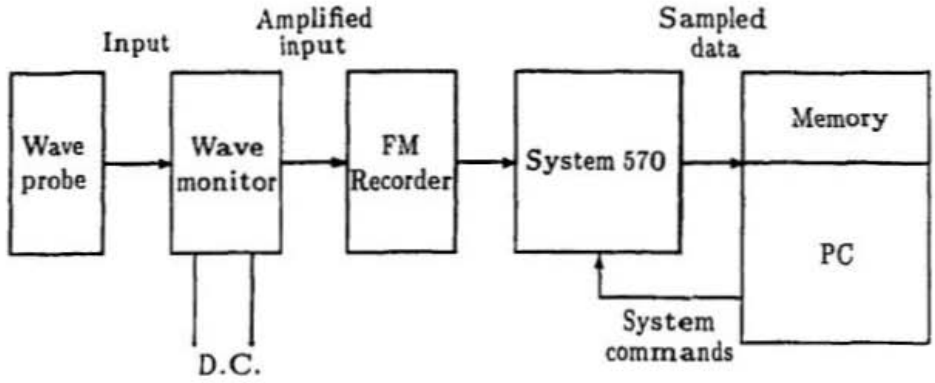

Figure 4.3 Information flow chart for wave experiments

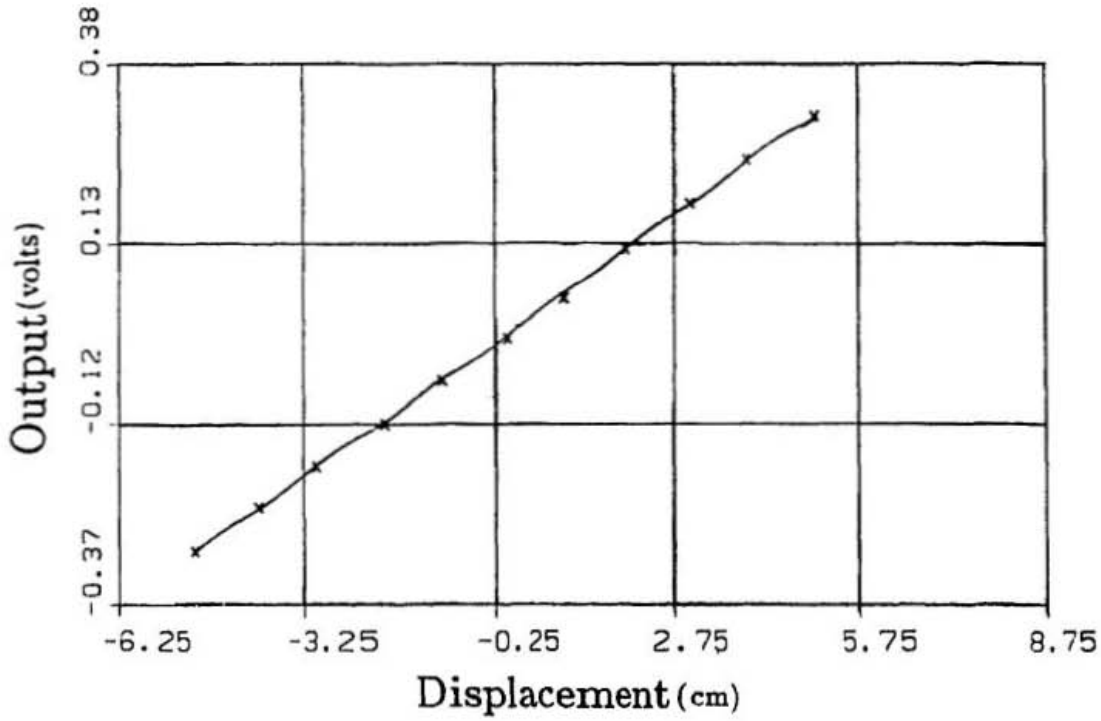

Figure 4.4 Wave probe calibration diagram; Date: Feb 12
Slope of least squares line = 5.99 V/m
× - Measured points

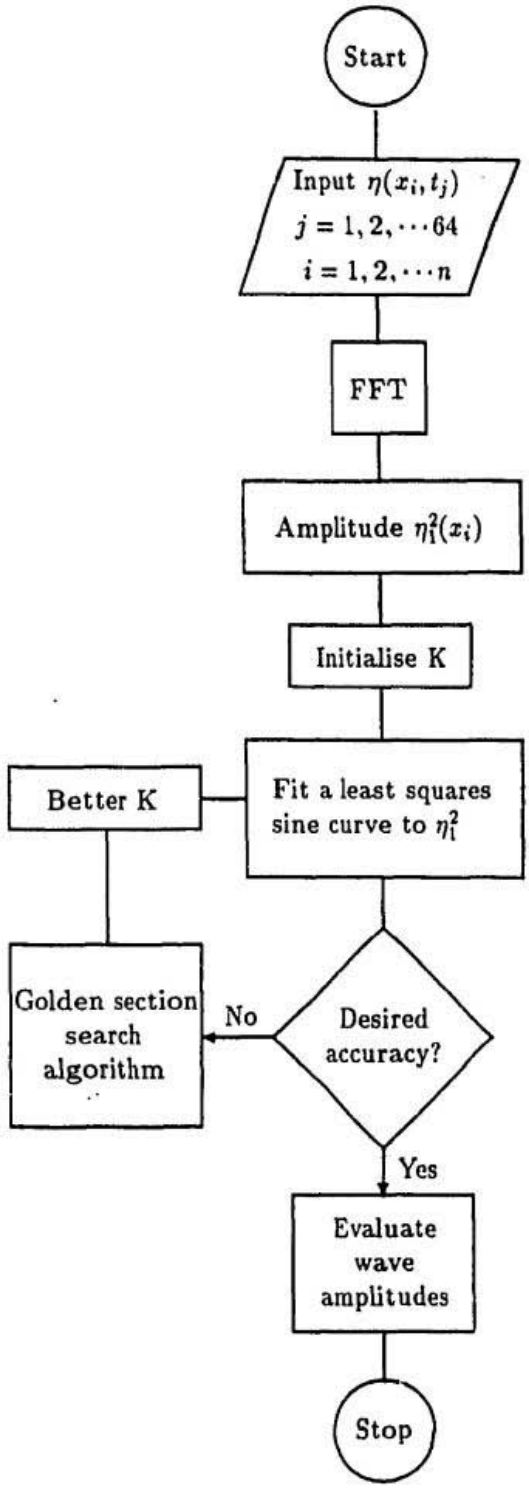

Figure 4.5 First order analysis flow chart for wave experiments

Chapter 5

Discussion of results

The experiments were designed to cover a range of parameters where Stokes second order theory would be valid. It was also important that third order effects be low in this range, as no third order wave generator theory was available. Further, the range was also subject to limitations of the apparatus used. The piston type generator was stroke limited at lower frequencies and power limited at higher frequencies. It was found to perform satisfactorily for frequencies of 0.35 - 1.3Hz. Considering all these factors, a set of 28 points were chosen in Fig. (2.1). The runs were composed of seven frequencies and four steepnesses at every frequency. These values and those of certain characterising parameters are given in Table (5.1). A constant water depth of 1.0m was maintained throughout.

Sample wave forms (time history of the free surface elevation) are shown in Figs. (5.1) to (5.5) as a plot of time vs surface elevation. Figures are

arranged according to the order of locations from where the data was taken. The time scale used depended on the sampling rate, which in turn was dependent on the frequency of the wave. Free surface elevation as shown is uncalibrated. The total wave amplitude can be seen to vary along the flume. The variation of the first and second order amplitudes is shown in Figs. (5.6) and (5.7) which are intermediate outcomes of the program ANALYS. First and second order mean square amplitudes at various locations are evaluated using a FFT and plotted as points in these figures. Least squares fits, corresponding to Eqs. (3.35) and (3.36) are also plotted. The proximity of the points to the curve shows that the model used for the wave field matches well with the actual field. Correlation was generally good for all the runs even at the second order, where the measured quantities are small (for example the mean squared amplitude in Fig. (5.7) is of the order of 0.025 sq.cm.) Discrepancies still existed which were possibly due to

- Other unknown and unaccounted effects
- Practical difficulties in exactly positioning a location. As was mentioned before, movement from one location to the next was by a carriage, with the help of a frequency counter. Precise movement to a location would be practically impossible though efforts were directed towards achieving that. This effect could be significant on waves of smaller wavelength.

5.1 First order results

The first order results from the program ANALYS consisted of the first order wave number, amplitudes of the first order Stokes wave and the first order reflected wave and the phase of the reflected wave with respect to the incident wave. Results are nondimensionalised and presented in Figs. (5.8) through (5.11). Fig. (5.8) is a plot of the relative depth parameter kh experiment versus theory. The graph is intended to show the efficiency of the golden section optimization technique to estimate the optimal wave number which would suit the data. Fig. (5.8) shows that the experimental kh differs from the theoretical kh by a margin of 10%. Further improvement of this technique is possible. To check whether the wave generator followed the linear generator theory, the wave height(H) to stroke length(S) ratio was plotted against kh in Fig. (5.9). The curve of Fig. (5.9) is a plot of Eq. (3.29) and the dots are the results from ANALYS. A scatter to the order of 20% is evident. This is not unprecedented. Chen (1978) reported of a similar scatter at approximately the same water depth. His explanations for this scatter were general. In the present study, the author expects two possible sources of this scatter.

- Presence of secondary reflected waves at the first order.
- Imperfections in the wave generator control system.

If the reflection from a beach is high, secondary reflected waves are created due to the reflection of the primary reflected waves at the generator surface. This effect is usually small if the primary reflected waves from the beach are small. If a secondary reflected wave were to be present, it would be impossible to separate it out from the primary incident wave because both of them would be of the same frequency. Depending on the phase difference, these waves interfere constructively or destructively. Comparison of the results of Fig. (5.9) with the reflection coefficients plotted in Fig. (5.10) shows no apparent correlation. There are cases where the reflection coefficient is high but scatter in Fig. (5.9) low and vice versa. On the second aspect of the wave generator control system, four possible sources of errors are:

- imperfections in knob control
- voltage setting for maximum stroke of the board
- variation of generator efficiency with depth
- temporal variation of board movement due to poor seating of the teflon seal.

Manual errors in knob control for span setting to the extent of 5% are possible. The voltage setting for maximum stroke of the generator is an initialising parameter for the control system. Small changes in this parameter can occur over the course of time, if not checked periodically. The

amount of error will however, be small. The generator was designed for an optimal depth of 1.8m. Lower depth can result in a bigger stroke than required because of reduced hydrostatic load. Improper seating of the teflon seal around the board was noticed in the early stages of the experiment and rectified. The scatter in Fig. (5.9) could have had contributions from all these four sources.

First order reflection coefficients defined by

$$R = \frac{a_R}{a_i} \times 100\%$$

are plotted in Fig. (5.10) versus the relative depth parameter kh. Beach mechanisms are still a subject of study and hence it is possible that R could depend on any parameter. The graph shows a considerable scatter varying over 10 - 60%. The main source of this high reflection was the one foot gap between the beach and the tank floor. The author was also informed that the beach was designed for an optimal depth of 1.8m. So at a water depth of 1.0m, the reflection coefficients are likely to be higher than optimum. More intriguing than the reflection coefficient is the phase at which a wave is reflected from a beach. Fig. (5.11) shows a plot of the phase difference between the reflected wave and the incident wave, α vs kh. Results are widespread from -2π to 0. In all cases, α is negative, indicating that the reflected wave lags behind the incident wave. Apart from that, no conclusions seem possible.

5.2 Second order results

Expected results for second order were:

- Free wave number, κ
- Second order Stokes wave amplitude, a_2
- Second harmonic free wave amplitude, a_{22}
- Phase difference between the free wave and incident wave, δ
- Second order reflected wave, a_{22R}
- Phase difference between the second order reflected wave and the incident wave, γ

Figs. (5.12) through (5.15) are plots of the Stokes amplitude ratio, a_2/a_1 versus kh. This would be a test on the validity of Stokes theory over the range of testing. Each plot is for one of the four different steepnesses, characterised by the parameter, H/gT^2. Fig. (5.12) shows that at the lowest steepness, where a_2 is typically of the order of $0.01a_1$, experimental results are quite close to theory. This was the first indication of the efficiency of the algorithm behind ANALYS. Though the obtained values of a_1 were considerably different from expected (see Fig. (5.9)), it did not seem to have affected the amplitude ratios. Results are higher than theory in Fig. (5.12) but the difference narrows down with increasing steepness. This is because

the second order quantities become comparatively bigger thus enabling a better measurement, within the scope of the instruments used. A local high in Fig. (5.13) at a kh of 3.0 was inexplicable. At a H/gT^2 of 0.003, the theory line almost corresponds to the mean curve, if drawn through the points. A drawback of Stokes theory is reflected in Fig. (5.15). As can be seen in Fig. (2.1), waves with $H/gT^2 = 0.005$ almost fall in the Stokes third order theory range. In and around this value, second order theory predicts a higher value for the second order wave amplitude, causing a secondary crest to appear in the primary wave trough, (Dean and Dalrymple, 1984). This would be even more conspicuous at lower kh or higher Ur. Fig. (5.15) demonstrates this effect, with experimental points lying below theory at lower kh values. Overall, results for Stokes amplitude ratio are satisfying and demonstrate the efficiency of the analysis strategy.

Results for the free wave number are plotted in Fig. (5.16). The free wave number ratio can be defined based on the dispersion relationships, Eqs. (3.19) and (3.33) as:

$$\frac{\kappa}{4k} = \frac{\tanh kh}{\tanh \kappa h}$$

The ratio tends to 1 as water gets progressively deeper. Experimental results can be seen to be close to theory, scatter in the order of 10%. In this context, significantly higher free wave celerities than theory were reported by Buhr Hansen and Svendsen (1974) and Ellix (1984). These authors attributed part of the variation to the mass transport velocity effects in the

tank. Relation between celerity and wave steepness was also discussed in Buhr Hansen and Svendsen (1974). Compared to these authors' results, scatter in Fig. (5.16) seems small. Further improvements are possible by refining the precision parameters of ANALYS. Fig. (5.17) is a plot of the free wave amplitude ratio a_{22}/a_2 vs kh. Theoretical curves of Daugaard (1972), Fontanet (1961) and Madsen (1970, 1971) are also shown in the figure. The theories of Fontanet and Daugaard show that the free wave amplitude ratio converges to 0.4 at deep water whereas the present study indicates considerably higher values of the ratio at around 0.8. Results for this ratio by Buhr Hansen and Svendsen (1974) also showed variations from theories but the results were generally less than 0.6. Their results showed two depressions in a_{22}/a_2, at $h/\lambda = 0.15$ ($kh = 0.942$) and $h/\lambda = 0.45$ ($kh = 2.827$) where the former was more pronounced and consistent. A similar depression around $kh = 1.0$ can be seen in Fig. (5.17). A second drop in the ratio occurs beyond $kh = 6.0$ which were not noticed by Buhr Hansen and Svendsen (1974) as their experiments were restricted to a kh of 4.0. While the theories used for comparison are in doubt, a quantitatively unknown second order effect is expected to have contributed to these variations. The free wave phase angle shown in Fig. (5.18) shows a heavy scatter and precludes any conclusion to be drawn. One intriguing aspect was to determine whether the second order reflection resembles first order. It has been reported by Ellix (1984) that second order coefficients upto 50% were

measured which compared with 5 - 6% at the first order. Fig. (5.19) is a plot of second order reflection coefficients plotted against κh. Values of this coefficient ranges from 5 - 100%. This range is higher than that of the first order reflection coefficient. It is felt that apart from the mere reflection of the incident free wave, the reflected wave at second order can also have contributions from the nonlinear processes associated with the breaking of the first order incident wave at the beach. This also explains the discrepancy in the results obtained by Ellix (1984) mentioned previously. The phase angle of the second order reflected wave plotted in Fig. (5.20) shows similar to Fig. (5.11) large scatter and no trends.

5.3 Conclusions

The results of the wave experiments are promising from the point of view of implementing a novel strategy of analysing the wave field in a wave tank. Some conclusions from these experiments are:

1. The total wave field formulation upto second order adequately represents the actual wave field present in a wave tank.

2. The golden section optimization technique used to evaluate wave numbers of beat patterns is accurate to $\pm 10\%$.

3. The wave generator performance was found to deviate from linear generator theory predictions by as much as 20%. This is very likely

due to control system imperfections.

4. First and second order reflections exhibit similarities, with most of the values lying in the range of 5 - 60%.

5. The proximity of the experimental results with theory for the Stokes wave amplitude ratio, a_2/a_1 indicates that the strategy employed in the analysis program served its purpose.

6. Within the range of testing done, second order Stokes theory adequately represents the progressive wave.

7. The free wave behaves like a linear wave and satisfies the linear dispersion relation, Eq. (3.33).

8. Results for free wave amplitude ratio are considerably higher than theory. Contributions could be from the inadequacy of existing theories and from unknown effects in the tank.

9. Phase differences of reflected and free waves are widely scattered and no trends are observed.

Recommendations for further research are included as part of the last chapter in this thesis.

Table 5.1 Parameters of experimental runs

Run	f $\sec^{-1}$	H cm	k m^{-1}	h/gT^2	H/gT^2	Ur
1	0.4	4.287	0.900	6.981	0.0007	2.090
2	0.5	2.744	1.206	5.210	0.0007	0.745
3	0.6	1.906	1.579	3.979	0.0007	0.302
4	0.9	0.847	3.272	1.920	0.0007	0.031
5	1.0	0.686	4.031	1.559	0.0007	0.017
6	1.1	0.567	4.875	1.289	0.0007	0.009
7	1.2	0.476	5.801	1.083	0.0007	0.006
8	0.4	6.125	0.900	6.981	0.0010	2.986
9	0.5	3.920	1.206	5.210	0.0010	1.065
10	0.6	2.722	1.579	3.979	0.0010	0.431
11	0.9	1.210	3.272	1.920	0.0010	0.045
12	1.0	0.980	4.031	1.559	0.0010	0.024
13	1.1	0.810	4.875	1.289	0.0010	0.014
14	1.2	0.681	5.801	1.083	0.0010	0.008
15	0.4	18.375	0.900	6.981	0.0030	8.958
16	0.5	11.760	1.206	5.210	0.0030	3.194
17	0.6	8.167	1.579	3.979	0.0030	1.293
18	0.9	3.630	3.272	1.920	0.0030	0.134
19	1.0	2.940	4.031	1.559	0.0030	0.071
20	1.1	2.430	4.875	1.289	0.0030	0.040
21	1.2	2.042	5.801	1.083	0.0030	0.024
22	0.4	30.625	0.900	6.981	0.0050	14.930
23	0.5	19.600	1.206	5.210	0.0050	5.324
24	0.6	13.611	1.579	3.979	0.0050	2.155
25	0.9	6.049	3.272	1.920	0.0050	0.223
26	1.0	4.900	4.031	1.559	0.0050	0.119
27	1.1	4.050	4.875	1.289	0.0050	0.067
28	1.2	3.403	5.801	1.083	0.0050	0.040

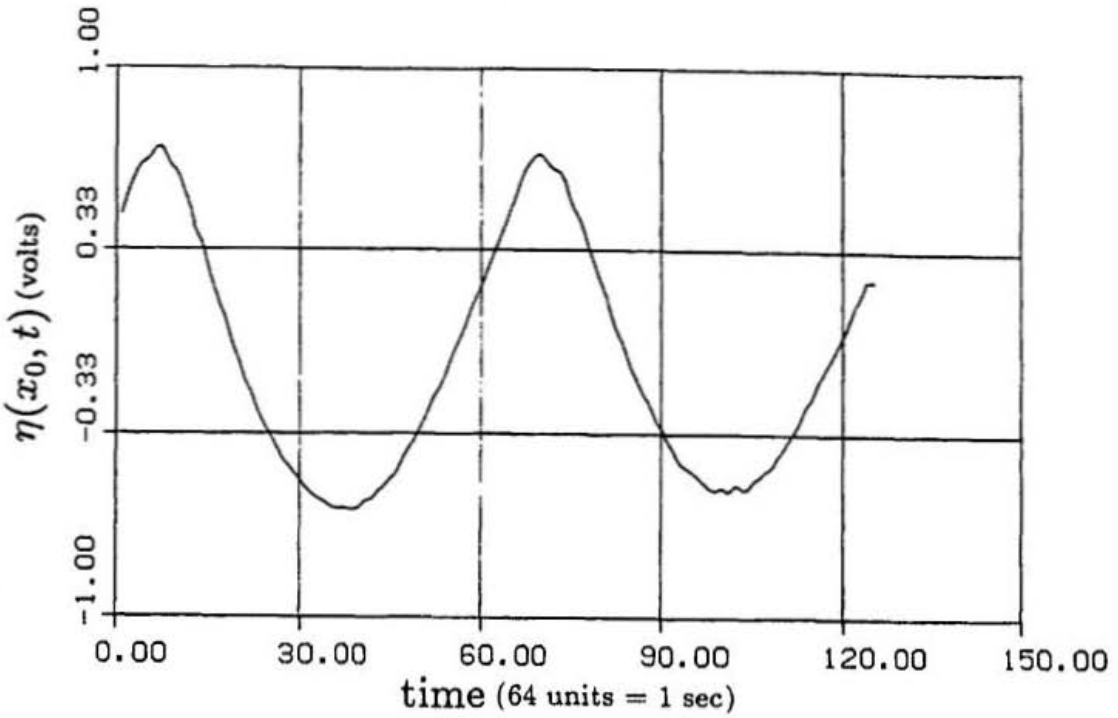

Figure 5.1 Sample wave form graphs: f = 1.0Hz, $H/gT^2 = 0.001$; Location zero (20m away from the wave board mean position).

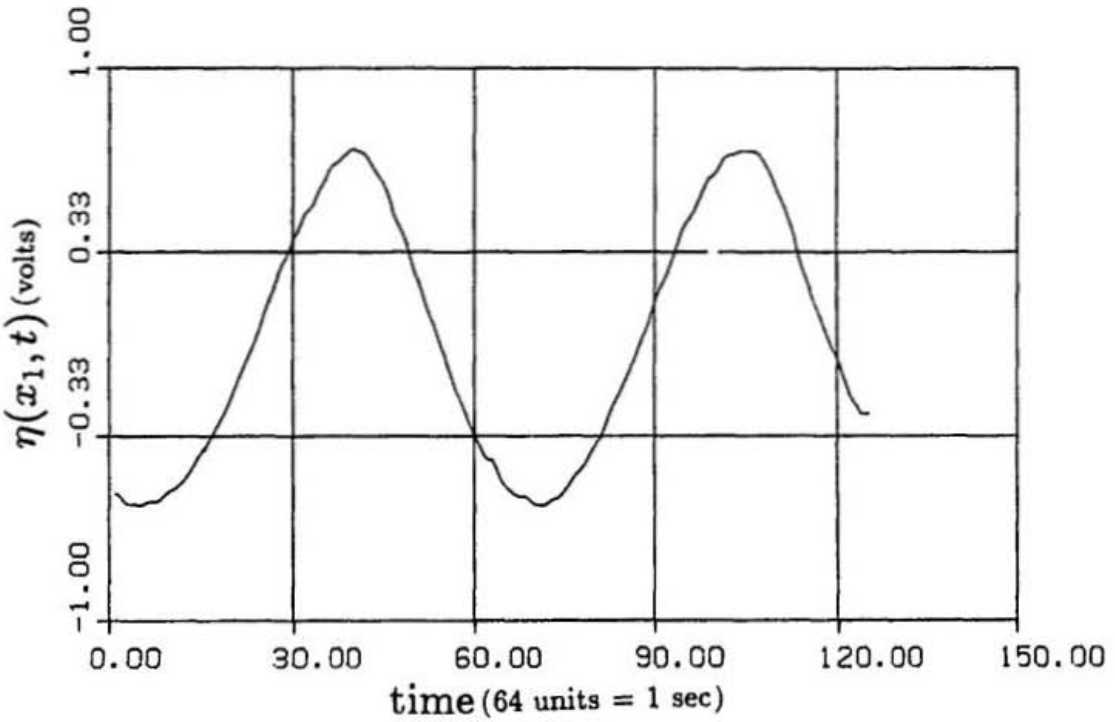

Figure 5.2 Sample wave form graphs: f = 1.0Hz, $H/gT^2 = 0.001$; Location one (0.2m from location zero).

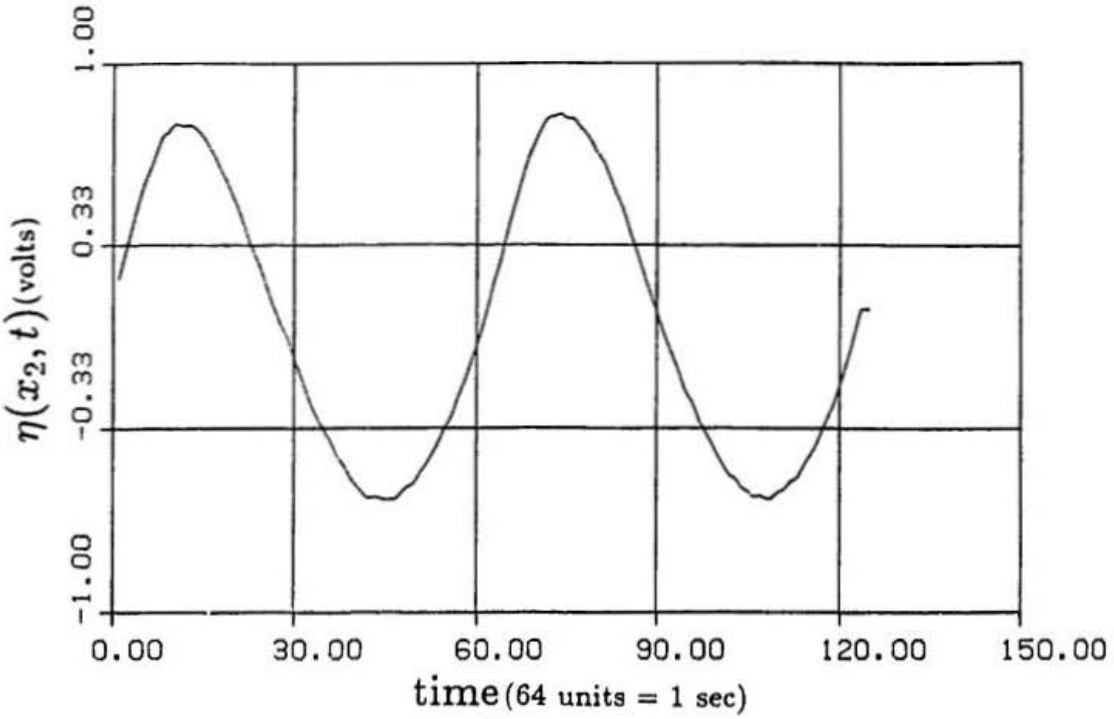

Figure 5.3 Sample wave form graphs: f = 1.0Hz, $H/gT^2 = 0.001$; Location two (0.4m from location zero).

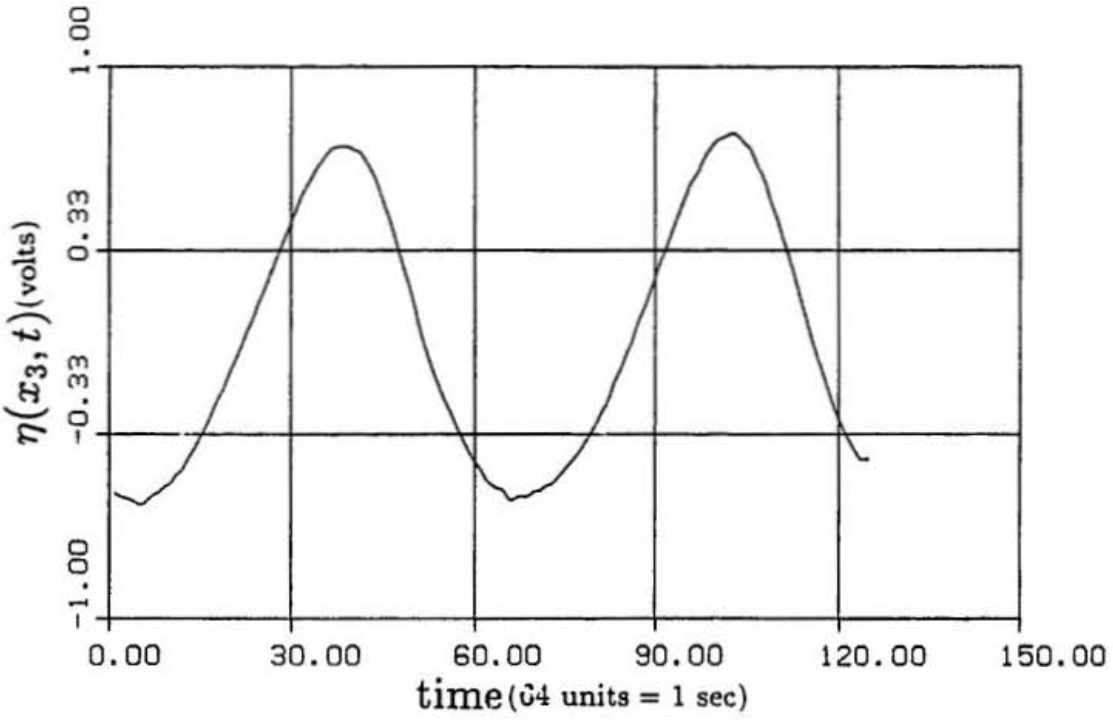

Figure 5.4 Sample wave form graphs: f = 1.0Hz, $H/gT^2 = 0.001$; Location three (0.6m from location zero).

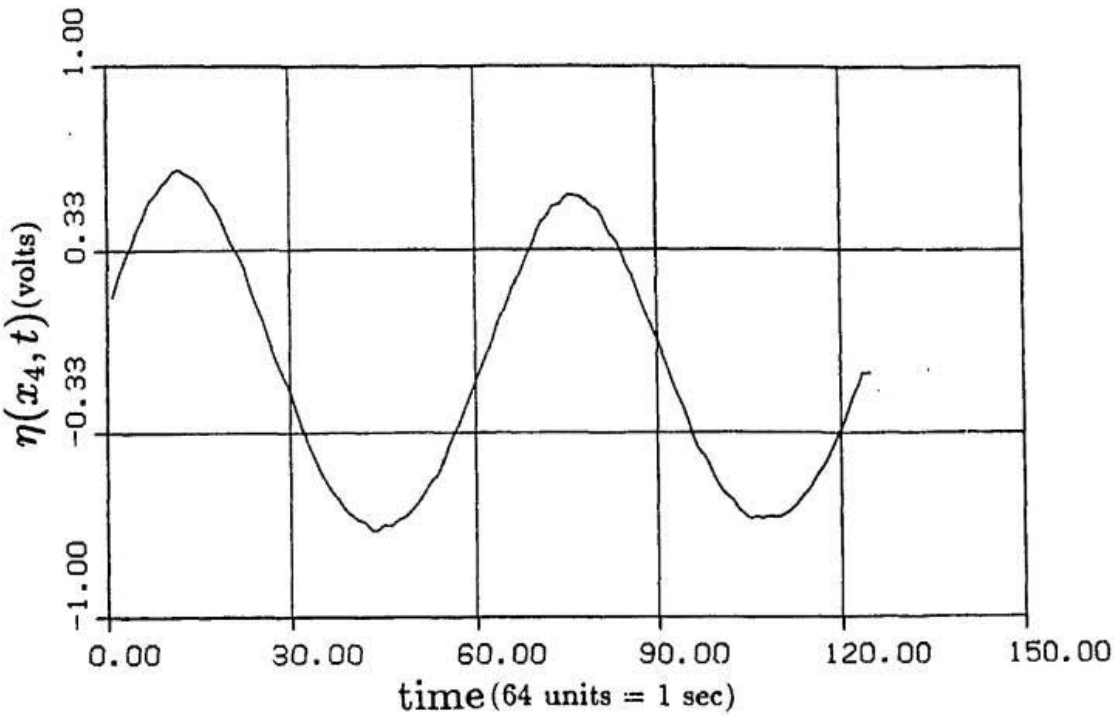

Figure 5.5 Sample wave form graphs: f = 1.0Hz, $H/gT^2 = 0.001$; Location four (0.8m from location zero).

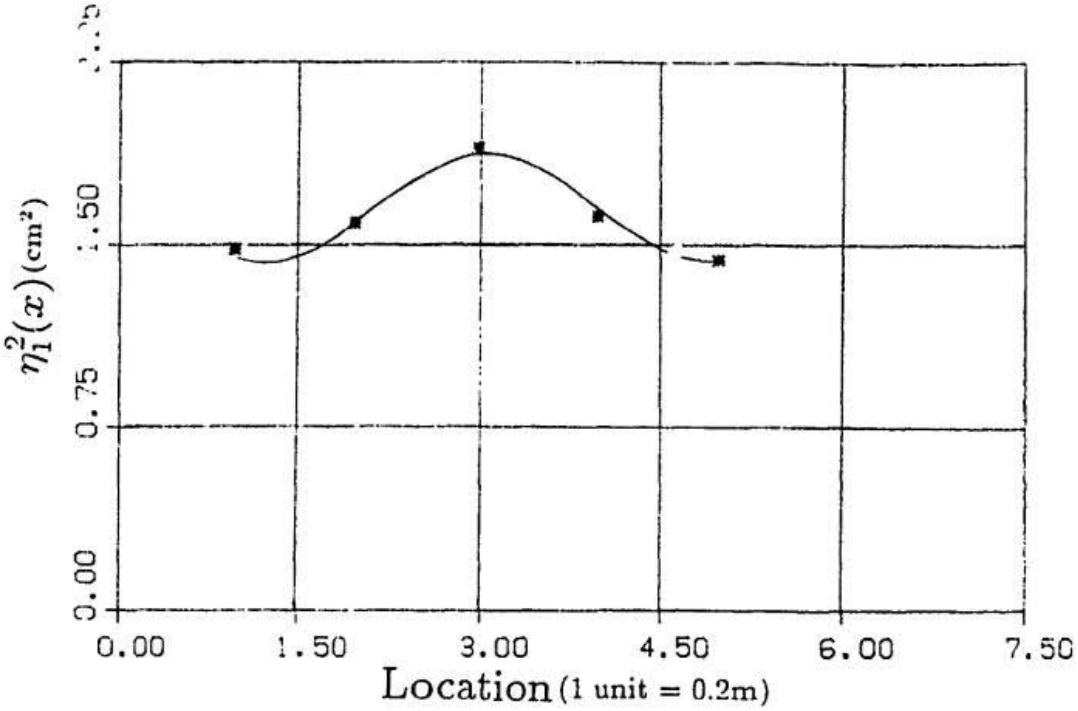

Figure 5.6 First order amplitude fit: f = 1.0Hz, $H/gT^2 = 0.001$.
—— eq (3.35) * ANALYS results

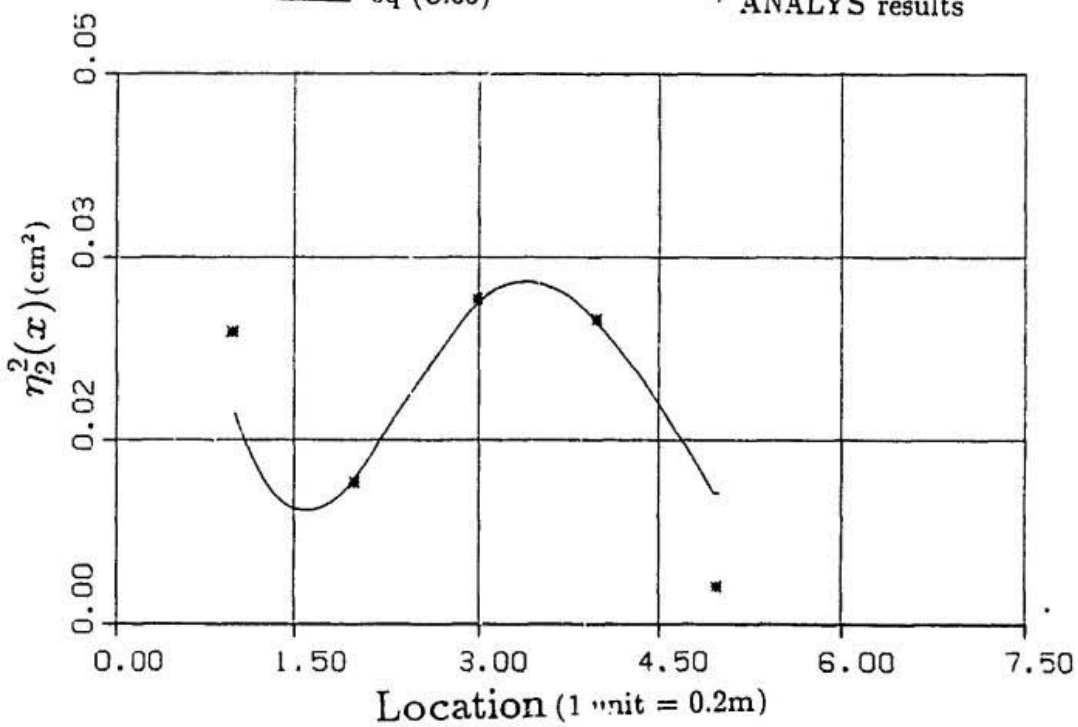

Figure 5.7 Second order amplitude fit: f = 1.0Hz. $H/gT^2 = 0.001$.
—— eq (3.36) * ANALYS results

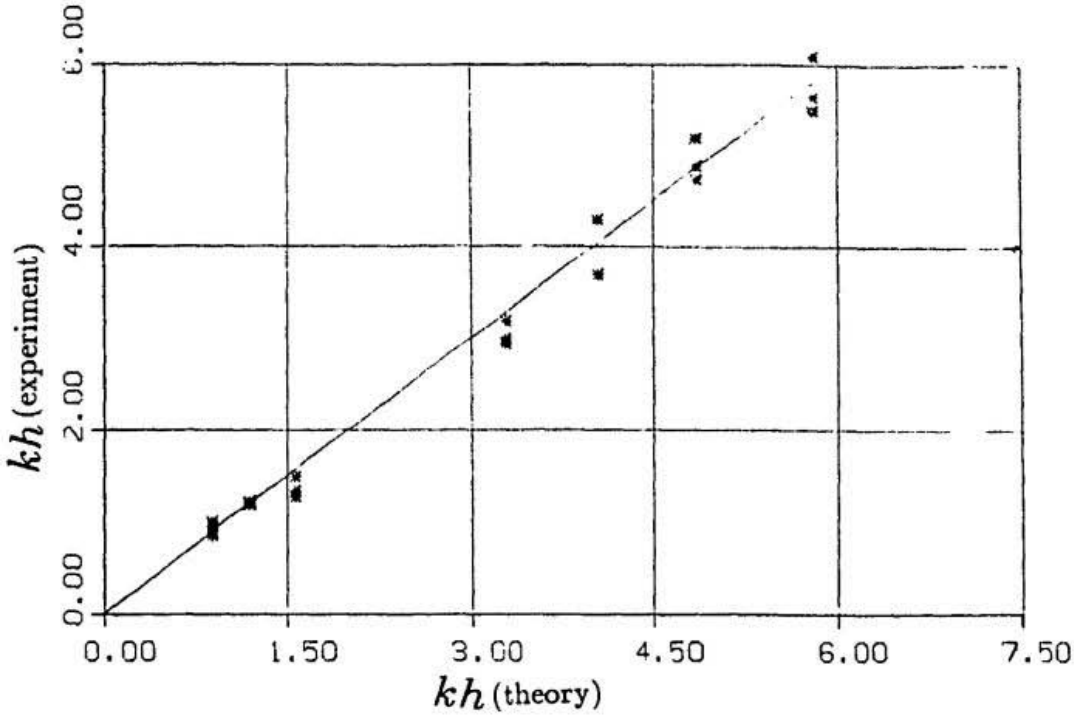

Figure 5.8 Relative depth: theory vs experiment.
—— Linear theory * experimental values

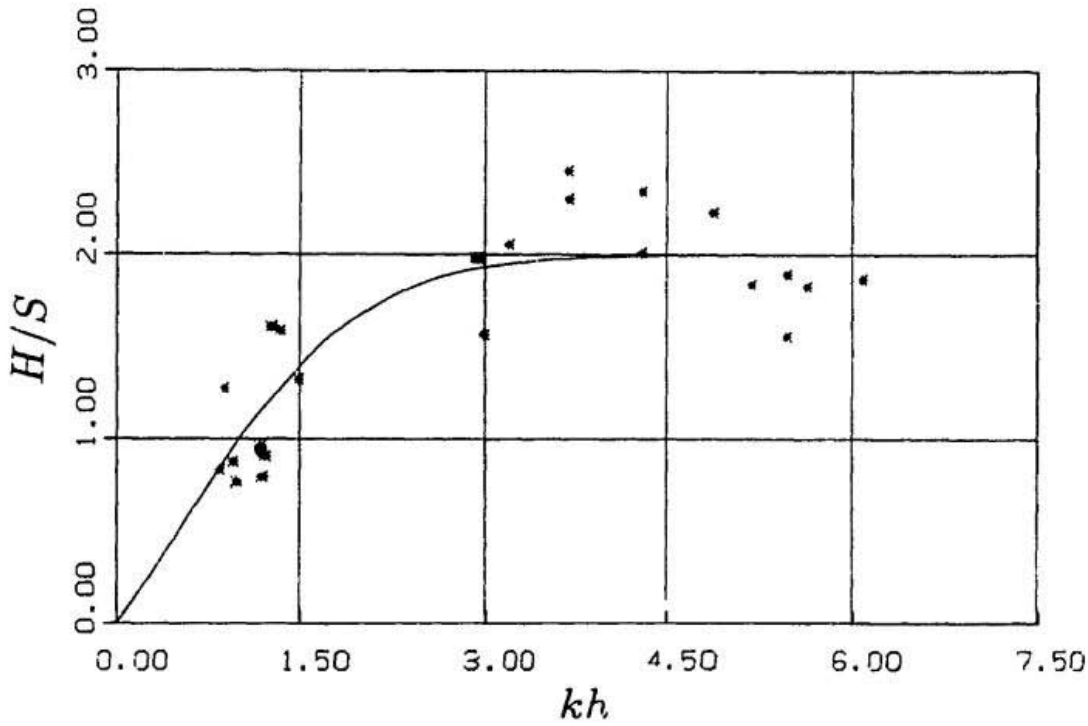

Figure 5.9 Wave maker amplitude ratio vs kh.
—— zero error line * experimental values

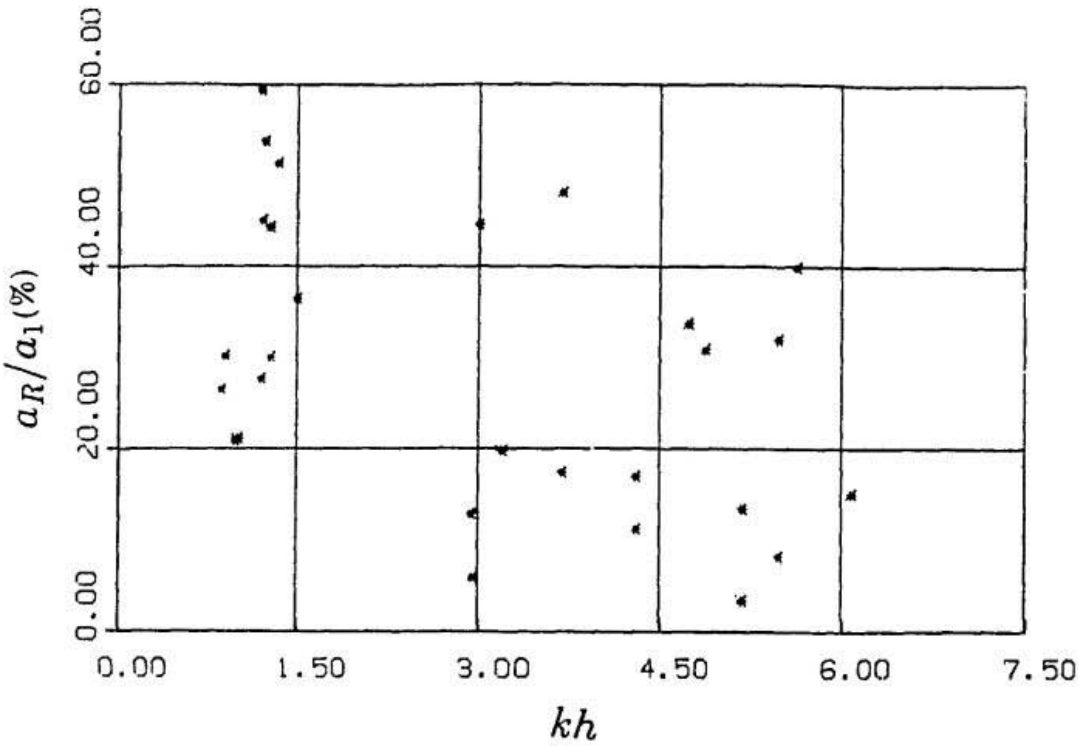

Figure 5.10 First order reflection coefficient vs kh.

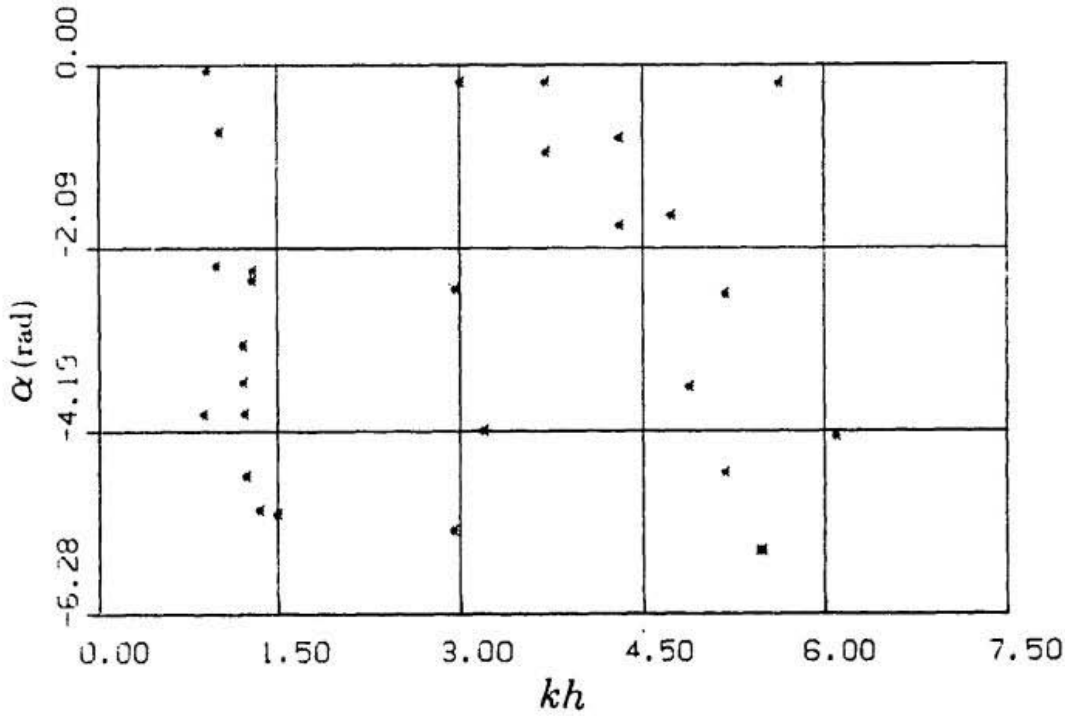

Figure 5.11 First order reflected wave phase angle vs kh.

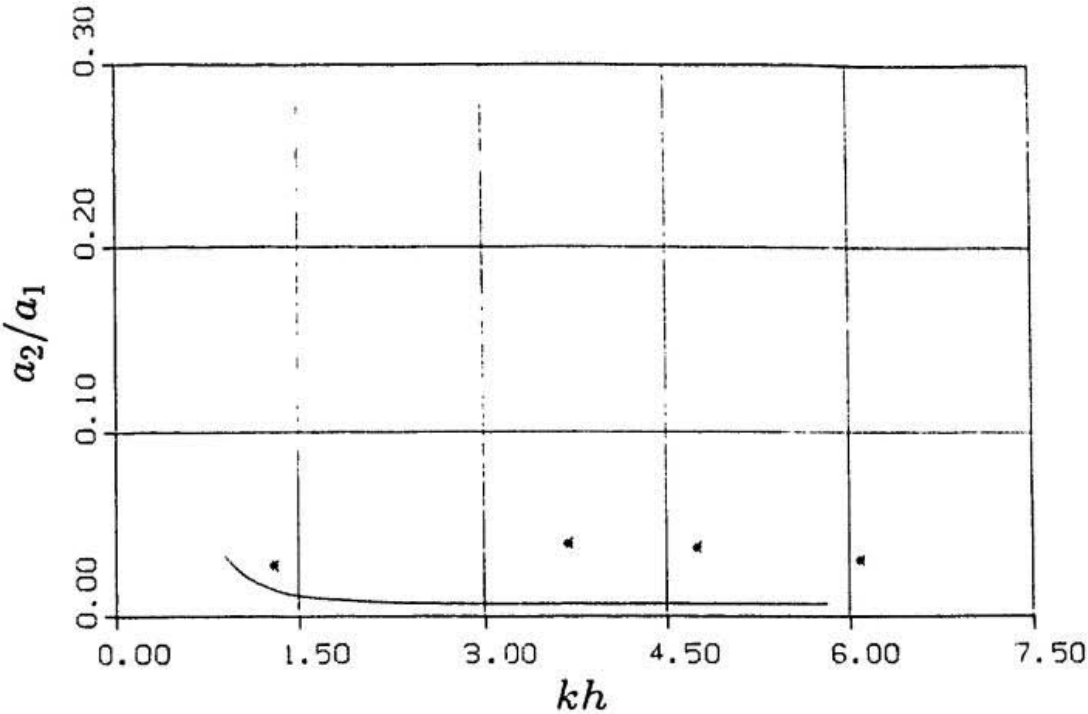

Figure 5.12 Stokes amplitude ratio vs kh; H/gT^2=0.0007.
——— Second order Stokes theory
* experimental values

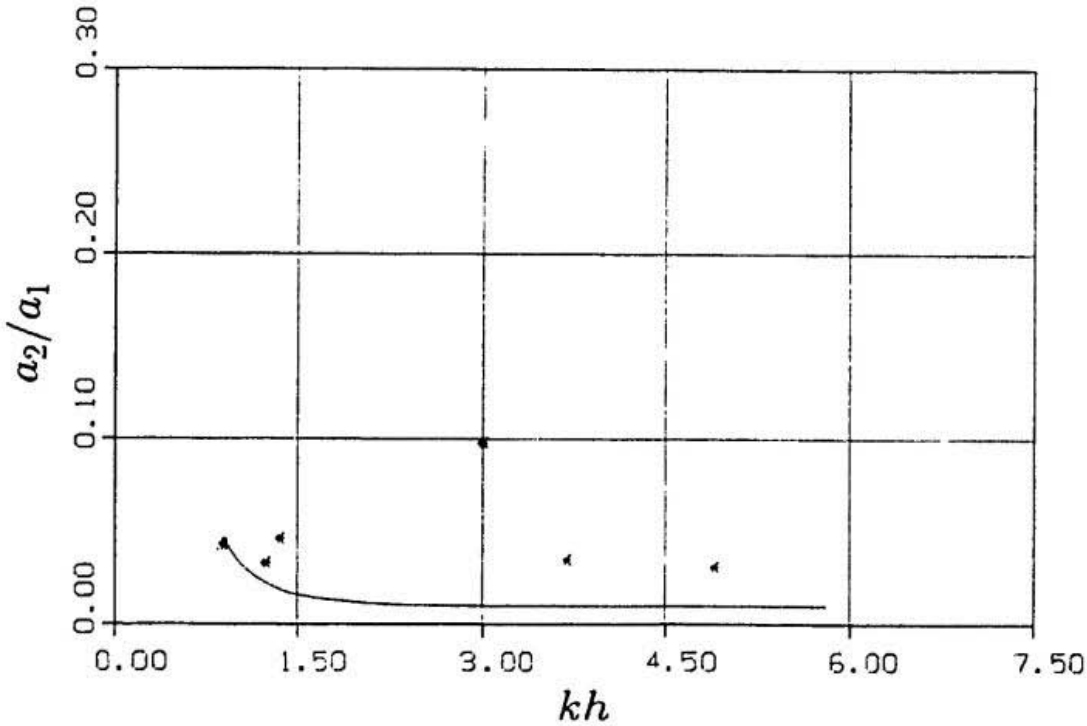

Figure 5.13 Stokes amplitude ratio vs kh; H/gT^2=0.001.
——— Second order Stokes theory
* experimental values

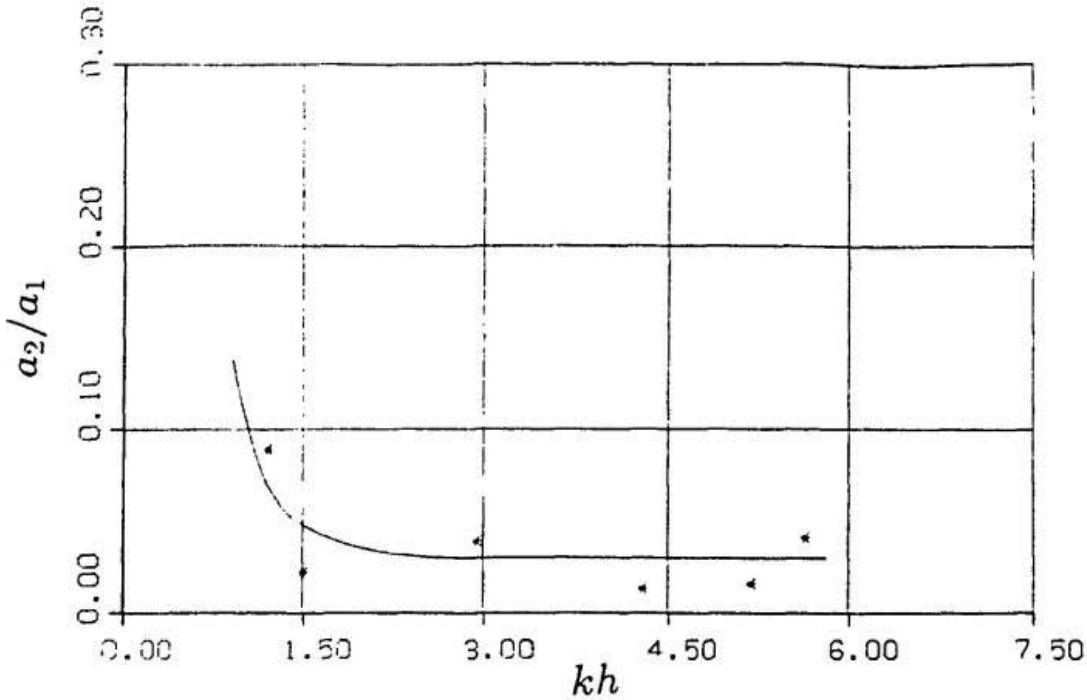

Figure 5.14 Stokes amplitude ratio vs kh; H/gT^2=0.003.

—— Second order Stokes theory

* experimental values

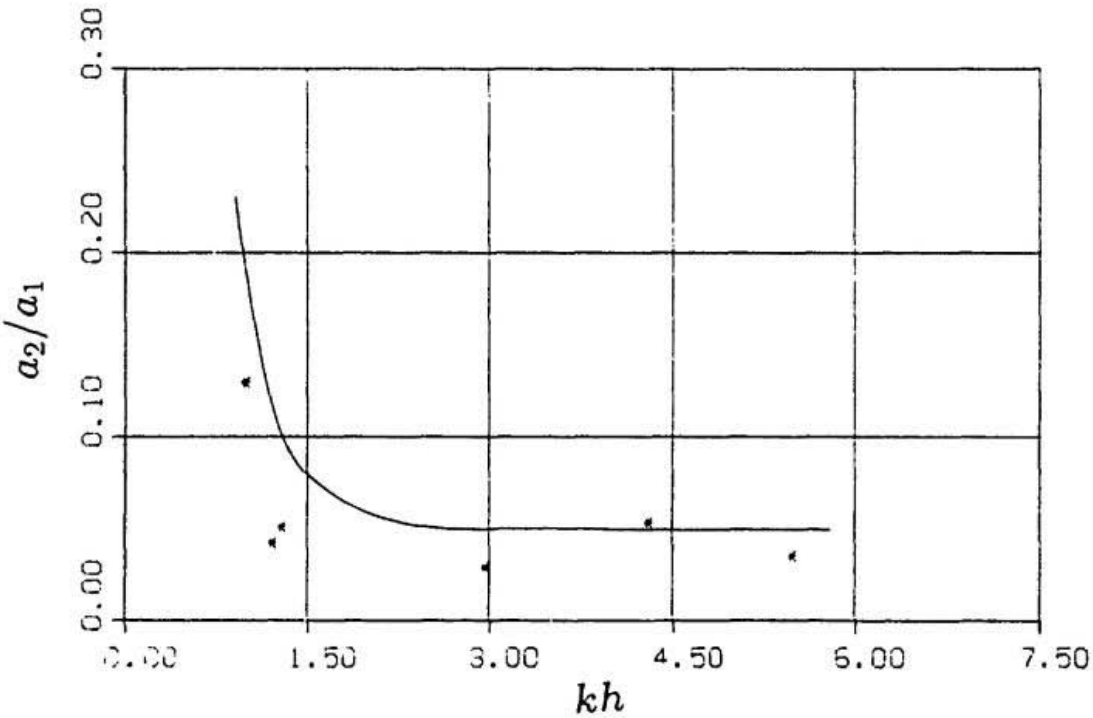

Figure 5.15 Stokes amplitude ratio vs kh; H/gT^2=0.005.

—— Second order Stokes theory

* experimental values

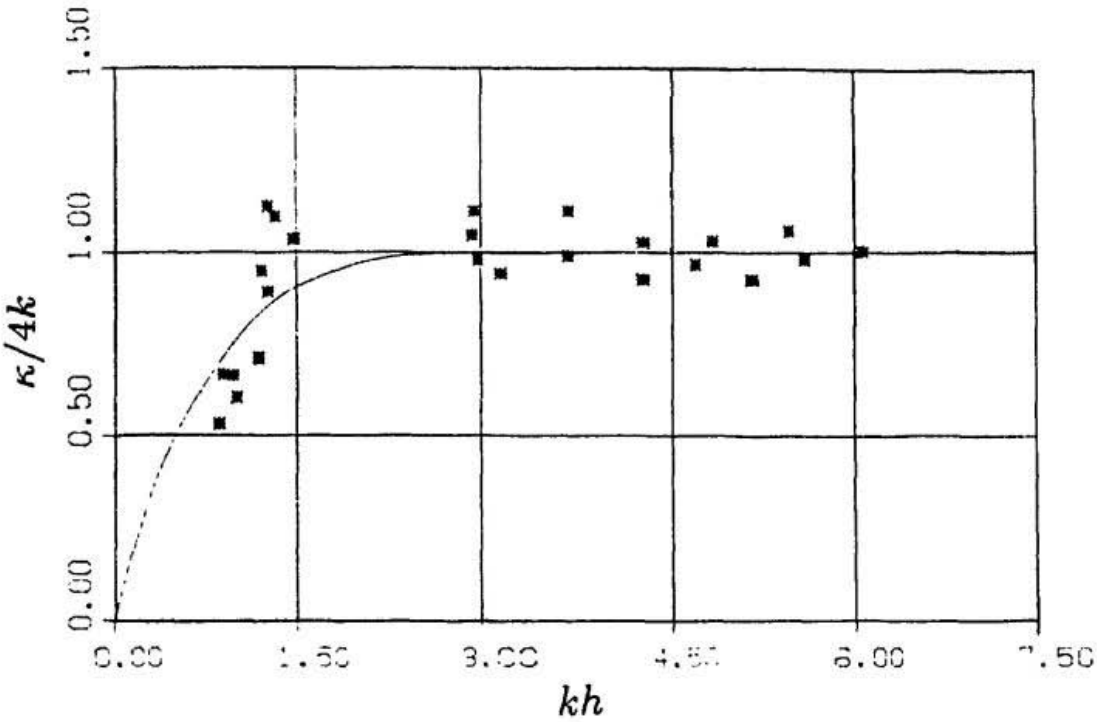

Figure 5.16 Free wave number ratio vs kh.

—— Second order theory

* experimental values

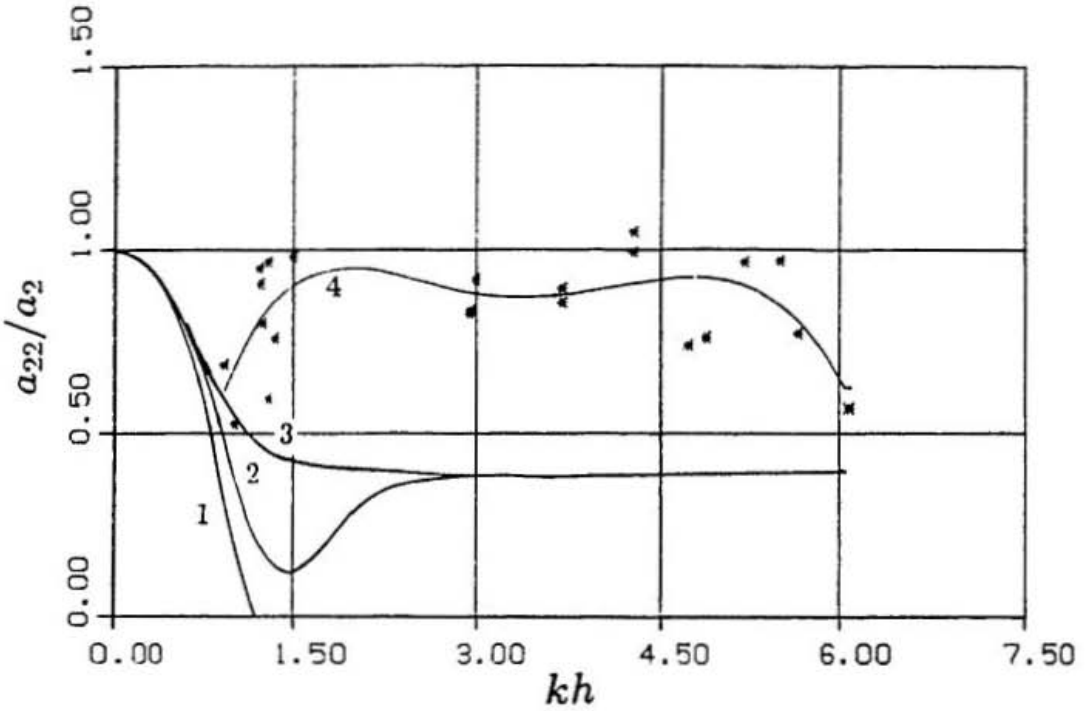

Figure 5.17 Free wave amplitude ratio vs kh.

1 Madsen (1970)

2 Daugaard (1972)

3 Fontanet (1961)

4 Fifth degree polynomial least square fit

• Experimental points

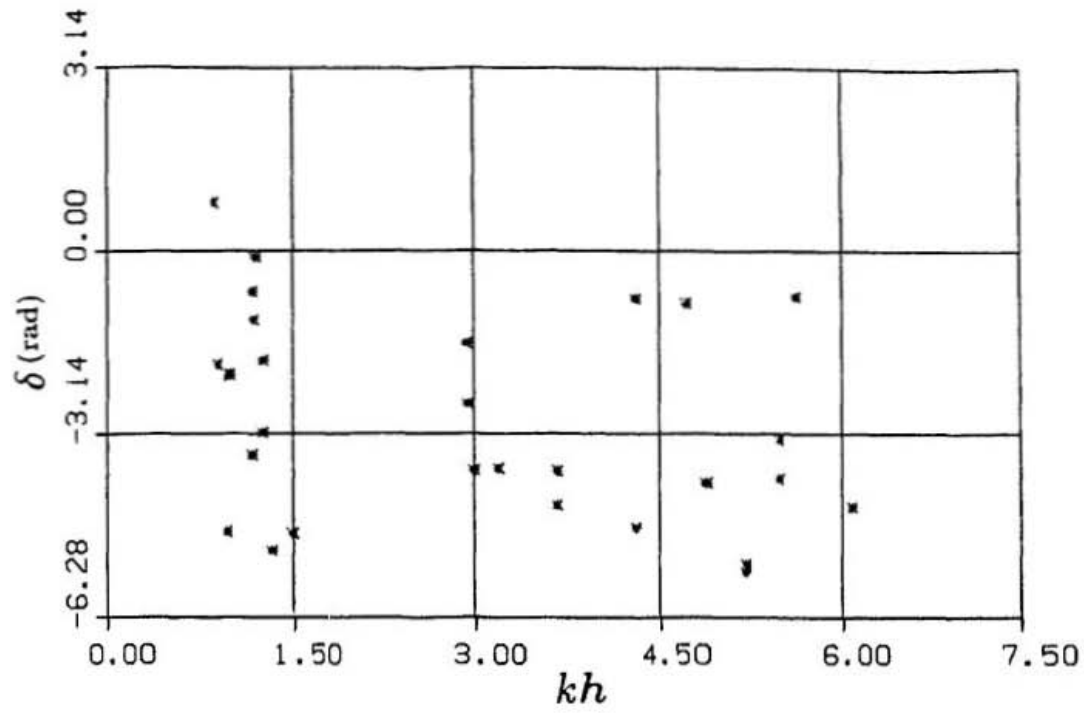

Figure 5.18 Free wave phase angle vs kh.

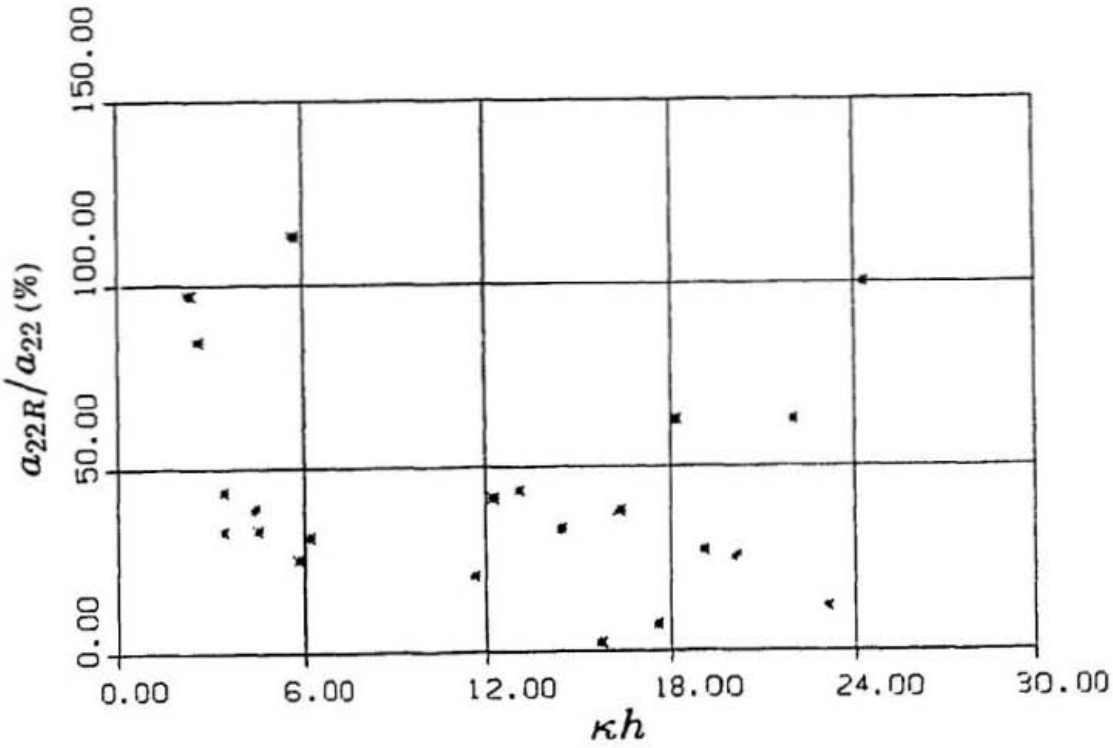

Figure 5.19 Second order reflection coefficient vs κh.

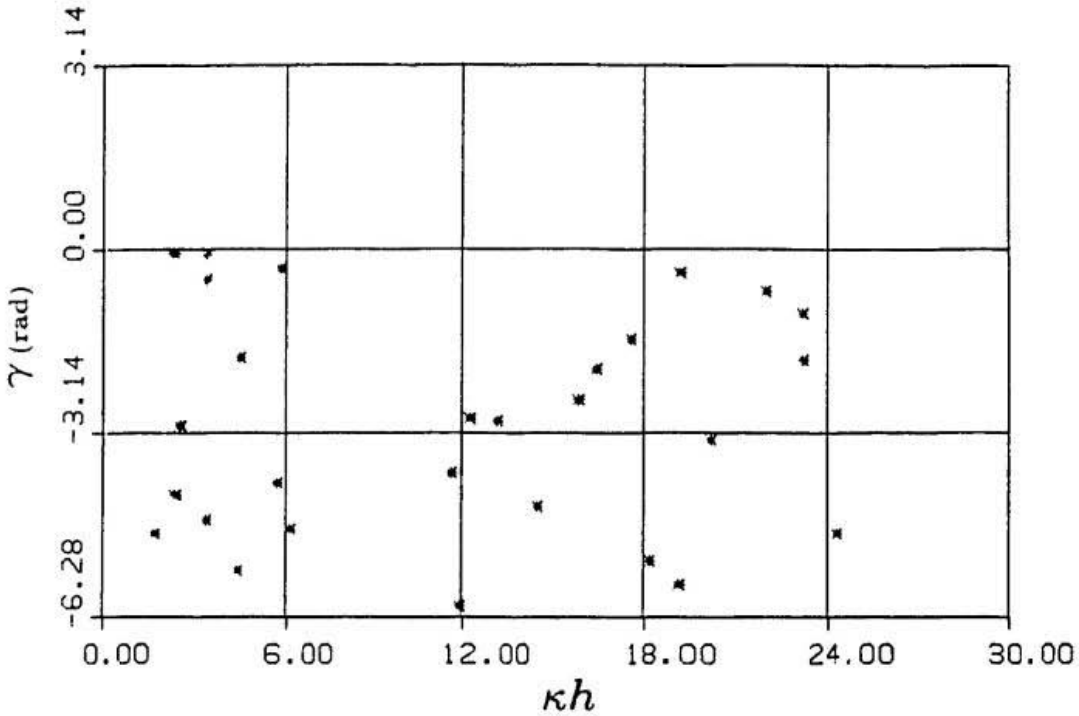

Figure 5.20 Second order reflected wave phase angle vs κh.

Part II

Wave Forces: Theoretical Formulation and Experiments

Chapter 6

Background and Literature Review

Estimation of hydrodynamic loading on vertical cylinders had for long been accomplished using Morison's equation, which was proposed by Morison et al (1950). This equation is composed of two parts inertia and drag and, each component contains an unknown coefficient, C_m and C_d the inertia and drag coefficients respectively. Efforts to evaluate these coefficients in the laboratory have shown a wide scatter in data and conclusions are varied among researchers. (Sarpkaya and Isaacson, 1981; Wiegel, 1964). Further developments on this equation were also attempted. Vugts (1979) has broadly reviewed formulations of wave forces and possible interactions with a structure's response. With a view that linear formulations more often satisfy engineering requirements Vugts (1979) has emphasized on the usefulness of the probabilistic and spectral techniques. In nonlinear problems where the maximum force is to be estimated, use of a higher order theory would

be sufficient. If an actual sea state is to be formulated non-linearly, Vugts (1979) indicated the importance of a systematic, consistent and formal description of the problem. Sarpkaya and Isaacson (1981, section 3.8.3) have reviewed experimental studies on the hydrodynamic coefficients and their parametric dependency on the Keulegan - Carpenter number (KC) and Reynold's number (Re) (chapter 9 of this thesis gives the definition of these numbers). The authors have mentioned the significance of Sarpkaya's parameter β (chapter 9) in interpreting data. They have also refined and presented the results of Sarpkaya obtained previously from experiments done with smooth and roughened cylinders in a U - shaped vertical water tunnel. These results showed that C_m increased with KC beyond 15 for all β. A reverse trend was noted for C_d.

Lighthill (1979, 1986) had set out to describe current techniques for estimating wave loading on offshore structures. While outlining the energy and momentum approaches to Morison's equation, the author was skeptical about fitting all wave loading results within the framework of Morison's equation. Significant second order potential flow forces were the quadratic force associated with the nonlinear free surface condition, the dynamic pressure force and the waterline force, both resulting from the linear potential. Lighthill (1979) also showed that it was possible to evaluate all these terms from the computed solutions to the linear problem.

Chakrabarti et al (1976) have conducted force experiments on a 3.0 in.

cylinder placed vertically in small amplitude waves of periods between 1.0 - 3.5 sec at a constant water depth of 3.0 m. His results showed that at low KC, C_m was of the order of 3.5. Wide scatter in C_d was attributed to the smallness of the drag term in the total force. Further experiments were done on 1.5 in. and 3.0 in. diameter cylinders by Chakrabarti (1980a) for a KC range of 0.0 - 85.0. The coefficients were computed from Morison's equation using Stream function theory to represent water particle kinematics. These experiments showed that for low KC, C_m was high, assuming values upto 2.5. For KC in the range of 10.0 to 70.0, C_M remained in between 1.0 - 1.5 decreasing gradually beyond $KC = 70.0$. C_d was found to be as low as 0.2 at $KC = 0.0$, increasing and taking a maximum of 1.75 at KC approximately equal to 10.0 and remaining around 1.5 beyond that. Chen (1978) had done wave force experiments at the MUN wave tank facility on a 6 in. bottom fixed cylinder in wave conditions $0.059 < h/\lambda < 0.6977$ and $0.0012 < H/\lambda < 0.1$. Two strain gage bridges were used to estimate the longitudinal and transverse overturning moments on the cylinder. The estimated values of C_m varied from 0.675 to 1.22 and values of C_d varied from 0.307 to 7.118 for a KC range of 0.69 to 11.83.

The work of Lighthill (1979) had been used by many researchers in their analysis. Demirbilek and Gaston (1985) have used Lighthill's approach to modify the linear diffraction theory and Morison's equation to include second order forces. Their formulation showed better correlation

with previously established data than linear diffraction theory. Ellix (1984) had proposed a second order wave force formulation for a vertical slender cylinder in a laboratory environment. He included forces due to the second order Stokes wave, convective acceleration, waterline and dynamic pressures and also due to reflected waves from the beach and free waves generated by the wave maker. His experiments were conducted in a 20.0 m long, 0.75 m wide tank at a constant water depth of 0.5 m. The wave amplitudes varied between 15 - 40 mm. Results for C_m and C_d were in general agreement with the results of Sarpkaya (Sarpkaya and Isaacson, 1981 section 3.8.3) and Chakrabarti (1980a). Scatter in C_m data was explained as due to its dependence on Re. For second order forces, results were heavily scattered and no explanations were possible. Use of equivalent coefficients also showed heavy scatter. Results were found to be better in cases where free wave activity was low. Ellix and Arumugam (1985) have used the data of Ellix (1984) and have attempted to quantitatively analyse the so - called Lighthill forces. Results for inertia forces showed considerable scatter which was explained as due to free wave. The drag force results were even more scattered which was possibly due to inertia dominated loading.

Other second order force formulations have also been reported. Isaacson (1979) has arrived at a second order equation for the inertia force acting on a body in an unsteady non - uniform flow of an inviscid fluid. The forces thus calculated were smaller than those obtained by the linear approach. The

author has introduced a second order inertia force function for comparison of various approaches. Madsen (1986) had arrived at a different result for the same problem where the forces estimated were greater than the linear force. These two approaches are discussed in chapter 7 of this thesis.

Diffraction forces are generally considered negligible as far as slender cylinders are concerned. The linear diffraction theory by MacCamy and Fuchs (1954) had been used to estimate the forces on a cylinder of diameter comparable to the wave length of the incident wave. Hunt and Baddour (1981) have included second order diffraction effects in their computation of maximum horizontal force on a vertical cylinder under a non linear progressive wave in deep water. Their results showed that for large cylinders, the maximum force would be greater than that predicted by linear theory. The force on a slender cylinder obtained as a limiting case also wa. higher than linear predictions. Eatock Taylor and Hung (1987) have attempted to provide a complete solution for second order diffraction forces on a vertical cylinder in regular waves. Their results showed the significance of the forces due to second order scattered potential and that the pressures due to this potential were significant compared to first order pressures. The quadratic forces similar to Lighthill (1979) have also been evaluated.

The above literature survey was focussed on obtaining insight into a complete second order force analysis. Available information was used to construct a suitable force formulation for a vertical surface piercing cylinder

for the present study. Experiments were then conducted on cylinders in wave environments in the following range:

$$0.0066 < \frac{D}{\lambda} < 0.0704$$

$$0.137 < \frac{h}{\lambda} < 0.971$$

$$0.0044 < \frac{H}{\lambda} < 0.04738$$

and the total force on the test cylinders were measured. The experimental results for first and second order were obtained from a fourier analysis. Results of first order were used to evaluate the hydrodynamic coefficients of the cylinders. At second order, the measured results were fitted into the formulated model and the efficiency of the model studied. Chapter 7 of this thesis presents the theoretical formulation adopted in the study. The experimental and analysis procedures are mentioned in chapter 8, to be followed by a chapter on results and conclusions.

Chapter 7

Theoretical development

Wave forces experienced by a vertical surface piercing circular cylinder are treated in this chapter. Herein considered is a flow of a real fluid. The cylinder is assumed to be slender so that diffraction effects are negligible and rigid so that hydroelastic effects are negligible. The representative diagram of the flow with chosen coordinate system and cylinder position is shown in Fig. (7.1).

7.1 Force equation in a real flow

A real fluid flow is theoretically treated as made of two components: *i*) irrotational flow and *ii*) vortex flow, (Lighthill, 1979). The irrotational flow satisfies the instantaneous boundary conditions of the flow and, the vortex flow has all the vorticity associated with the flow and satisfies no boundary conditions, Lighthill (1979). The force on a body placed in such a flow along the direction of the flow comprises of contributions from both components.

The irrotational flow forces in the direction of the flow can be analysed into two components, the Froude - Krylov force and the added mass force (see for eg. Dean and Dalrymple, 1984). The Froude - Krylov force is caused by the pressure gradient of $-\rho\partial u/\partial t$ required for the fluid to flow (in the absence of the cylinder). The added mass force is thought of as the rate of change of kinetic energy of the fluid retarded by the body. This is written as $M_a\partial u/\partial t$ where M_a is the so - called added mass of the body. The net force is usually given as:

$$C_m\rho V\cdot\frac{\partial u}{\partial t}$$

where $C_m = 1 + M_a/V$ and V is the immersed volume of the body.

Vorticity in real flows is created on the surface of a body due to the property of viscosity. As fluid flows around a body, a wake of growing length is formed behind the body. The kinetic energy per unit wake length manifests itself as the drag force on the body, (Lighthill 1979) and is given as

$$\frac{1}{2}\rho A u^2 C_d$$

where A is the frontal area of the body and C_d is an unknown drag coefficient.

Apart from the inline forces discussed above, a flow also causes a transverse force on a body, normal to the direction of flow. Details of this force can be obtained from Sarpkaya and Isaacson, (1981) and Lamb, (1932). In the following text, the term 'force' is assumed to represent only the inline forces and not the transverse force on a body.

Morison et al (1950) produced a formula based on the above principles for the inline force on a circular, rigid and vertical cylinder in two-dimensional waves. This force was made of two components, inertia and drag with two corresponding coefficients C_m and C_d. Their equation in differential form was given as:

$$\frac{\mathrm{d}f}{\mathrm{d}z} = C_m \rho \frac{\pi D^2}{4} \frac{\partial u}{\partial t} + C_d \rho \frac{D}{2} u|u| \tag{7.1}$$

where the force f was in the x-direction (the chosen direction of wave propagation) and D the diameter of the cylinder. The drag force was related to $u|u|$ to retain its directionality, parallel to u. The expression for the inertia force in Eq. (7.1) can be generalized in the case of a non uniform unsteady flow by replacing the local derivative of the velocity, $\partial u/\partial t$ with the total derivative, $\mathrm{D}u/\mathrm{D}t$ as:

$$\frac{\mathrm{d}f}{\mathrm{d}z} = C_m \rho \frac{\pi D^2}{4} \frac{\mathrm{D}u}{\mathrm{D}t} + C_d \rho \frac{D}{2} u|u| \tag{7.2}$$

where

$$\frac{\mathrm{D}u}{\mathrm{D}t} = \frac{\partial u}{\partial t} + u\frac{\partial u}{\partial x} + w\frac{\partial u}{\partial z}$$

The two nonlinear terms in $\mathrm{D}u/\mathrm{D}t$ are collectively called convective acceleration. The adopted generalization can be justified by the view that $\mathrm{D}u/\mathrm{D}t$ would be the acceleration experienced by the volume of the body if it were replaced by the fluid in a non-uniform unsteady flow, (Madsen 1986). Eq. (7.2) is also the commonly accepted form of Morison's equation (see for eg. Dean and Dalrymple, 1984).

The use of Eq. (7.1) to evaluate wave forces on cylinders under various wave conditions involves using appropriate wave theories for estimating the water particle kinematics and values for C_m and C_d from established data. For force evaluation upto higher orders, Morison's equation assumes that all nonlinearities with respect to the fluid velocity are associated with the drag force only. Recent studies (see for eg. Lighthill, 1979; 1986) have drawn attention on additional nonlinear terms arising as part of the irrotational flow force.

A second order wave force formulation for the present study was constructed based on the literature survey. The wave conditions in a wave tank have been considered in the formulation. It was decided that all force measurements during experiments would be conducted before reflection from the beach, as the length of the wave tank was sufficient to achieve this purpose. In the present context the wave field experienced by the test cylinder is assumed to be of the form (cf. 3.4)

$$\eta = a_1 \cos(kx - \omega t) + a_2 \cos 2(kx - \omega t) + a_{22} \cos(\kappa x - 2\omega t + \delta) \qquad (7.3)$$

The variables in Eq. (7.3) are defined in section 3.4 of this thesis.

Using Stokes second order theory to represent the water particle kinematics of the incident wave, we have the following expressions for the particle velocities u and w in the x and z - directions respectively and $\partial u/\partial t$

at the cylinder location x_0:

$$u = \frac{\omega H}{2}\frac{\cosh k(h+z)}{\sinh kh}\cos(kx_0-\omega t)+\frac{3}{16}\frac{\omega H^2 k\cosh 2k(h+z)}{\sinh^4 kh}\cos 2(kx_0-\omega t) \tag{7.4}$$

$$w = \frac{\omega H}{2}\frac{\sinh k(h+z)}{\sinh kh}\sin(kx_0-\omega t)+\frac{3}{16}\frac{\omega H^2 k\sinh 2k(h+z)}{\sinh^4 kh}\sin 2(kx_0-\omega t) \tag{7.5}$$

$$\frac{\partial u}{\partial t} = \frac{gkH}{2}\frac{\cosh k(h+z)}{\cosh kh}\sin(kx_0-\omega t)+\frac{3}{4}\frac{gk^2H^2\sinh 2k(h+z)}{\sinh 2kh\sinh^2 kh}\sin 2(kx_0-\omega t) \tag{7.6}$$

The water particle kinematics associated with the free wave are:

$$u_{\text{free}} = 2\omega a_{22}\frac{\cosh\kappa(h+z)}{\sinh\kappa h}\cos(\kappa x_0 - 2\omega t+\delta) \tag{7.7}$$

$$\left(\frac{\partial u}{\partial t}\right)_{\text{free}} = g\kappa a_{22}\frac{\cosh\kappa(h+z)}{\cosh\kappa h}\cos(\kappa x_0 - 2\omega t+\delta) \tag{7.8}$$

7.2 Inertia forces on a cylinder

The inertia force on a vertical, surface piercing, rigid, slender, circular cylinder is found by integrating the elementary inertia force given by Eq. (7.2), over the entire immersed length of the cylinder. This integral is split into two parts, with limits from $-h$ to 0 and 0 to η respectively as

$$\int_{-h}^{\eta} \mathrm{d}f_i = \int_{-h}^{0} \mathrm{d}f_i + \int_{0}^{\eta} \mathrm{d}f_i \tag{7.9}$$

The second integral gives rise to the so-called waterline force, Lighthill (1979). This force has been shown by Lighthill (1979) to be the resultant of the forces due to transient and hydrostatic pressures acting on the cylinder

length from 0 to η. Evaluation of this force can be approximated as (Ellix, 1984)

$$\int_0^\eta \mathrm{d}f_i \simeq \eta \frac{\mathrm{d}f_i}{\mathrm{d}z}|_{z=0} \tag{7.10}$$

where $\eta = H/2\cos(kx_0 - \omega t)$ for second order evaluation. Consistent upto the second order, the waterline and convective acceleration forces will be evaluated using linear expressions of the water particle kinematics, the first terms of Eqs. (7.4) - (7.6).

Contributions to the inertia force due to the incident wave are:

1. First order force due to the linear part of $\partial u/\partial t$, the first term in Eq. (7.6)

2. Second order force due to the second order part of $\partial u/\partial t$, the second term of Eq. (7.6)

3. Convective acceleration force of second order using linear expressions for the water particle kinematics, first terms of Eqs. (7.4) and (7.5)

4. Waterline force of second order using linear expressions for u and η.

Since scattering of the wave by the cylinder is neglected, no diffraction forces are included. If the above calculations are performed, the inertia force on the cylinder due to the Stokes wave can be obtained as:

$$F_i = C_m\rho\frac{\pi D^2}{4}\left[\frac{\omega^2 H}{2k}\sin(kx_0-\omega t)\right.$$

$$+\frac{3}{4}\frac{gkH^2}{(\cosh 2kh-1)}\sin 2(kx_0-\omega t)$$

$$-\frac{\omega^2 H^2 kh}{8\sinh^2 kh}\sin 2(kx_0-\omega t)$$

$$\left.+\frac{gH^2k}{8}\sin 2(kx_0-\omega t)\right] \qquad (7.11)$$

The terms of Eq. (7.11) correspond to the four contributions mentioned previously.

The free wave present in the tank would cause an additional inertia force on the cylinder at its frequency 2ω. The force due to the free wave is given as:

$$F_{i\,free} = C_m\rho\frac{\pi D^2}{4}\frac{\omega^2 a_{22}}{\kappa}\cos((\kappa-2k)x_0+\delta)\sin 2(kx_0-\omega t) \qquad (7.12)$$

Thus the first order inertial loading is assumed solely due to the incident wave while the second order inertial loading considered here consists of contributions from the incident wave, waterline effects, convective accelerations and the free wave. The second order inertia force formulation presented by Ellix (1984) included apart from the terms discussed above, a force due to the dynamic pressure term in the unsteady Bernoulli's equation, (Ellix, 1984; sec 3.3.2 and 3.3.4). It was felt by the present author that

the dynamic pressure force is inherently present in the generalised Morison's equation and gives rise to the convective acceleration terms in the equation. Hence adding the dynamic pressure force to the force predicted by the generalised Morison's equation (7.2) would lead to a redundancy in the formulation. [1]

A different formulation of the inertia force neglecting diffraction effects upto second order has been presented by Isaacson (1979). The author has used G.I.Taylor's results for the force on a body in steady, non uniform flow coupled with the force due to an unsteady , non-uniform flow in the absence of the body. The equation for the inertia force on a cylinder in the x-direction has been obtained as:

$$\frac{\mathrm{d}f_i}{\mathrm{d}z} = \rho\frac{\pi D^2}{4}\frac{\mathrm{D}u}{\mathrm{D}t} + m_{11}\left(\frac{\partial u}{\partial t} + u\frac{\partial u}{\partial x}\right) + m_{22}v\frac{\partial v}{\partial x} + m_{33}w\frac{\partial w}{\partial x} \qquad (7.13)$$

Isaacson (1979) has mentioned that for a vertical cylinder, the added masses in the x and y directions, m_{11} and m_{22} assume a value $\rho\pi D^2/4$ whereas the vertical added mass, m_{33} was given a value zero thus obtaining the result,

$$\frac{\mathrm{d}f_i}{\mathrm{d}z} = \rho\frac{\pi D^2}{4}2\left(\frac{\partial u}{\partial t} + u\frac{\partial u}{\partial x} + \frac{w}{2}\frac{\partial w}{\partial x}\right) \qquad (7.14)$$

While this result differs with the generalized form of the Morison's equation, it can be seen that if the author had adopted an assumption inherent in

[1] In the derivation of the unsteady Bernoulli's equation from the Navier - Stokes equation, the dynamic pressure component $\nabla\phi^2/2$ can be seen to arise from the convective acceleration terms of the total acceleration of the fluid, see for eg. Lamb (1932). The reverse is assumed here that the dynamic pressure is integrated over the cylinder surface to obtain the convective acceleration terms of Eq. (7.2).

the generalised Morison's equation, that the added masses in both in line and vertical directions were equal to $\rho\pi D^2/4$, his result would be identical to the latter.

Madsen (1986) has proposed yet another formulation. He has obtained an approximate solution by formulating the force as a series expansion in the parameter $kD/2$ and the velocity potential split into two parts, one solely due to the undisturbed flow and the other due to the flow perturbation caused by the body. Free surface diffraction effects have been neglected. The result obtained by Madsen for the case of a two - dimensional flow with negligible body velocities and a theoretical value of 2 for C_m was:

$$\frac{\mathrm{d}f_i}{\mathrm{d}z} = \rho\frac{\pi D^2}{4}2\left(\frac{\partial u}{\partial t} + \frac{u}{2}\frac{\partial u}{\partial x} + w\frac{\partial u}{\partial z}\right) \tag{7.15}$$

where all derivatives were evaluated at the cylinder axis.

Isaacson (1979) has introduced a second order inertia force function in the inertia force equation to compare various approaches. This function appropriate to the present study is implicitly given by $f(kh)$ in:

$$F_{2i} = (\rho g H D^2)\frac{\pi}{4}\tanh kh(kH)f(kh)\sin 2(kx_0 - \omega t) \tag{7.16}$$

where F_{2i} is the total second order inertia force. The function $f(kh)$ formulated for various approaches is given in Table 7.1 where C_m has to be estimated. When $C_m = 2$ the formulations (2) and (3) reduce to the formulas given by Isaacson (1979) and Madsen (1986) respectively.

7.3 Drag forces on a cylinder

The drag force on a vertical surface piercing cylinder is evaluated by integrating the elementary drag force given by Eq. (7.2) over the entire length of the cylinder. This integration, similar to the inertia force can be split into two parts, one with limits from $-h$ to 0 and 0 to η. The second integral gives rise to the waterline component of the drag force. The first integral would be simpler to evaluate, if the $u|u|$ term is split into harmonic components. This can be accomplished using fourier analysis for the case $u_2 << u_1$ where

$$u = u_1 \cos\theta + u_2 \cos 2\theta$$

IF θ has a periodicity of 2π, then

$$u|u| = \left(\frac{2.667}{\pi}u_1^2 + \frac{3.349}{\pi}u_2^2\right)\cos\theta + \frac{4.461}{\pi}u_1 u_2 \cos 2\theta \qquad (7.17)$$

The algebraic details are presented in Appendix D of this thesis. It can be seen that the second order amplitude of the velocity contributes to the first order term of $u|u|$. The relative magnitude of the u_2^2 term increases with increasing steepness. Apart from a precise harmonisation of the $u|u|$ expression, inclusion of this term is also consistent with a second order formulation. The left and right hand sides of Eq. (7.17) are plotted in Figs. (D.2) and (D.3) in Appendix D. The significance of the u_2^2 term in the first order is that this also leads to a reduction in the drag coefficient.

If the velocity is represented using Stokes theory, then u_1 and u_2 would

be the amplitudes of the $\cos(kx_0 - \omega t)$ and $\cos 2(kx_0 - \omega t)$ respectively in Eq. (7.4). If a free wave is present, the second order particle velocity in the combined wave field will have an amplitude

$$u_2 = \frac{3}{16}\omega H^2 k \frac{\cosh 2k(h+z)}{\sinh^4 kh} + 2a_{22}\omega \frac{\cosh \kappa(h+z)}{\sinh \kappa h} \cos((\kappa - 2k)x_0 + \delta) \tag{7.18}$$

where u_2 would again be the amplitude associated with $\cos 2(kx_0 - \omega t)$. It can be seen that $\cos((\kappa - 2k)x_0 + \delta)$ in the equation arises due to the approximate conversion of $\cos(\kappa x_0 - 2\omega t + \delta)$ to $\cos 2(kx_0 - \omega t)$.

Integration of the drag force may now be performed. The components of the drag force are:

1. At frequency ω, due to the $\cos\theta$ term in Eq. (7.17)

2. At frequency 2ω, due to the $\cos 2\theta$ term in Eq. (7.17)

3. Waterline force at 2ω using linear expressions for u and η.

It is important to note that the free wave makes no individual contribution, as it is coupled in the expression for u_2 in Eq. (7.18). Neglecting free wave effects temporarily (the second term of Eq. (7.18)), and representing u_1 and u_2 using Stokes theory, integration over depth can be performed to obtain the total drag force as

$$F_d = 0.5\rho C_d D \left\{ \frac{2.667}{\pi} \frac{\omega^2 H^2 (\sinh 2kh + 2kh)}{16k \sinh^2 kh} \cos(kx_0 - \omega t) \right.$$

$$+\frac{3.349}{\pi}\frac{9}{1024}\frac{\omega^2 H^4 k(\sinh 4kh+4kh)}{\sinh^8 kh}\cos(kx_0-\omega t)$$

$$+\frac{4.461}{\pi}\frac{\omega^2 H^3(\cosh 2kh+2)}{16\sinh^4 kh}\cos 2(kx_0-\omega t)$$

$$+\frac{H^3}{8}\left(\frac{gk}{\omega}\right)^2\left[\frac{8}{6\pi}+\frac{8}{5\pi}\cos 2(kx_0-\omega t)\right]\Bigg\} \qquad (7.19)$$

The last term is the contribution due to the waterline effect.

Including the free wave in the wave field, the drag force expression takes on the form:

$$\begin{aligned}\frac{F_d}{0.5\rho C_d D} = \quad & \Bigg\{\frac{2.667}{\pi}\frac{\omega^2 H^2(\sinh 2kh+2kh)}{16k\sinh^2 kh} \\ & + \frac{3.349}{\pi}\Bigg[\frac{9}{1024}\frac{\omega^2 H^4 k}{\sinh^8 kh}(\sinh 4kh+4kh) \\ & + \frac{a_{22}^2\omega^2}{\kappa}\frac{\cos^2((\kappa-2k)x_0+\delta)}{\sinh^2\kappa h}(\sinh 2kh+2kh) \\ & + \frac{3\omega^2 H^2 a_{22}k\cos((\kappa-2k)x_0+\delta)}{4\sinh^4 kh\sinh\kappa h} \\ & \times \frac{(\kappa\sinh\kappa h\cosh 2kh-2k\cosh\kappa h\sinh 2kh)}{\kappa^2-4k^2}\Bigg]\Bigg\}\cos(kx_0-\omega t) \\ & + \frac{4.461}{\pi}\Bigg\{\frac{\omega^2 H^3}{32\sinh^5 kh}(\sinh 3kh+3\sinh kh)\end{aligned}$$

$$+ \quad \left. \frac{\omega^2 H a_{22}(\kappa \sinh \kappa h \cosh kh + k \sinh kh \cosh \kappa h)}{\sinh kh \sinh \kappa h(\kappa^2 - k^2)} \right\} \cos 2(kx_0 - \omega t)$$

$$+ \quad \frac{H^3}{8}\left(\frac{gk}{\omega}\right)^2 \left[\frac{8}{6\pi} + \frac{8}{5\pi}\cos 2(kx_0 - \omega t)\right] \tag{7.20}$$

The free wave thus contributes to two additional terms in the first order drag force and one extra term in the second order drag force.

Table 7.1 Formulation of the second order inertia force function $f(kh)$.

	Author	Formulation
1.	Generalised Morison's equation	$\frac{C_m}{8\sinh^2 kh}\left[3\coth kh + \frac{1}{2}\sinh 2kh - kh\right]$
2.	Isaacson (1979)	$\frac{C_m}{8\sinh^2 kh}\left[3\coth kh + \frac{1+1/C_m}{4}\sinh 2kh - \frac{1+1/C_m}{2}kh\right]$
3.	Madsen (1986)	$\frac{C_m}{8\sinh^2 kh}\left[3\coth kh + \frac{3-1/C_m}{4}\sinh 2kh - \frac{1+1/C_m}{2}kh\right]$
4.	Experimental	$\frac{F_{2i}}{(\rho g H D^2)(\pi/4)\tanh kh(kH)} - C_m\frac{a_{22}}{\kappa H^2}\cos((\kappa - 2k)x_0 + \delta)$

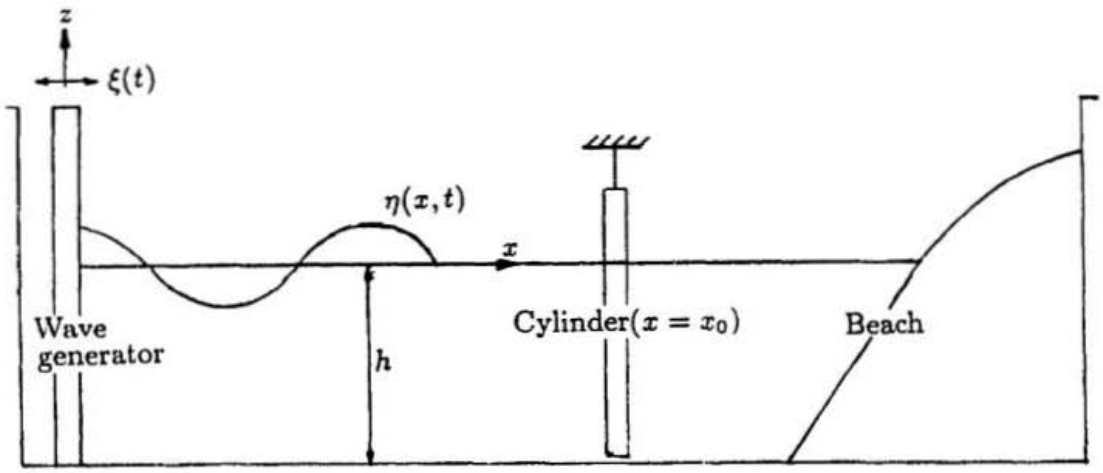

Figure 7.1 Representative diagram of the wave flume with the wave generator, beach and coordinate system.

Chapter 8

Experiments and Analysis

Experiments were conducted at the MUN wave tank facility to estimate the total inline wave force on cylinders of different diameters in various wave conditions. The wave tank had dimensions of 58.27m × 4.57m × 3.04m. Waves were generated by a hydraulically operated piston generator at one end of the tank and were partially absorbed at the other end by a parabolic beach. A description of the wave tank is given in chapter 4 of this thesis.

Two cylinders of diameters of 72.5mm (wall thickness = 5mm) and 48.9 mm (wall thickness = 3mm) were used during the experiments. The cylinders were made of aluminium and were 1.40m long, Fig. (8.1). A holder was constructed which was attached to a stationary carriage on top of the tank, Fig. (8.1). The test cylinder was connected to the holder with a force transducer plate, by means of bolts. The position of the holder was adjusted such that the cylinder was equally away from either side walls, a precaution expected to reduce the influence of cross tank oscillations.

The bottom of the cylinder was sealed and left unsupported. There was approximately 1.0cm gap between the cylinder and the bottom of the tank. The cylinders were initially weighed and their volume estimated. An excess in buoyancy was compensated by ballasting the cylinder with water.

The transducer plate was made of steel with an overall length of 0.52m, 3cm width and 2mm thick as shown in Fig. (8.2). The plate hosted eight strain gages at two elevations separated by a distance of 20cm. The strain gages used were the Micro - Measurements EA series of general purpose constantan strain gages of high precision. Each gage had a resistance of 120 ohms and a gage factor of 2.04 at 24^0C. The gages were bonded by a systematic procedure and water proof coatings were applied on them. Four gages at the same elevation were connected to a full bridge circuit. An advantage in using four gages in a full bridge circuit was that the effects of ambient temperature on the strain measurements were automatically adjusted. Each set of four gages was connected to a strain gage conditioner which housed a Wheatstone bridge network and a signal amplifier. The amplifier gain was initially set for a certain input voltage range. This range was in turn decided based on the maximum and minimum voltage expected from the gages. The output from the conditioner was directly recorded on an eight channel FM recorder.

The transducer plate acted as a cantilever beam, rigidly supported on one end and a load on the unsupported end. Let the total wave force

experienced by the cylinder be F and the centroid of its vertical distribution be $\bar{h}$, from the mean free surface. Let it also be that the two bridges were h_1 and h_2 from the free surface. The strains measured by each of the gages in bridge 1 according to elastic beam theory will be

$$\epsilon_1 = \frac{y}{EI}[F(h_1 + \bar{h})]$$

where y, E, I are characteristic parameters of the size and material of the beam. The strains measured by the gages in bridge 2 will be

$$\epsilon_2 = \frac{y}{EI}[F(h_2 + \bar{h})]$$

so that the difference in strain will be linear in F as

$$\epsilon_1 - \epsilon_2 = \left[\frac{y}{EI}(h_1 - h_2)\right] F \tag{9.1}$$

Fig. (8.3) shows a calibration chart of the transducer which is a plot of the difference in strains between the two bridges and the applied load. The calibration was performed by loading the cylinder with known weights at different leverage and evaluating the strain difference between the bridges. As part of the calibration process, free vibration tests were performed on the cylinder - transducer setup placed in the wave tank at the desired depth of 1.0 m. An arbitrary initial displacement was given to the setup and the response from the strain gages were measured and analyzed by the FFT. These tests revealed that the fundamental frequencies of the cylinders with diameters 72.5 mm and 48.9 mm were 3.12 Hz and 4.25 Hz respectively.

The procedure of the wave force experiments may now be described. A constant water depth of 1.0 m was maintained during the experiments. The frequency of the wave was varied from 0.4 - 1.2 Hz and, the stroke length of the generator was varied from 0.5% to 59.4% to give rise to the range of parameters used for the wave experiments. A total of 56 runs were performed, 28 runs for each cylinder. Since the tank was sufficiently long, all data acquisition was completed before the first wave front reached the beach. The effects of the reflected wave were thus avoided. Effects of the free wave were however, inevitable and had to be included in the analysis. A wave probe was placed in-line with the cylinder to obtain the phase difference between the wave and force signals.

The recorded data was digitised using the Keithley system 570 described in chapter 4. The sampling rate was set at 64 samples per wave period. The digitised uncalibrated data was stored as files in the VAX/VMS 8530 computer. Files were coded with four digits, the first two representative of the cylinder used and the last two digits indicated the run number. The first and second order sine and cosine components of the wave force were obtained from the calibrated data using a fast fourier transform subroutine explained in chapter 4. The initial phase information for the FFT was provided from the wave probe output.

The first order analysis consisted of evaluating the hydrodynamic coefficients C_m and C_d from the measured first order forces. The following formulae

were used, which are obtained from Eqs. (7.11) and (7.19).

$$C_m = F_{1\sin} / \left(\rho \frac{\pi D^2}{4} \frac{\omega^2 H}{2k} \right) \tag{9.2}$$

$$C_d = F_{1\cos} / \left(0.5 \rho D \frac{2.667}{\pi} \frac{\omega^2 H^2 (\sinh 2kh + 2kh)}{16k \sinh^2 kh} \right) \tag{9.3}$$

where $F_{1\sin}$ and $F_{1\cos}$ are the first order sine and cosine force components as evaluated by the FFT. Values of H, k, ω etc. were obtained from the results of the corresponding wave experiment, discussed in part 1 of this thesis.

In the second order analysis, it was desired to verify the second order force formulation presented in chapter 7. Second order forces were calculated as per formulae (7.13) and (7.22) using the values of C_m and C_d obtained from first order analysis. The measured values were then compared with the calculated ones. Another analysis performed was to compare the function $f(kh)$ for various approaches, as mentioned in Table 7.1.

A schematic diagram of the force analysis procedure is given in Fig. (8.4).

Figure (8.1) Cylinder configuration in the wave tank

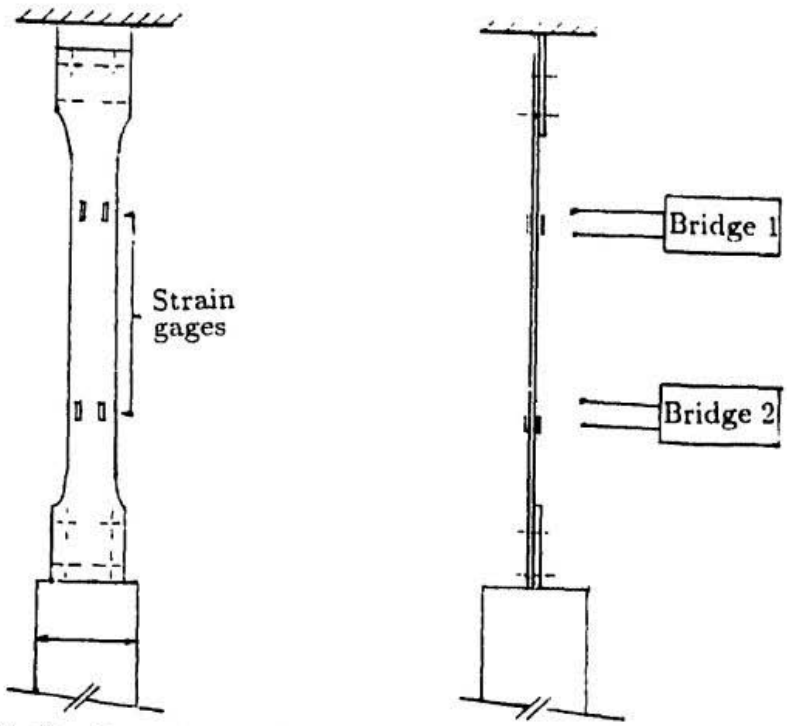

Figure (8.2) Configuration of the force transducer

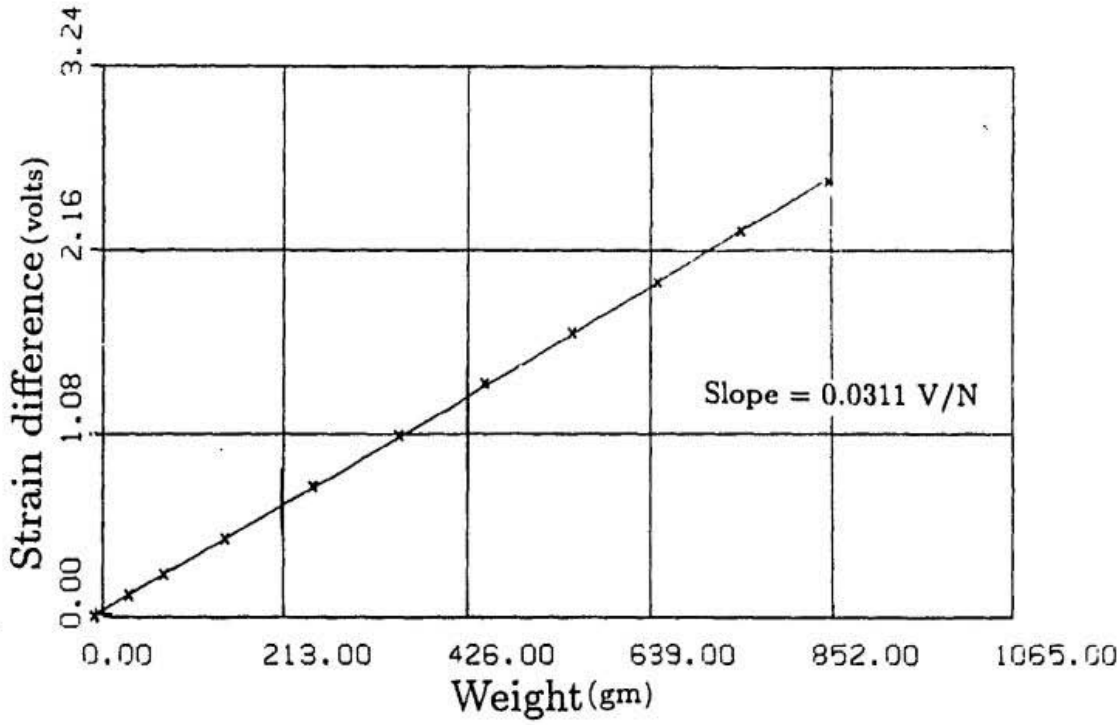

Figure (8.3) Calibration chart for the force transducer

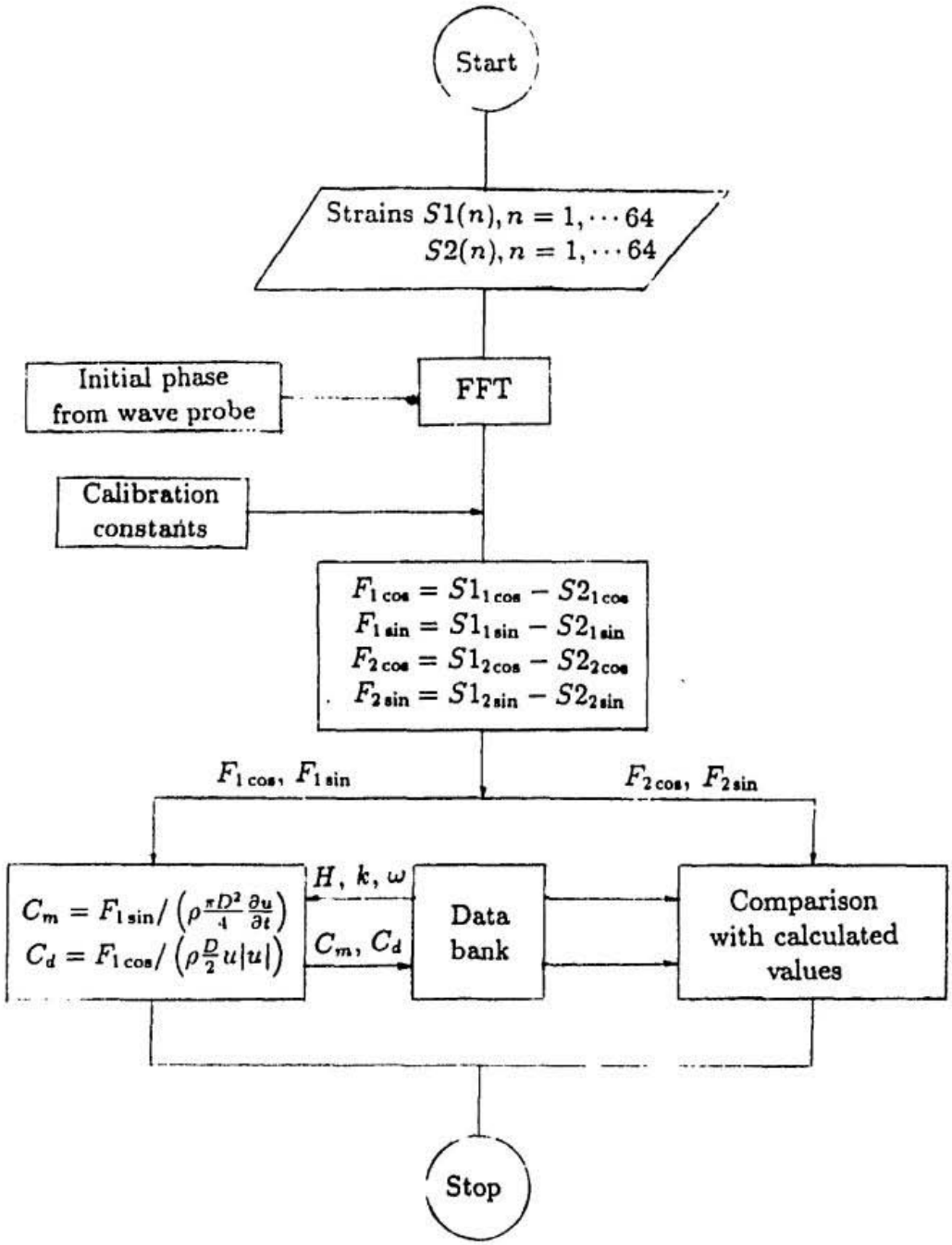

Figure (S.4) Schematic diagram of wave force analysis

Notes: Subscripts 1 and 2 indicate the order of the force.
Subscripts 'sin' and 'cos' indicate the component of the FFT

Chapter 9

Discussion of results

The range of testing for the wave force experiments followed the range of wave experiments in accordance with the values tabulated in Table 5.1. A value of 0.2 for the cylinder diameter to incident wave length ratio (D/λ) characterises the diffraction regime, beyond which scattering of waves becomes important. For the present study, the range of D/λ was 0.0066 - 0.0701. Thus scattering was neglected in the present study. The dimensionless parameters used in the analysis were

1. Keulegan - Carpenter number defined as

$$KC = U_m T/D$$

where U_m is the amplitude of the water particle velocity at the mean free surface as predicted by linear theory.

2. Reynold's number defined as

$$Re = U_m D/\nu$$

where ν is the kinematic viscosity of water.

3. Sarpkaya's parameter defined as the ratio of Reynold's number to Keulegan - Carpenter number

$$\beta = D^2/\nu T$$

The values of these parameters for all the experimental runs are given in Table 9.1.

Figs. (9.1) and (9.2) show the sample curves of outputs from the strain gage bridges and the wave probe. The results are presented in an uncalibrated form so that they could be qualitatively analysed. In Fig. (9.1), KC is low where the inertia force dominates over drag. This is reflected in the figure with the wave and force curves out of phase by $\pi/2$. Fig. (9.2) in contrast is in the high KC range where the drag force is comparable or greater than the inertia force, thus the force is almost in phase with the wave. The force spectra corresponding to the above two wave conditions are shown in Figs. (9.3) and (9.4), where the fundamental frequency of the spectrum corresponds to the first harmonic frequency of the incident wave.

Forces evaluated experimentally for the two cylinders are presented in Table 9.1. Values of F_{1sin} and F_{2sin} correspond to those of the first and

second order inertia forces. First and second order drag forces are respectively given by F_{1cos} and F_{2cos}. The table is intended to provide the reader with a quantitative estimate of the wave forces experienced by cylinders of the specified dimensions. A maximum inertia force of 4.95 N occurs at the steepest wave for the 0.0725m diameter cylinder.

The results for the two hydrodynamic coefficients are presented in graphs, (9.5) and (9.6), plotted against the Keulegan-Carpenter number (KC). A third and fourth order polynomial least squares fits are also shown in the graphs. Also shown are the results obtained by Chakrabarti (1980a) and Sarpkaya (Sarpkaya and Isaacson, 1981; section 3.8). The results of Sarpkaya have been plotted for two different values of β, within which most of the present experimental points lie. These results show that at very low KC, the values stagger around the theoretical value of 2.0 as opposed to a higher value of 2.5 by Chakrabarti. The fourth order polynomial fit seem to follow the trend of Sarpkaya's results. Results for C_d in the low KC range are scattered due to unreliable drag measurements. This arises because of inertia dominance, also noticed by other researchers, (see for eg. Sarpkaya and Isaacson, 1981, sec 3.8.3). There is evidence of some scatter at higher values of KC too, but the polynomial fits to the data points follow the trend of both Sarpkaya (Sarpkaya and Issacson, 1981) and Chakrabarti (1980).

The ratios of second order to first order force amplitudes are plotted in Figs. (9.7) and (9.8). It is apparent that the second order forces can be as

much as 80% of the first order forces and thus contribute significantly to the total loading. In many other cases the ratio is less than 30%. Higher values occur in both graphs at low β because steeper waves were generated only at low frequencies, a limitation of the capacity of the wave generator.

A comparison between the calculated second order forces and the measured ones are made in Figs. (9.9) - (9.12). Second order forces are calculated from Eqs. (7.11) and (7.20) using the estimated values of the hydrodynamic coefficients. Graphs show values only upto 0.3 Newtons. Beyond that value, points are sparse and data insufficient. Results are classified into:

i) at low steepness, corresponding to $H/gT^2 = 0.0007$ and 0.001;

ii) at high steepness, corresponding to $H/gT^2 = 0.003$ and 0.005.

At low steepness, second order effects are low and hence measurement of second order forces becomes exceedingly difficult and is prone to errors. Results of Figs. (9.9) and (9.11) attest to that, as measured values of upto five times the calculated ones are present in the figures. Measured results become more reliable at higher steepnesses, as can be seen in Figs. (9.10) and (9.11). The margin of error in these two figures is in the order of $\pm 50\%$, which may well be regarded as good, as scatter to this order or more have been reported even for first order measurements (Wiegel, 1964; also Chakrabarti, 1980).

In view of the above discussions on first and second order forces, the following points should be considered while perusing Table 9.1:

- At higher values of KC (> 4), measured values of the first order drag force are more reliable than at low KC (< 4).
- At high steepness (corresponding to $H/gT^2 = 0.003$ and 0.005), measured values of the second order forces are more reliable than at low steepness.
- In those runs comprising of low KC (< 4)and low steepness ($H/gT^2 = 0.0007$, 0.001), it is possible that some values of the second order forces.are greater than the first order force values.

The second order inertia force function mentioned in Table 7.1 was calculated for the three mentioned approaches and determined experimentally. These values are plotted in Figs. (9.13) to (9.16). Experimental results were far higher than the calculated ones at low steepness. This was anticipated based on the results of Figs. (9.9) and (9.11). At higher steepnesses the points were in the vicinity of of the calculated values and in Fig. (9.11) the experimental values follow the theoretical trend. The three approaches for the second order inertia force function differ only marginally. Due to experimental errors of the same order, it was not possible to ascertain in definite terms, the best of the three approaches.

The influence of the free wave on the force measurements requires attention. It was observed by Ellix (1984) and Ellix and Arumugam (1985) that correlation of second order force results with theory was very poor when the free wave activity was high. Such a trend was not observed during the present study, though measured values of free wave amplitude were generally higher than theoretical predictions, Fig. (5.17). The correction made for the free wave in entry 4 of Table 7.1 was found to satisfy the requirement.

Many sources of error are possibly due to the physical limitations of the wave tank. The following are expected to have contributed significantly to the scatter in the wave force results, Figs. (9.5) through (9.16):

1. The sources that contributed to the scatter in the wave height to stroke length ratio of Fig. (5.9). These include *i*) human errors in span setting, *ii*)wave generator control system imperfections.

2. Round off errors in estimating the force from the measured strains. This error arises due to the subtraction of two quantities of the same order of magnitude (the strains from the two bridges), further magnified by a small quantity (the distance between the bridges) in the denominator, see Eq. (8.1).

3. Ripples and disturbances present in the tank. These are created due to experiments conducted previously during the day and, take a long

time to die down. When waves of small height are generated, the forces measured might also include the response of the gages to these disturbances. This strongly depends on the sensitivity of the transducer.

4. The transducer plate was designed to be slender and flexible, so that small force quantities be sensed. An increased sensitivity on the other hand leads to small disturbances being recorded along with the desired quantities.

5. Effects of cross tank oscillations and other side effects in the tank. Quantifying these effects is beyond the scope of the present study.

The following conclusions were obtained from the results of the experiments on wave forces:

1. The first order results were within the expected range. Results for the hydrodynamic coefficients followed the trends of established data. There was evidence of a scatter in data.

2. At low KC, C_m converged to a value of 2.0, decreased upto $KC = 10$ and remaining around 1.0 upto $KC = 15$.

3. At low KC, C_d results were scattered and unreliable. Values in general, increased upto $KC = 12$ and decreased beyond that.

4. Second order forces were found to be significant compared to first order. Second order forces upto 80% of first order were recorded during experiments.

5. Results for second order forces were unreliable at low steepness. This occurs because second order effects are small at low steepness. It is felt that measuring second order forces below a H/gT^2 of 0.001 with the present setup leads to inaccurate results.

6. Measured second order forces at high steepness were within 50% of the calculated forces. This was observed to hold good for both inertia and drag components.

7. Theoretical formulation of the second order forces appears to be adequate. Inclusion of quadratic forces following Lighthill (1979) might lead to a better formulation.

8. The second order inertia force function is found to be an effective tool to compare different approaches. Experimental values for this function showed correlation with calculated values at higher steepnesses.

9. A complete comparison of the approaches for second order inertia forces of Lighthill (1979), Madsen (1986) and Isaacson (1979) was prevented by experimental errors. But it was observed that all three approaches closely represented the actual forces.

Table 9.1 Experimental wave forces and related parameters

Run	D=0.0479m					
	KC	Re	$F_{1\sin}$ N	$F_{1\cos}$ N	$F_{2\sin}$ N	$F_{2\cos}$ N
1	3.21	2672.33	0.4782	0.0312	0.0891	0.0993
2	1.79	1871.75	0.3357	0.6557	0.0669	0.0298
3	1.63	2037.18	0.2151	0.7390	0.1011	0.0247
4	0.58	1091.98	0.1659	0.1944	0.0109	0.0009
5	0.55	1145.72	0.1654	0.1743	0.0204	0.0095
6	0.58	1332.64	0.1628	0.2705	0.0573	0.0108
7	0.30	738.28	0.0750	0.0072	0.0095	0.0130
8	8.11	6755.88	0.4600	0.3568	0.1093	0.0597
9	2.39	2488.85	0.4484	0.4136	0.1883	0.0323
10	2.25	2810.63	0.3720	0.7275	0.0465	0.0490
11	0.64	1205.63	0.2802	0.3621	0.0298	0.0313
12	0.74	1549.52	0.2327	0.3501	0.0128	0.0162
13	0.60	1377.71	0.1660	0.3098	0.0101	0.0259
14	0.35	871.19	0.0935	0.1988	0.0068	0.0402
15	15.83	13188.67	0.9210	1.1472	0.2827	0.3935
16	6.35	6610.94	0.8956	0.2926	0.2199	0.2234
17	5.43	6792.42	0.8477	0.2439	0.1855	0.2061
18	2.43	4554.16	0.7559	0.0862	0.1336	0.1281
19	2.28	4759.48	0.5664	0.5407	0.1202	0.0904
20	2.19	5030.79	0.5580	0.7136	0.0971	0.0705
21	1.23	3069.63	0.3684	0.5215	0.0752	0.0560
22	26.56	22129.84	2.0650	3.4385	0.8733	0.0960
23	12.33	12849.49	1.0056	2.6479	0.5220	0.9856
24	11.62	14531.46	1.2640	2.5281	0.5059	0.8742
25	4.04	7571.72	1.2619	1.1146	0.1977	0.6699
26	3.26	6789.43	0.7650	1.2300	0.0595	0.1663
27	2.46	5632.37	0.6329	1.2060	0.0594	0.1037
28	2.12	5299.31	0.5516	1.1142	0.0185	0.1033

Table 9.1 Contd.

Run	D=0.0725m					
	KC	Re	$F_{1\sin}$ N	$F_{1\cos}$ N	$F_{2\sin}$ N	$F_{2\cos}$ N
1	2.12	4048.97	0.7616	0.0369	0.0225	0.0687
2	1.19	2835.97	0.6575	0.0200	0.0698	0.0319
3	1.07	3086.63	0.5039	0.0324	0.1063	0.0663
4	0.38	1654.50	0.3497	0.4480	0.0576	0.0362
5	0.36	1735.93	0.3670	0.4227	0.0707	0.0481
6	0.38	2019.14	0.2487	0.0052	0.0364	0.0156
7	0.19	1118.60	0.1678	0.0907	0.0436	0.0050
8	5.35	10236.14	0.8559	0.4011	0.1434	0.1197
9	1.58	3770.97	0.7357	0.3572	0.0559	0.0951
10	1.48	4258.51	0.6344	0.1582	0.0693	0.0596
11	0.42	1826.66	0.4387	0.2129	0.0922	0.0661
12	0.49	2347.75	0.4969	0.1564	0.0310	0.0484
13	0.40	2087.43	0.3457	0.0166	0.0131	0.0361
14	0.23	1319.97	0.2242	0.0163	0.0245	0.0126
15	10.45	19982.76	2.1343	3.6861	0.4826	0.6942
16	4.19	10016.54	1.9500	2.1112	0.3868	0.5453
17	3.59	10291.50	1.8428	1.7827	0.2899	0.2845
18	1.60	6900.22	1.6811	1.7127	0.1126	0.2174
19	1.51	7211.31	1.3926	1.6396	0.0781	0.1490
20	1.45	7622.37	1.1890	1.3952	0.0740	0.1390
21	0.81	4650.94	0.8601	1.1656	0.0461	0.1294
22	17.53	33529.93	4.9485	5.8846	2.5173	2.2124
23	8.14	19468.85	3.9007	4.9018	2.4803	1.7041
24	7.67	22017.27	3.7865	3.4307	1.7972	0.9616
25	2.67	11472.26	2.6972	2.8319	0.9399	0.7364
26	2.15	10286.97	1.7329	2.1031	0.6694	0.3011
27	1.62	8533.37	1.2778	1.7120	0.3737	0.2053
28	1.40	8029.22	1.2374	1.3437	0.4356	0.0361

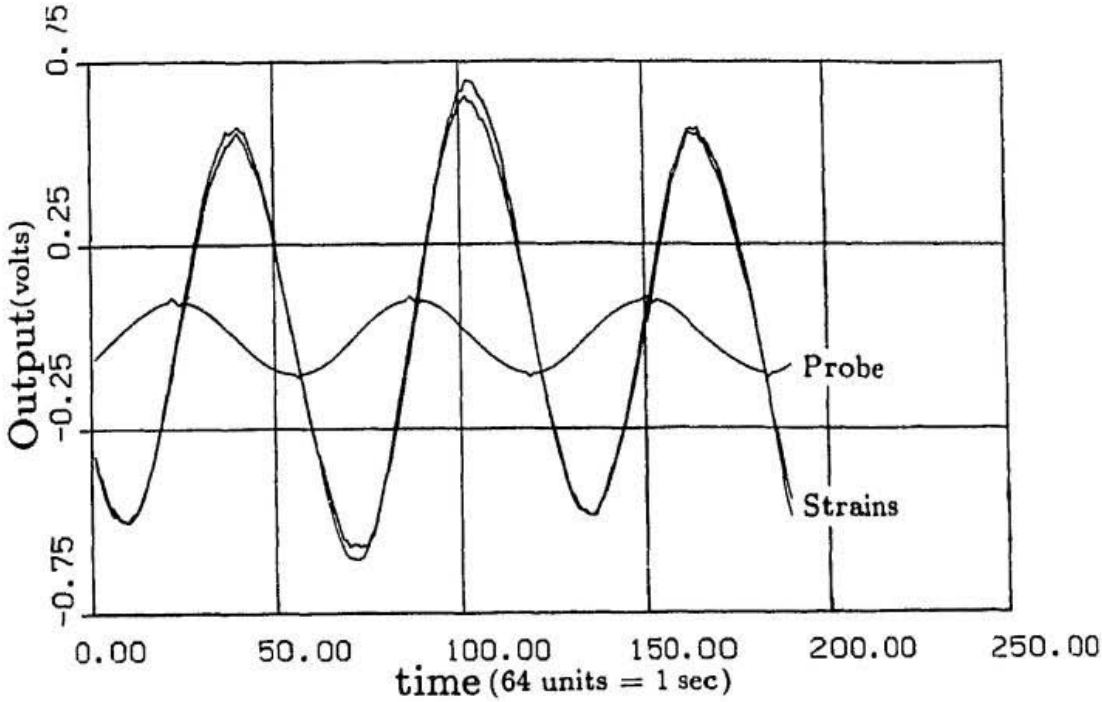

Figure 9.1 Sample wave force graph: Run 01, D=0.0725m, f = 0.9Hz, $H/gT^2 = 0.003$, $KC = 2.12$

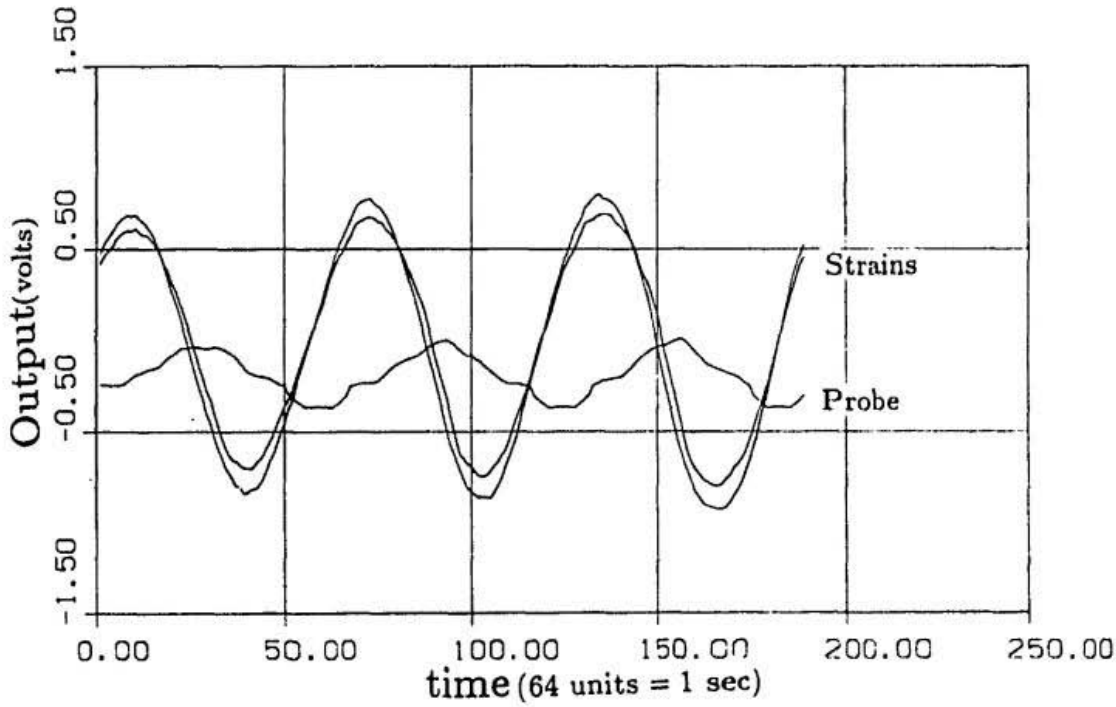

Figure 9.2 Sample wave force graph: Run 22, D=0.0479m, f = 0.4Hz, $H/gT^2 = 0.005$, $KC = 26.56$

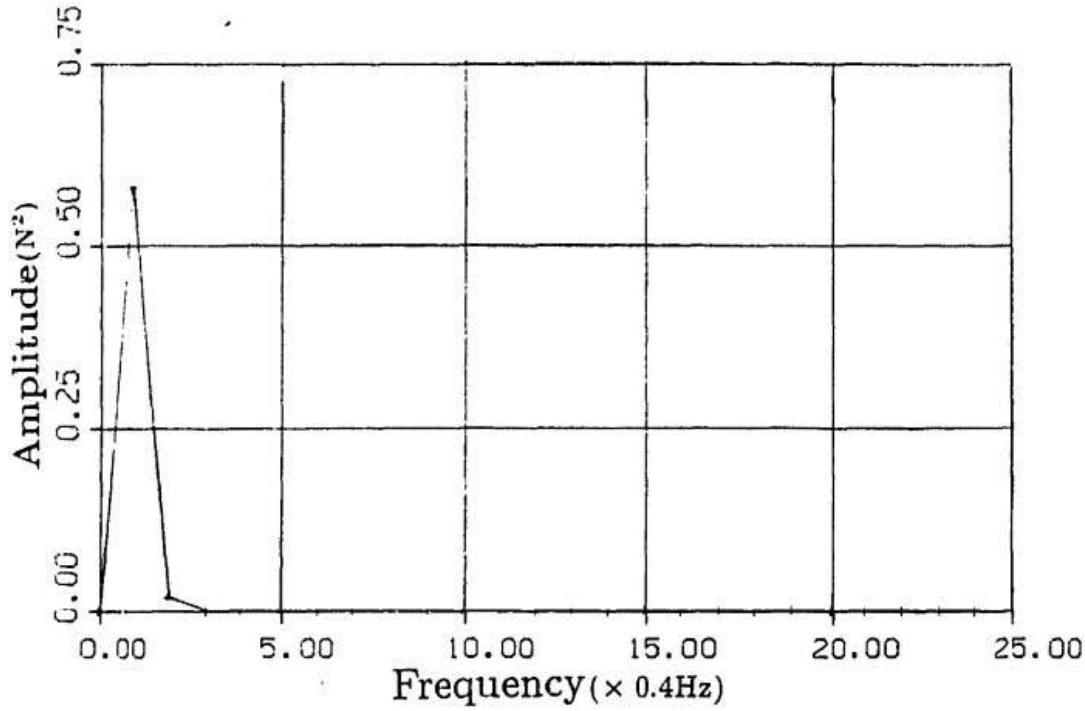

Figure (9.3) Wave force spectrum for run 01, D=0.0725m

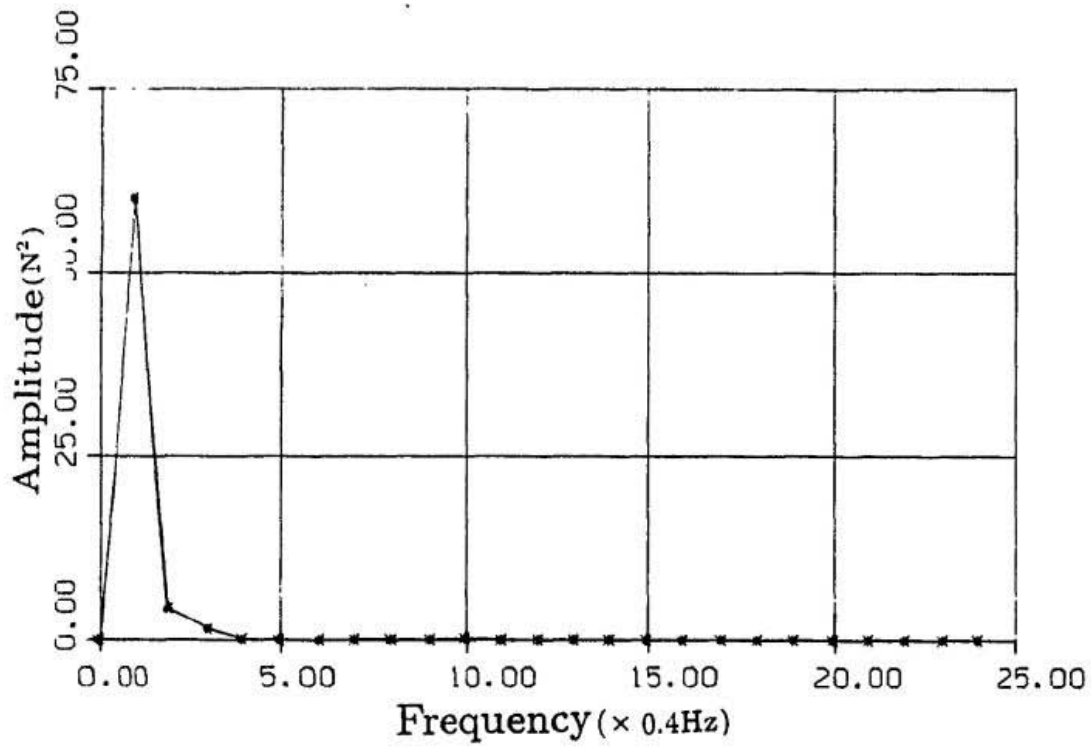

Figure (9.4) Wave force spectrum for run 22, D=0.0479m

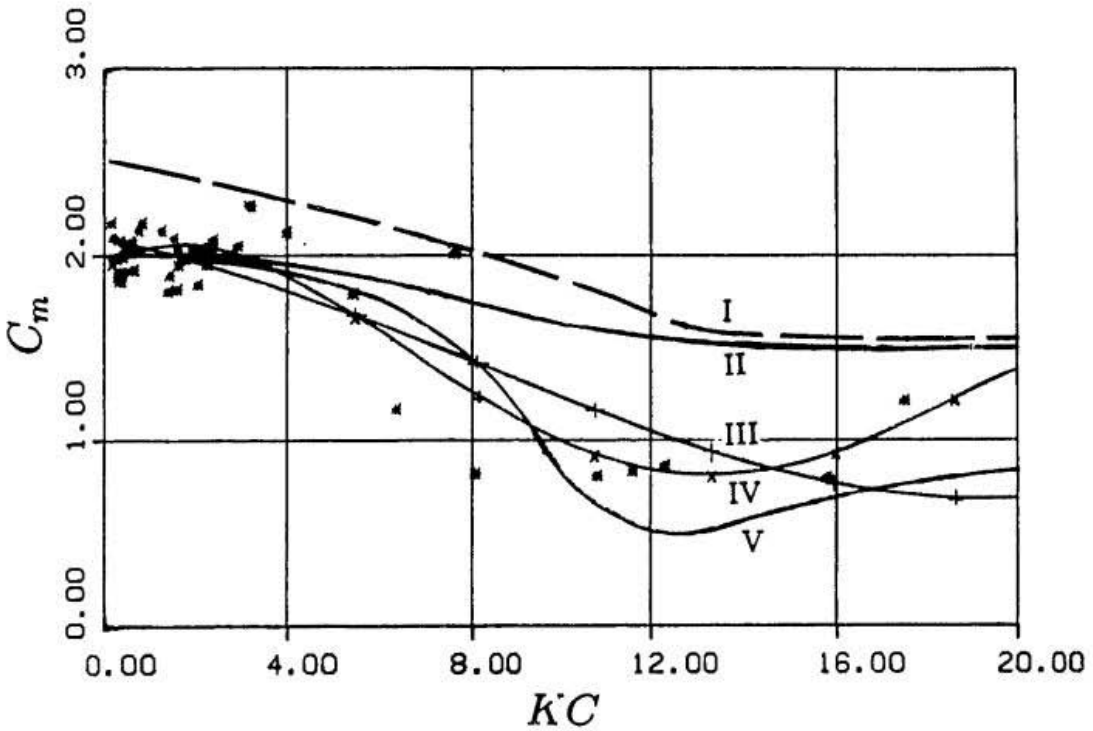

Figure 9.5 Inertia coefficient (C_m) vs Keulegan Carpenter number (KC)

I - Chakrabarti (1980);
II - Sarpkaya (Sarpkaya and Isaacson 1981), $\beta = 5260$;
III - Third order polynomial fit to data;
IV - Fourth order polynomial fit to data;
V - Sarpkaya (Sarpkaya and Isaacson 1981), $\beta = 784$;
■ - Experimental data points.

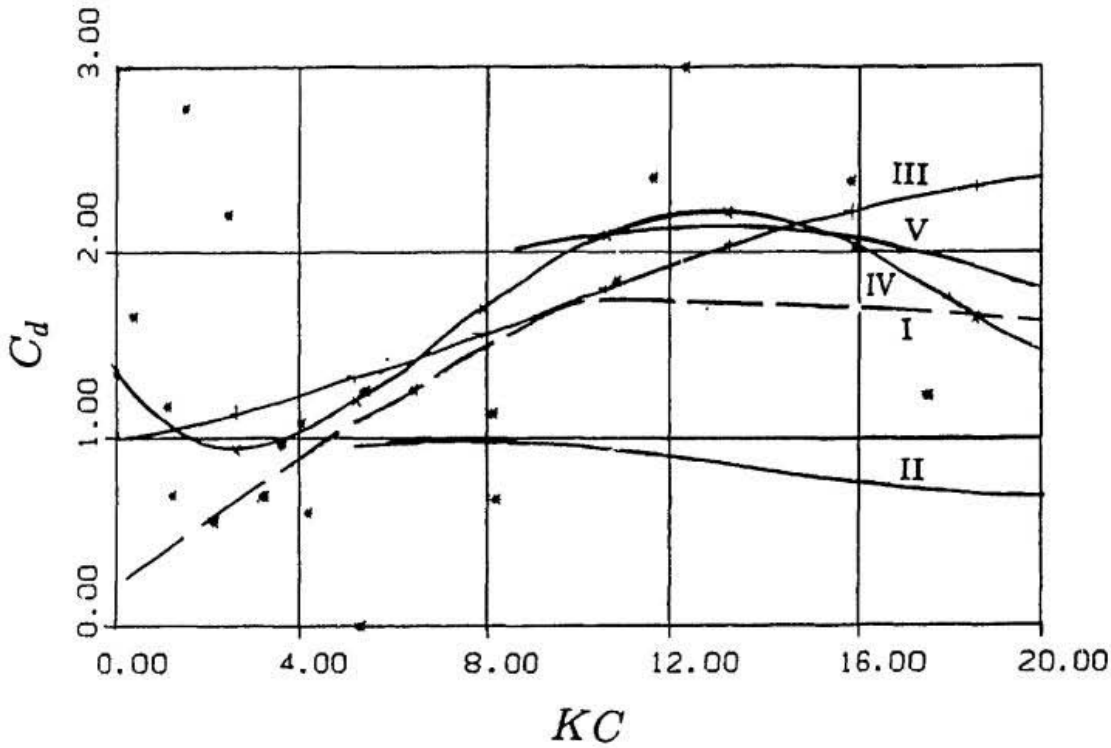

Figure 9.6 Drag coefficient (C_d) vs Keulegan Carpenter number (KC)

I - Chakrabarti (1980);
II - Sarpkaya (Sarpkaya and Isaacson 1981), $\beta = 5260$;
III - Third order polynomial fit to data;
IV - Fourth order polynomial fit to data;
V - Sarpkaya (Sarpkaya and Isaacson 1981), $\beta = 784$;
▪ - Experimental data points.

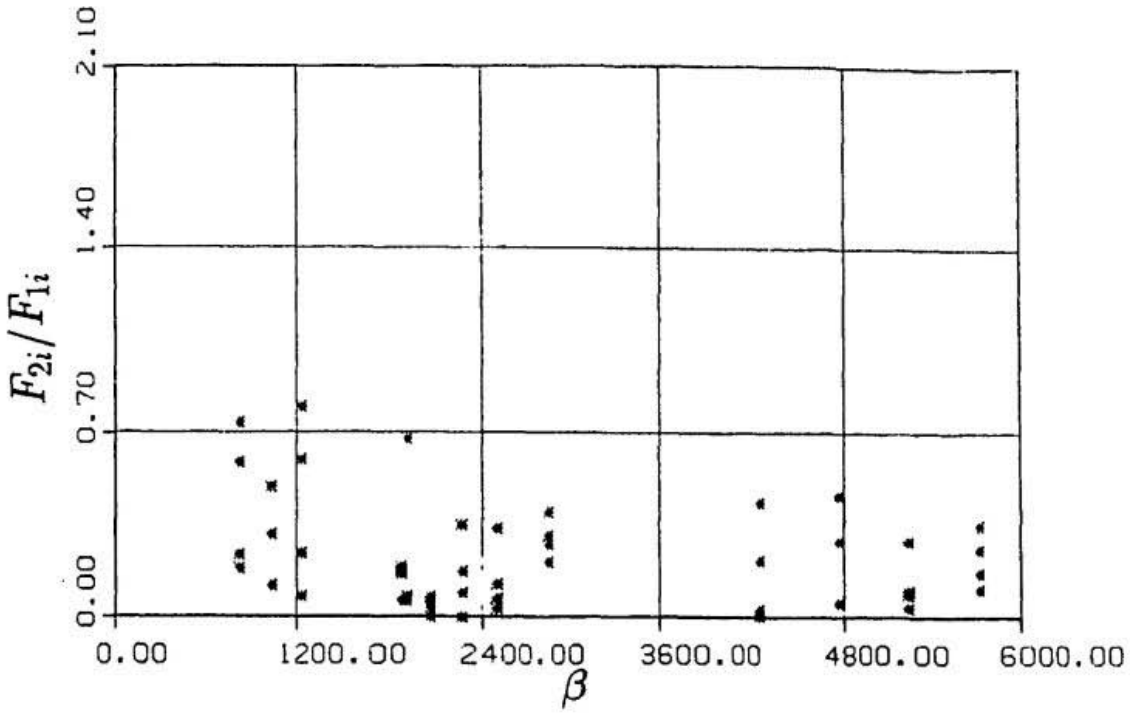

Figure 9.7 Ratio of second to first order inertia forces versus Sarpkaya's parameter (β).

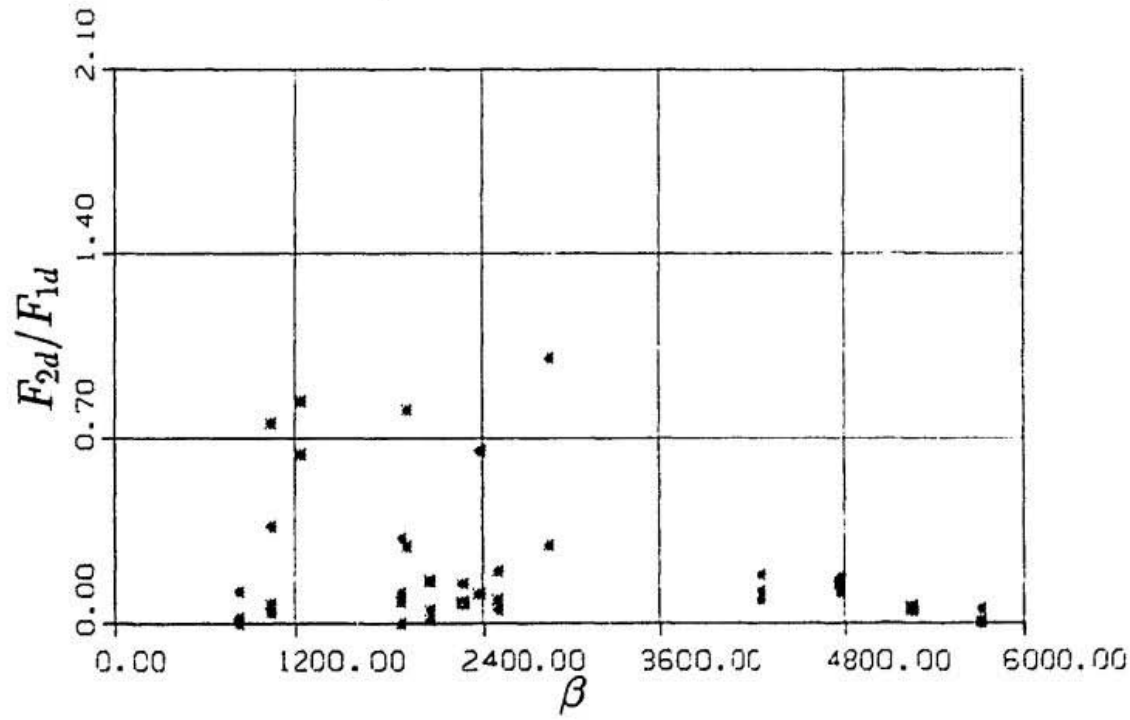

Figure 9.8 Ratio of second to first order drag forces versus Sarpkaya's parameter (β).

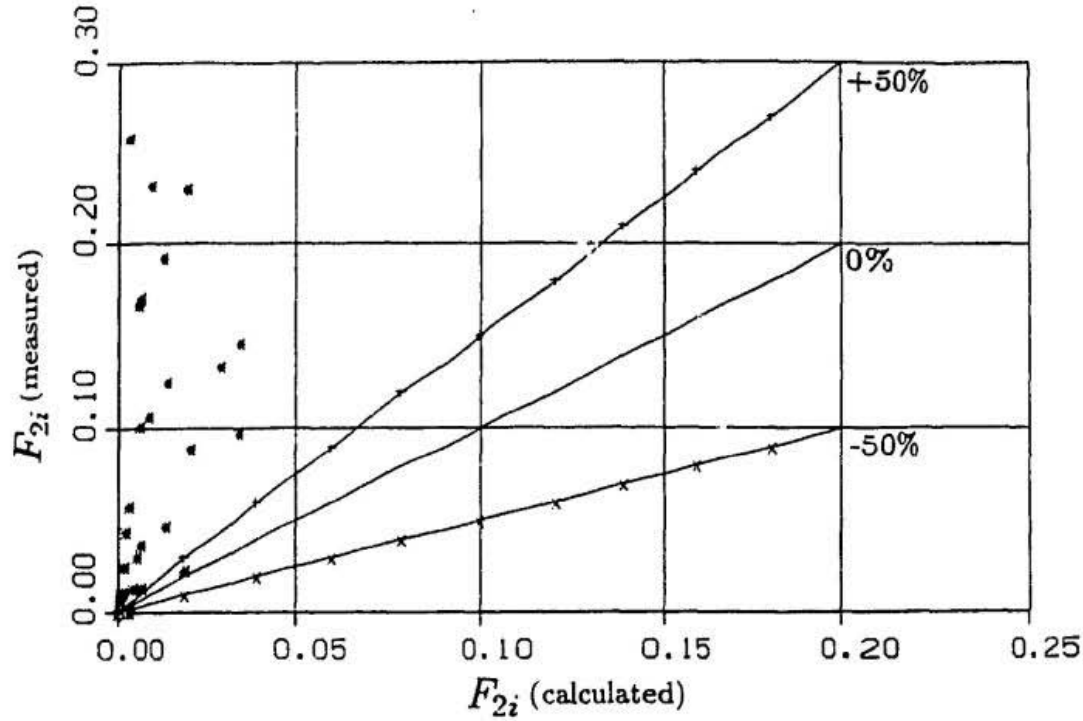

Figure 9.9 Comparison between calculated and measured second order inertia force at low steepness ($H/gT^2 = 0.0007, 0.001$).

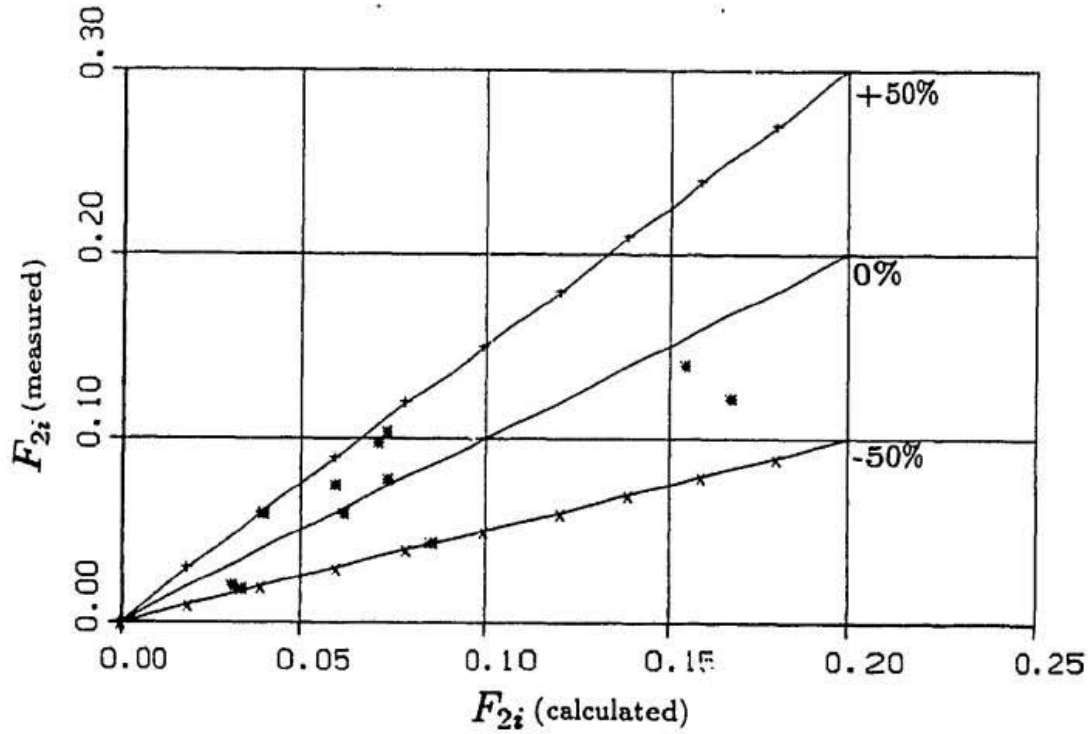

Figure 9.10 Comparison between calculated and measured second order inertia force at high steepness ($H/gT^2 = 0.003, 0.005$).

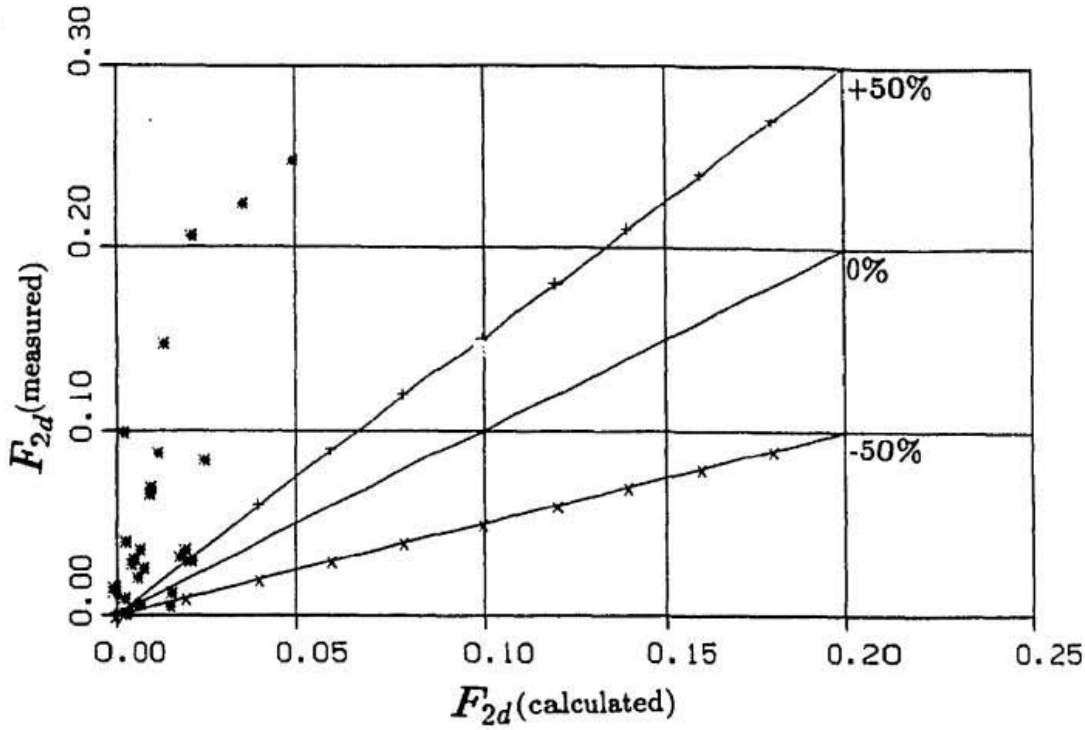

Figure 9.11 Comparison between calculated and measured second order drag force at low steepness ($H/gT^2 = 0.0007, 0.001$).

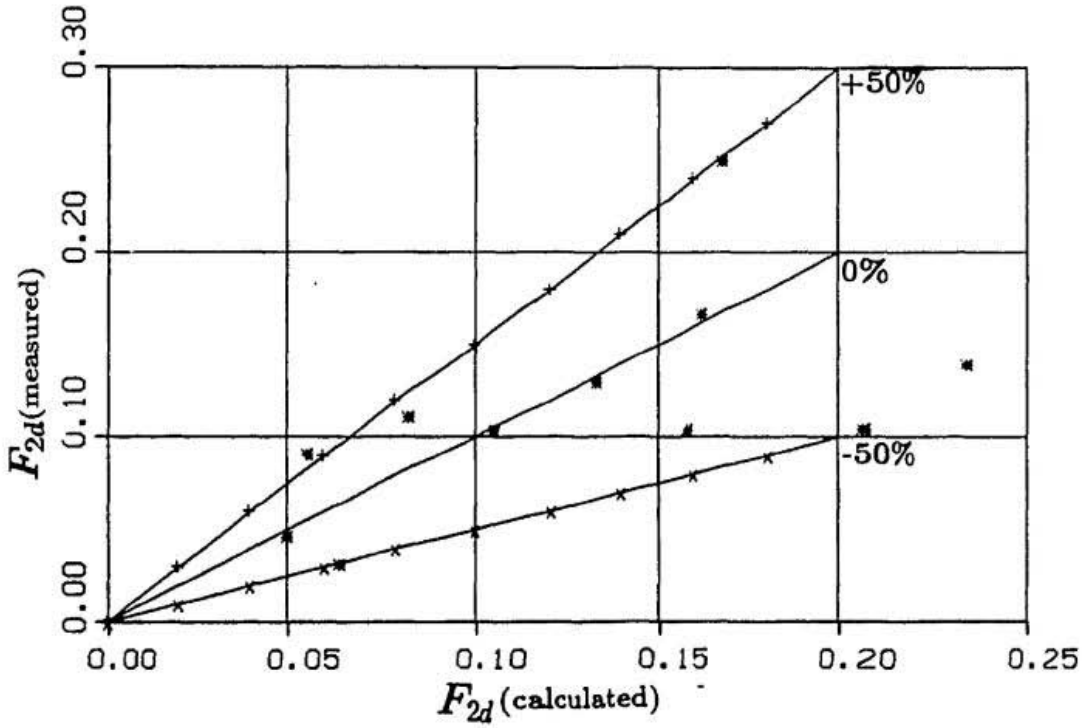

Figure 9.12 Comparison between calculated and measured second order drag force at high steepness ($H/gT^2 = 0.003, 0.005$).

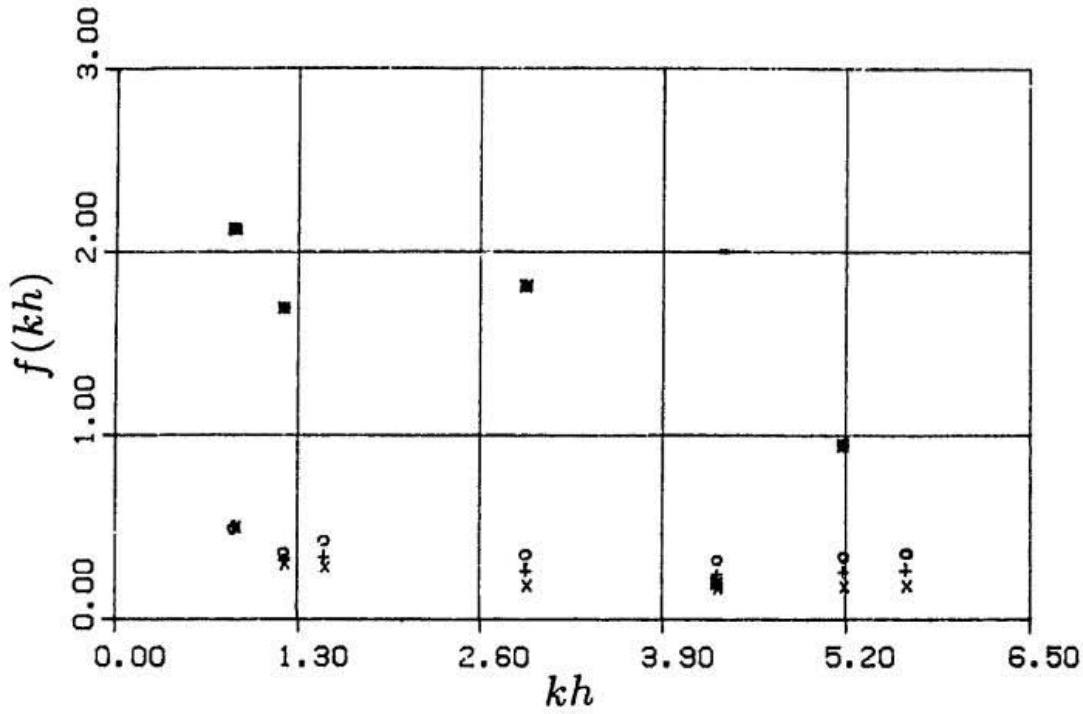

Figure 9.13 Comparison between measured and calculated second order inertia force function vs kh; $H/gT^2 = 0.003$; $D = 0.0479$m.

- o Madsen (1986)
- × Isaacson (1979)
- \+ Generalised Morison's equation
- * Experimental

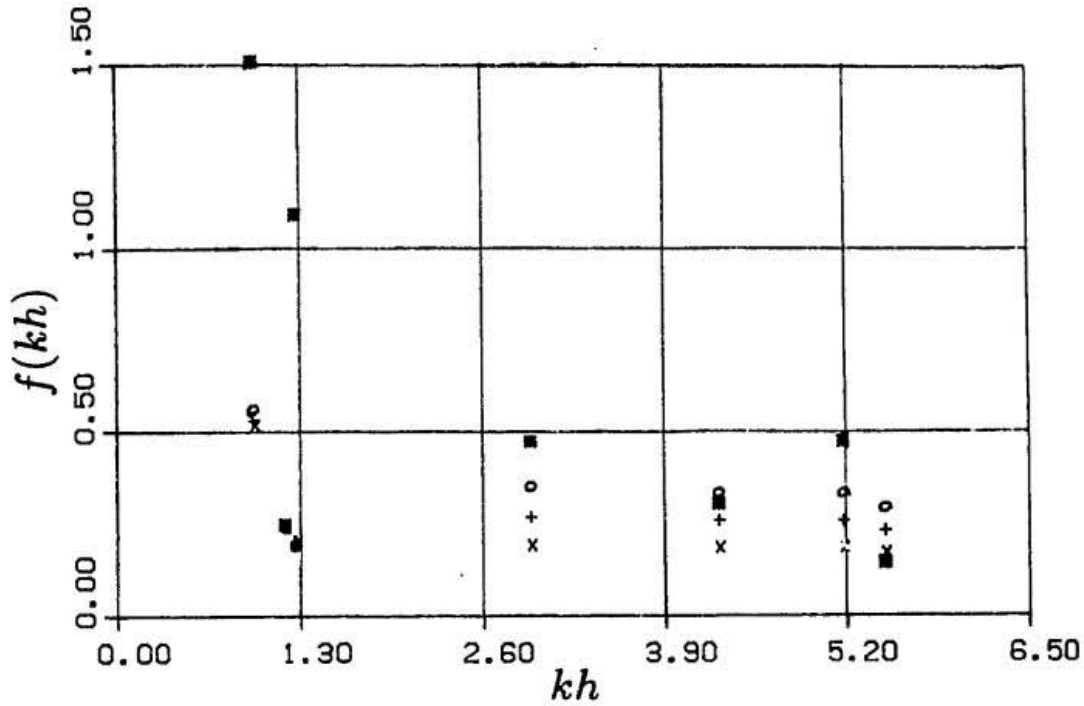

Figure 9.14 Comparison between measured and calculated second order inertia force function vs kh; $H/gT^2 = 0.005$; $D = 0.0479$m.

- o Madsen (1986)
- × Isaacson (1979)
- \+ Generalised Morison's equation
- * Experimental

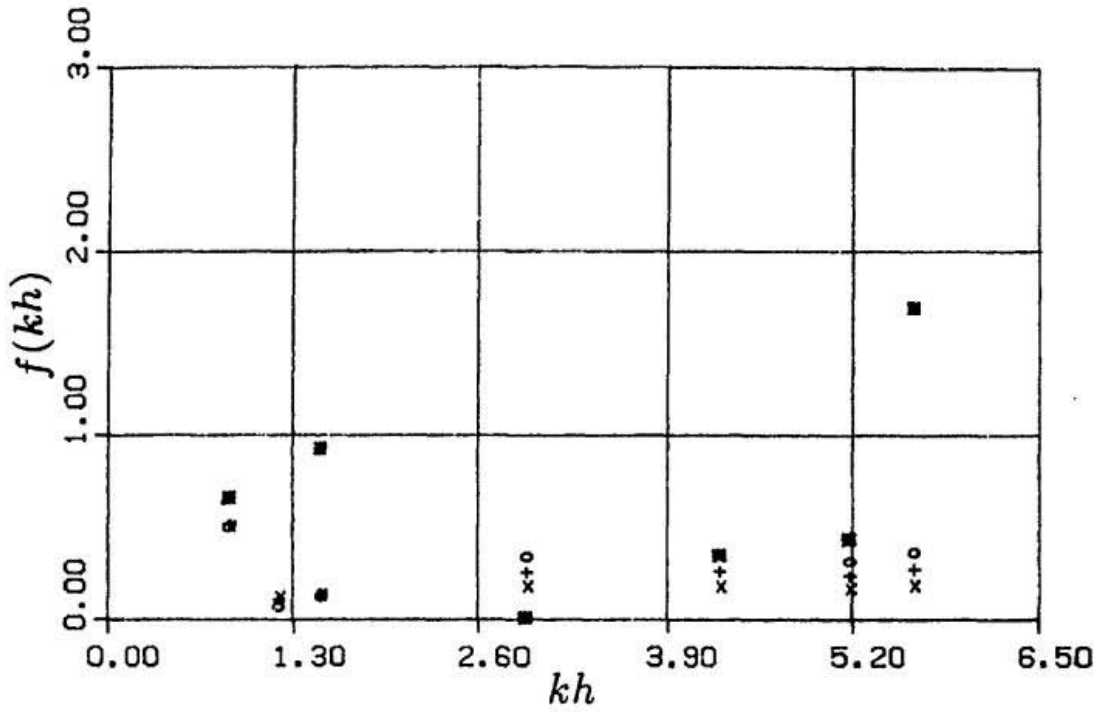

Figure 9.15 Comparison between measured and calculated second order inertia force function vs kh; $H/gT^2 = 0.003$; $D = 0.0725$m.

o Madsen (1986)

× Isaacson (1979)

\+ Generalised Morison's equation

* Experimental

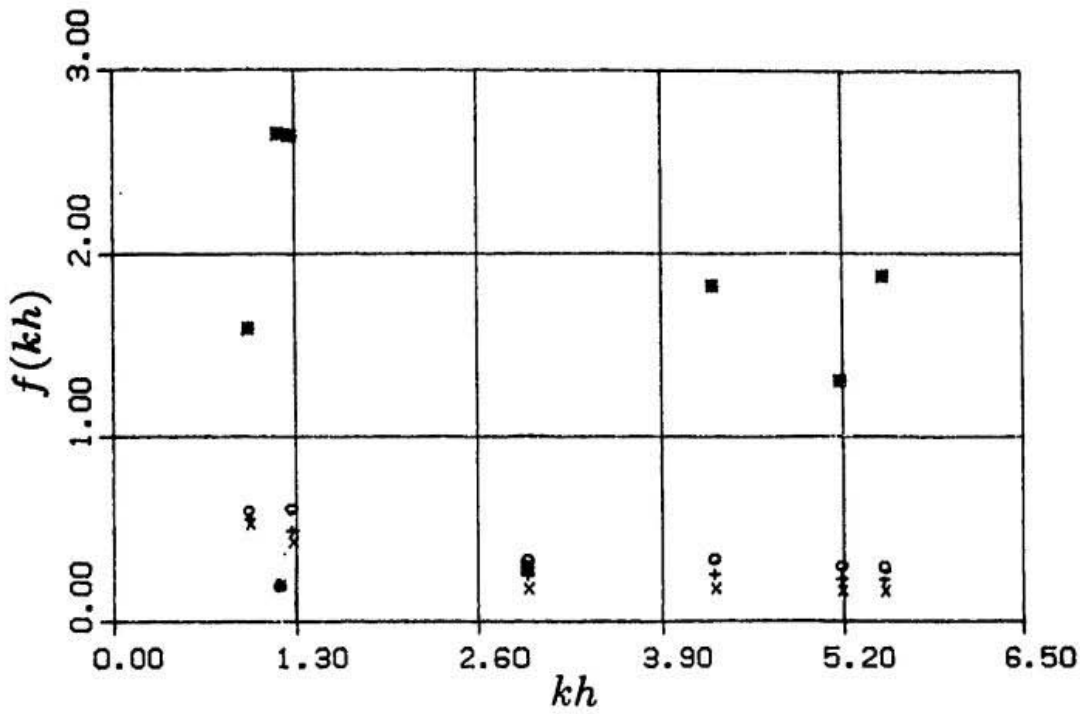

Figure 9.16 Comparison between measured and calculated second order inertia force function vs kh; $H/gT^2 = 0.005$; $D = 0.0725$m.

- o Madsen (1986)
- × Isaacson (1979)
- \+ Generalised Morison's equation
- * Experimental

Chapter 10

Concluding remarks

This study presented a formulation of the wave field upto second order in a wave tank. Experiments were conducted by measuring the free surface elevations at locations sequentially down the tank. Results were analysed using a fast fourier transform and least squares analyses. Amplitudes of wave components at first and second order were identified. These results were used in evaluating the wave forces on a cylinder. Experiments on cylinders were conducted in similar wave environments and forces measured by a strain gage force transducer. A theoretical formulation of wave forces was presented based on a literature survey. The force results were fitted in the formulation and first and second order force results obtained.

Smallness of quantities was identified as an inherent problem in a second order analyses. Further, the apparatus also exhibited second order effects, which have not been completely treated in theory. Notwithstanding the above, the following conclusions were arrived at the end of the present

study.

1. The total wave field formulation upto second order in a wave tank comprising of a Stokes wave upto second order, a second order free wave, a first order and a second order reflected wave was found to adequately represent the actual wave field in the tank.

2. The analysis strategy of using a Fast Fourier Transform to separate frequency components, golden section optimization technique to identify the wave numbers of beat patterns and least squares curve fitting for the beat patterns was found to be satisfactory. Results were close to the expected ones even at low steepnesses.

3. The free wave caused due to a second order effect of the wave generator was found to behave like a linear wave satisfying the linear dispersion relationship (Eq. 3.33). Its amplitude was found to be consistently twice the values predicted by existing theories.

4. Similarities existed between first and second order reflection coefficients. Their phases with respect to the Stokes wave were widely scattered.

5. The available second order formulations for the wave forces on a vertical slender surface piercing cylinders are adequate.

6. Results for the hydrodynamic coefficients in general followed the published trends, with a certain amount of scatter in C_d results.

7. Measurements of second order forces at low steepness ($H/gT^2 =$ 0.0007 and 0.001) were unreliable because the forces were very small in magnitude.

8. Results for the second order forces at high steepness ($H/gT^2 = 0.003$ and 0.005) were within 50% of the calculated values. This demonstrates the adequacy of the formulation.

9. Relative comparison of the second order formulations following Lighthill (1979), Madsen (1986) and Isaacson (1979) was hampered by experimental errors.

During the course of the present study it was found that more research needs to be done on second order effects in a wave tank and also the phenomena affecting a second order experimental study. The following recommendations and suggestions for future research are cited:

1. A complete formulation and systematic experimentation of the wave field in a tank is a prerequisite for any experimental wave force studies.

2. Further research on second order wave generator theories and the qualities of the second order free wave is urged.

3. Beach reflection forms an intriguing and difficult phenomenon. More attention is required on the theory of beach reflection in a wave tank.

4. Many side effects in a wave tank have affected the experimental results, which could not be understood qualitatively and quantitatively. Side effects in general should not be considered negligible in an experimental study. Efforts should be directed to eliminate them to the maximum possible extent.

5. It is felt that measuring second order wave forces below a wave steepness (H/gT^2) of 0.001 will lead to inaccurate results with a simple experimental setup.

6. Force measuring devices with fine sensitivity and least side effects should be designed.

7. The significance of diffraction forces on slender cylinders at second order requires further experimental research.

8. More functions and parameters of comparison for wave forces at second order are required.

List of References

Biésel,F., 1949, "Calcul de l'amortissement d'une houle dans un liquide visqueux de profondeur finie," *La Houille Blanche*, vol 4, no 5, pp 630-634.

Biésel,F. and Suquet,F., 1951, "Les appareils générateurs de houle en laboratoire," *La Houille Blanche*, vol 6, no 2, pp 147-165.

Boussinesq,J., 1871, "Théorie de l'intumescence liquide, appelée onde solitaire ou de translation se propageant dans un canal rectangulaire," *Comptes Rendus Acad Sci.*, Paris, vol 72, pp 755-759.

Buhr Hansen,J. and Svendsen,Ib.A., 1974, "Laboratory generation of waves of constant form," *Proc. 14th Conf Coastal Eng.*, Ch.17, pp 321-339.

Chakrabarti,S.K., 1980a, "Inline forces on fixed vertical cylinder in waves," *Jl. of the Waterway Port Coastal and Ocean Div.*, vol 106, WW2, pp 145-155.

Chakrabarti,S.K., 1980b, Laboratory generated waves and wave theories," *Jl. of the Waterway Port Coastal and Ocean Div.*, vol 106, WW3, pp 349-368.

Chakrabarti,S.K., Wolbert,A.L. and Tam,W.A., 1976, " Wave forces on vertical circular cylinders," *Jl. of the Waterways Harbor and Coastal Eng. Div.*, ASCE, vol 102, WW2, pp 203-221.

Chen, C-M., 1978, "Calibration of a 200ft wave tank and a study of the response of a circular cylinder to sinusoidal waves," M.Eng. thesis, Faculty of Engineering, Memorial University, St.John's, Newfoundland.

Daugaard,E., 1972, "Generation of regular waves in the laboratory," Ph.D. thesis (in Danish), Inst. Hydrodynamics and Hydraulic Eng., Tech. Univ of Denmark, Denmark.

Dean, R.G., 1965, "Stream function representation of nonlinear ocean waves ," *J. Geophys Res.* vol 70, pp 4561-4572.

Dean,R.G., 1974, "Evaluation and development of water wave theories for engineering application," *Special Report no. 1* CERC, U.S Army Corps of Engrs., Fort Belvoir.

Dean,R.G. and Dalrymple,R.A., 1984, *Water wave mechanics for Engineers*

and Scientists, Prentice Hall pub., New Jersey.

Demirbilek,Z. and Gaston,J.D., 1985, "Nonlinear wave loads on a vertical cylinder," *Ocean Engng.* vol 12, no 5, pp 375-385.

Eatock Taylor,R. and Hung,S.M., 1987, "Second order diffraction forces in a vertical cylinder in regular waves," *Applied Ocean Res.*, vol 9, no 1, pp 19-30.

Ellix,D., 1984, "Second order wave loading on vertical cylinders," *Ph.D thesis*, The City University, London, England.

Ellix,D., and Arumugam,K., 1984, "An experimental study of waves generated by an oscillating wedge," *Jl. of Hydraulic Res.*, vol 22, no. 5, pp 299-313.

Ellix,D.M. and Arumugam,K., 1985, "Second order wave loading on surface piercing cylinders," *Proc. BOSS*, paper P1, pp 739-750.

Flick,R.E. and Guza,R.T., 1980, "Paddle generated waves in laboratory channels," *Jl. of Waterways Port Coastal and Ocean Div.*, ASCE, vol 106, WW1, pp 79-97.

Fontanet,P., 1961, "Theorie de la génération de la houle cylindrique par un batteur plan," *La Houille Blanche*, no 1, pp 3-28.

Goda,Y. and Suzuki,Y., 1976, "Estimation of incident and reflected waves in random wave experiments," *Proc. 15th Conf Coastal Eng.*, Honolulu, vol 1, pp 828-845.

Havelock,T.H., 1929, "Forced surface waves on water," *Philosophical Magazine*, Series F, vol 8, pp 569-576.

Hunt,J.N., 1952, " Viscous damping of waves over an inclined bed in a channel of finite width," *La Houille Blanche*, vol 7, no 6, pp 836-842.

Hunt,J.N. and Baddour,R.E., 1981, "The diffraction of nonlinear progressive waves by a vertical cylinder," *Q. Jl. Mech. Appl. Math.*, vol XXXIV, part 1, pp 69-87.

Isaacson,M. de St.Q., 1979, "Nonlinear inertia forces on bodies," *Jl. of the Waterways, Port, Coastal and Ocean div.*, ASCE, vol 105, WW3, pp 213-227.

Korteweg,D.J. and DeVries,G., 1895, "On the change of form of long waves advancing in a rectangular channel, and a new type of long stationary waves," *Phil. Mag.* series 5, vol 39, pp 422-443.

Kim,Y.Y. and Hibbard,H.C., 1975, "Analysis of simultaneous wave force and water particle measurements," *Offshore Tech. Conf.*, Dallas, paper 2192, pp 461-470.

Lamb,Sir H., 1932, *Hydrodynamics*, Dover pub., New York.

Lighthill,M.J., 1979, "Waves and Hydrodynamic loading," *BOSS*, London, Opening address, pp 1-40.

Lighthill,M.J., 1986, "Fundamentals concerning wave loading on offshore structures," *J. Fluid Mech.*, vol 173, pp 667-681.

MacCamy,R.C. and Fuchs,R.A., 1954, "Wave forces on piles: a diffraction theory," Tech. Memo no. 69, U.S. Army Corps of Engrs., Beach Erosion Board.

Madsen,O.S., 1970, "Waves generated by a piston-type wavemaker," *Proc. 12th Conf. Coastal Eng.*, pp 589-607.

Madsen,O.S., 1971, "On the generation of long waves," *Jl. of Geophys. Res.*, vol 76, no 36, pp 8672-8683.

Madsen,O.S., 1986, "Hydrodynamic force on circular cylinders," *Applied Ocean Res.*, vol 76, no 36, pp 151-165.

Morison,J.R., O'Brien,M.P., Johnson,J.W. and Schaaf,S.A., 1950, "The force exerted by surface waves on piles," *Petroleum Trans.*, AIME, vol 189, pp 149-154.

Muggeridge,D.B. and Murray,J.J., 1981, "Calibration of a 58m wave flume," *Canadian Jl. of Civil Eng.*, vol 8, no 4, pp 449-455.

Newland,D., 1975, *Random Vibration and Spectral Analysis*, Longman pub.,

Press,W.H., Flannery,B.P., Tenkolsky,S.A. and Vetterling,W.T., 1986, *Numerical recipes, the art of scientific computing,* Cambridge University Press, Cambridge.

Sarpkaya,T. and Isaacson,M., 1981, *Mechanics of Wave Forces on Offshore Structures*, van Nostrand Reinhold co., New York.

Shore protection manual, 1984, CERC, U.S. Army Corps of Engrs., Washington, D.C.

Skjelbreia,L. and Hendrickson,J.A., 1960, "Fifth order gravity wave theory," *Proc. 7th Coastal Eng. Conf.*, The Hague, pp 184-196.

Stokes,G.G., 1847, "On the theory of oscillating waves," *Trans. Camb. Phil. Soc.*, vol 8, pp 441-455.

Ursell,F., Dean,R.G. and Yu,Y.S., 1960, "Forced small amplitude water waves: a comparison of theory and experiment," *Jl. of Fluid Mech.*, vol 7, pp 33-52.

Vugts,J.H., 1979, "A review of hydrodynamic loads on offshore structures and their formulation," *BOSS*, London, paper 54, pp 693-708.

Wehausen,J.V. and Laitone,E.V., 1960, "Surface waves," *Handbuch der Physik*, Springer-Verlag, Berlin, vol 9, pp 446-778.

Wiegel,R.L., 1964, *Oceanographic Engineering*, Prentice-Hall Inc., Englewood Cliffs, N.J.

Appendix A

ANALYS - Source code

```
C THIS PROGRAM EVALUATES THE WAVE AMPLITUDES BY FOURIER
C TRANSFORMS AND LEAST SQUARES ANALYSIS.
C IMPORTANT VARIABLES ARE ALPHABETICALLY
C DEFINED HERE:
C ALPHA    - REFLECTED WAVE PHASE DIFFERENCE
C AR       - REFLECTED WAVE AMPLITUDE
C A1       - FIRST ORDER STOKES WAVE AMPLITUDE
C A2       - SECOND ORDER STOKES WAVE AMPLITUDE
C A22      - FREE WAVE AMPLITUDE
C A22R     - SECOND ORDER REFLECTED WAVE AMPLITUDE
C CALIB    - CALIBRATION FACTOR
C DELTA    - FREE WAVE PHASE DIFFERENCE
C GAMMA    - SECOND ORDER REFLECTED WAVE PHASE
C H        - WATER DEPTH
C HH       - WAVE HEIGHT
C JUMPS    - TOTAL NUMBER OF LOCATIONS
C K        - WAVE NUMBER
C KAPPA    - FREE WAVE NUMBER
C K0,K3    - USER-SPECIFIED INTERVAL FOR OPTIMAL K
C NP       - TOTAL INTERPOLATING POINTS FOR SPLINE
C POINTS   - NUMBER OF SAMPLES PER WAVE PERIOD
C TK0,TK3  - USER-SPECIFIED INTERVAL FOR OPTIMAL KAPPA
C XINT     - DISTANCE BETWEEN LOCATIONS
C-------------------------------------------------
      REAL K0,K3,K,KAPPA
      INTEGER POINTS,RUN,RUNS
```

```
      PARAMETER (POINTS=64,IPOINTS=2.0*POINTS+15,X0=20.0)
      PARAMETER (NP=50,TPOINTS=(2.0/FLOAT(POINTS))**2)
      PARAMETER (PI=3.141592654)
      DIMENSION SEQ(POINTS),COEF(POINTS),ORDER1(20),X(20)
      DIMENSION ORDER2(20),WFFTR(IPOINTS),FFF(NP),FFF2(NP)
      DIMENSION XS(NP),YS(NP),CSCOEF(4,20),BREAK(20)

C FILE FREQ.DAT CONTAINS USER-SPECIFIED PARAMETERS
C FILE ANALYS.DAT CONTAINS DIGITISED DATA FOR ONE CYCLE
C AT ALL LOCATIONS
C FILE ANALYS.OUT CONTAINS THE OUTPUT

      OPEN(5,FILE='FREQ.DAT',TYPE='OLD')
      OPEN(6,FILE='ANALY.DAT',TYPE='OLD')
      OPEN(10,FILE='ANALYS.OUT',TYPE='NEW')

C INITIALISING FFT ROUTINES
      CALL FFTRI(POINTS,WFFTR)

C READING INPUT PARAMETERS
      READ(5,*) XINT,K0,K3,TK0,TK3,CALIB,JUMPS

      X(1)=0.0
      DO 50,I=2,JUMPS
      X(I)=X(I-1)+XINT
 50   CONTINUE
100   DO 500, JUMP=1,JUMPS
      DO 150,I=1,POINTS
      READ(6,*)SE
      SEQ(I)=SE/CALIB
15    CONTINUE

C IDENTIFY FREQUENCY CONTENT (COEF) FROM TIME DATA (SEQ)
160   CALL F2TRF(POINTS,SEQ,COEF,WFFTR)

C EVALUATE FIRST AND SECOND ORDER COMBINED WAVE AMPLITUDES
C AT ALL LOCATIONS
      ORDER1(JUMP)=TPOINTS*(COEF(2)**2+COEF(3)**2)
      ORDER2(JUMP)=TPOINTS*(COEF(4)**2+COEF(5)**2)

500   CONTINUE
      INTCEP=1
C LSSIN IS THE LEAST SQUARES CURVE FITTING ROUTINE
      CALL LSSIN(K0,K3,INTCEP,JUMPS,X,ORDER1,ONEK,SQE,AI,
```

```
     1  AA,ALPH)
        IF(AI.LT.0.)THEN
        PRINT*,'ILL-CONDITIONED DATA AT FIRST ORDER')
        GO TO 1000
        ENDIF

C EVALUATE FIRST ORDER WAVE AMPLITUDES, NUMBERS AND PHASES
        A1=0.5*((AI+AA)**0.5+(AI-AA)**0.5)
        AR=0.5*((AI+AA)**0.5-(AI-AA)**0.5)
        ALPHA=ALPH-ONEK*XO
        K=ONEK/2.0
        HH=A1*2.

C SPLINING OF SECOND ORDER DATA PERFORMED BY THE IMSL ROUTINES
C CSINT AND CSVAL
        XS(1)=X(1)
        SINT=X(JUMPS)/FLOAT(NP)
        DO I=2,NP
        XS(I)=XS(I-1)+SINT
        ENDDO
        CALL CSINT(JUMPS,X,ORDER2,BREAK,CSCOEF)
        NINTV=JUMPS-1
        DO I=1,NP
        YS(I)=CSVAL(XS(I),NINTV,BREAK,CSCOEF)
        ENDDO
C SPLINING ENDS

C EVALUATE THE PREDOMINANT BEAT PATTERN AT SECOND ORDER
C (THE ONE WITH NUMBER (KAPPA-2K))
        CALL LSSIN(TKO,TK3,INTCEP,NP,XS,YS,TWOK,SQE,B1,B2,DEL)
        IF(B1.LT.0.)THEN
        PRINT*,'ILL-CONDITIONED DATA AT SECOND ORDER')
        GO TO 1000
        ENDIF

C EVALATE FREE WAVE NUMBER
        DELTA=DEL-TWOK*XO
        TWOK1=TWOK+4.*K
        TWOK2=TWOK+TWOK1
        KAPPA=TWOK+2.*K

C SUBTRACT THE EVALUATED SECOND ORDER BEAT PATTERN FROM
C THE TOTAL SECOND ORDER WAVE PATTERN TO EVALUATE THE
C NEXT PREDOMINANT PATTERN (WITH NUMBER (KAPPA+2K)
```

```
        DO 600  I=1,NP
        FFF(I)=YS(I)-B1-B2*COS(TWOK*XS(I)+DEL)
600     CONTINUE
        INTCEP=0
        CALL ERROR(TWOK1,INTCEP,NP,XS,FFF,SQE,AI,B3,GAMM)
        GAMMA=GAMM-TWOK1*XO

C SUBTRACT THE EVALUATED BEAT PATTERN AGAIN TO LASTLY
C EVALUATE THE PATTERN WITH NUMBER 2KAPPA
        DO 700 I=1,NP
        FFF22=B3*COS(TWOK1*XS(I)+GAMM)
        FFF2(I)=FFF(I)-FFF22
700     CONTINUE
        CALL ERROR(TWOK2,INTCEP,NP,XS,FFF2,SQE,AI,B4,DEL)

C EVALUATE ALL SECOND ORDER WAVE AMPLITUDES
        IF((B1+B2-B3-B4).LT.0.)GO TO 701
        A22R=0.5*((B1+B2+B3+B4)**0.5-(B1+B2-B3-B4)**0.5)
701     IF((B1-B2-B3+B4).LT.0.)THEN
        PRINT*,'ILL-CONDITIONED DATA AT SECOND ORDER')
        GO TO 703
        ENDIF
        A2=0.5*((B1+B2+B3+B4)**0.5-(B1-B2-B3+B4)**0.5)
703     IF((B1-B2+B3-B4).LT.0.)GO TO 990
        A22=0.5*((B1+B2+B3+B4)**0.5-(B1-B2+B3-B4)**0.5)

C WRITE RESULTS IN AN OUTPUT FILE
990     WRITE(10,991)RUN,K,HH,AR,DELTA,A2,KAPPA,BETA,A22,
     1  GAMMA,A22R
991     FORMAT(//2X,I2,3X,F5.3,2X,F7.4,3X,F6.4,2X,F7.2,2X,
     1  F6.4,3X,F6.3,2X,F7.2,2X,F6.4,2X,F7.2,2X,F6.4)
1100    STOP
        END

C -------------------------------------------------------
C SUBROUTINE LSSIN FITS A LEAST SQUARES SINE CURVE WITH
C OPTIMAL WAVE NUMBER TO A GIVEN SET OF POINTS

        SUBROUTINE LSSIN(KO,K3,INTCEP,JUMPS,X,FF,XK,SQE,
     1  AI,AA,DELTA)
        DIMENSION FF(50),X(50)
        REAL KO,K1,K2,K3
        PARAMETER (R=0.61803399,C=1.0-R)
```

```
C EVALUATE LEAST SQUARED ERROR AT THE INITIAL WAVE
C NUMBERS K1 AND K2
        K1=K0*R+K3*C
        CALL ERROR(K1,INTCEP,JUMPS,X,FF,SQ1,A1,A2,DEL)
        K2=K1*R+K3*C
        CALL ERROR(K2,INTCEP,JUMPS,X,FF,SQ2,A1,A2,DEL)

C START NEXT ITERATION
100     IF(SQ2.LT.SQ1)THEN
         K0=K1
         K1=K2
         SQ0=SQ1
         SQ1=SQ2
         K2=R*K1+C*K3
         CALL ERROR(K2,INTCEP,JUMPS,X,FF,SQ2,A21,A22,DEL1)
        ELSE
         K3=K2
         K2=K1
         SQ3=SQ2
         SQ2=SQ1
         K1=R*K2+C*K0
         CALL ERROR(K1,INTCEP,JUMPS,X,FF,SQ1,A11,A12,DEL2)
        ENDIF

C CHECK FOR TOLERANCE
       IF(ABS(K3-K0).LE.0.0001)GO TO 200
       GO TO 100
200    IF(SQ1.LT.SQ2)THEN
        XK=K1
       ELSE
        XK=K2
       ENDIF
C FINAL CALL TO ERROR
       CALL ERROR(XK,INTCEP,JUMPS,X,FF,SQE,AI,AA,DELTA)
       RETURN
       END

C -------------------------------------------------
C FOR A SPECIFIED WAVE NUMBER SUBROUTINE ERROR FITS
C A LEAST SQUARES CURVE. THE CURVE TO BE FITTED IS
C DEFINED BY THE EXTERNAL FUNCTION F

       SUBROUTINE ERROR(KN,INTCEP,NOBS,X,FF,SSE,AI,AA,DEL)
       DIMENSION A(3),X(50),XX(50)
```

```
      PARAMETER (PI=3.141592654)
      EXTERNAL F
      REAL KN
      DO 100,I=1,NOBS
      XX(I)=X(I)*KN
100   CONTINUE
      NBASIS=2
      IWT=0

C CALLS IMSL LEAST SQUARES ROUTINE FNLSQ
200   CALL FNLSQ(F,INTCEP,NBASIS,NOBS,XX,FF,IWT,WEIGHT,A,SSE)
      IF(INTCEP.EQ.0)THEN
      A(3)=A(2)
      A(2)=A(1)
      A(1)=0.
      ENDIF
      AI=A(1)
      AA=(A(2)**2+A(3)**2)**0.5
      PHI=ATAN(ABS(A(3))/ABS(A(2)))
      IF(A(2).GT.0.)THEN
       IF(A(3).GT.0.)THEN
        DEL=-PHI
       ELSE
        DEL=PHI
       ENDIF
      ELSE
       IF(A(3).GT.0.)THEN
        DEL=PI+PHI
       ELSE
        DEL=PI-PHI
       ENDIF
      ENDIF
      RETURN
      END

      REAL FUNCTION F(K,XX)
      IF(K.EQ.1)THEN
        F=k*1./K*COS (XX)
      ELSE
        F=(1./K)*K*SIN (XX)
      ENDIF
      RETURN
      END
```

Appendix B

The Fast Fourier Transform

A function $x(t)$ can be represented using fourier series as

$$x(t) = a_0 + 2\sum_{n=1}^{\infty} a_n \sin(2\pi nt/T) + b_n \cos(2\pi nt/T) \qquad \text{(B.1)}$$

where a_n and b_n are the amplitudes of order n. Using complex notation,

$$x(t) \; = a_0 + 2\sum_{n=1}^{\infty} X_n \, e^{i(2\pi nt/T)} \qquad \text{(B.2)}$$

where $i = \sqrt{-1}$ and $X_n \; = \; a_n \; - \; ib_n$ is the complex amplitude. The value of X_n can be found by integrating the function over one period

$$X_n = 1/T \int_0^T x(t) e^{-i(2\pi nt/T)} \mathrm{d}t \qquad \text{(B.3)}$$

If the function $x(t)$ is sampled at a rate of N samples per period, we generate a discrete time series

$$\{x_r\}, r = 0, 1, 2, \cdots N-1$$

The fourier coefficients can be represented using the discrete time series as

$$X_n = 1/N \sum_{r=0}^{N-1} x_r e^{-i(2\pi nr/N)} \tag{B.4}$$

X_n is now called the discrete fourier transform (DFT) of the function $x(t)$, Newland (1975).

The Fast Fourier Transform (FFT) is a computer algorithm for calculating discrete Fourier transforms. The FFT works by partitioning the full sequence $\{x_r\}$ into a number of shorter sequences. The DFTs of the shorter sequences are evaluated and combined to give the DFT of the full sequence. If N is even, $\{x_r\}$ can be partitioned into shorter sequences as

$$y_r = x_{2r} \tag{B.5}$$

$$z_r = x_{2r+1} \tag{B.6}$$

$$r = 0, 1, 2, \cdots, (N/2 - 1) \tag{B.7}$$

The DFT of these two sequences are Y_n and Z_n where,

$$Y_n = \frac{1}{N/2} \sum_{r=0}^{N/2-1} y_r \, e^{-i\frac{2\pi nr}{N/2}} \tag{B.8}$$

$$Z_n = \frac{1}{N/2} \sum_{r=0}^{N/2-1} z_r \, e^{-i\frac{2\pi nr}{N/2}} \tag{B.9}$$

$$n = 0, 1, 2, \cdots, (N/2 - 1) \tag{B.10}$$

The DFT of the original sequence can be obtained from the DFT of the half sequences as

$$X_n = 1/2 \left\{ Y_n + e^{-i(2\pi n)/N} \, Z_n \right\} \tag{B.11}$$

If the original number of samples N is a power of 2, then the half sequences can themselves be partitioned into quarter sequences and so on, until eventually the last subsequences have only one term each. In fact a FFT algorithm works in the reverse way i.e., it starts with the individual terms and finally estimates the DFT of the full sequence.

Defining a new complex variable

$$W = e^{-i(2\pi/N)}$$

and using the fact that Y_n and Z_n are periodic in n and repeat themselves with period $N/2$, we obtain the so called computational "butterfly" formulae, Newland (1975).

$$X_n = 1/2(\, Y_n + W^n Z_n \,) \tag{B.12}$$

$$X_{n+N/2} = 1/2(Y_n - W^n Z_n \,) \tag{B.13}$$

$$n = 0, 1, 2, \ldots, (N/2 - 1) \tag{B.14}$$

While a direct approach for estimating the DFT would involve N^2 multiplications, the FFT requires $N \log_2 N$ multiplications, thus offering an enormous reduction in computer time.

Appendix C

Description of the subroutine LSSIN

LSSIN is a subroutine of the main program ANALYS of appendix A. This subroutine performs the task of fitting a sine curve to a given set of data points, the wave number of the curve being an unknown. If the wave number is known, the subroutine performs a simple least squares curve fitting operation as follows:

Given a set of data points $y_i, i = 1, 2, \cdots n$, a curve of the form

$$f(x) = A_0 + A_1 \cos kx + A_2 \sin kx \tag{C.1}$$

has to be fitted through these points. Define a squared error as

$$\epsilon_i^2 = [y_i - f(x_i)]^2 \tag{C.2}$$

To minimize the sum of squared errors with respect to the variables of the

fit, we require that

$$\frac{\partial \sum \epsilon_i^2}{\partial A_0} = \frac{\partial \sum \epsilon_i^2}{\partial A_1} = \frac{\partial \sum \epsilon_i^2}{\partial A_2} = 0 \qquad \text{(C.3)}$$

This would yield three simultaneous equations in A_0, A_1 and A_2 from which the three parameters can be estimated.

If the wave number k in Eq. (C.1) is not known *à priori* and given an interval within which the expected number lies, LSSIN locates the best wave number as the one which provides a fit with the minimum 'least squared error'. Basically, it assumes $\sum \epsilon_i^2$ as a function of k and identifies where the function attains a minimum within the interval. An optimization technique is employed to subdivide the interval effectively to identify the minimum. Once the best wave number is obtained, a least square fit at that number is performed to identify the desired amplitudes, A_0, A_1 and A_2 which are the outputs of the subroutine.

The optimization technique involved in identifying the wave number is called the golden section search method see for eg. Press et al (1986). Say a function $f(x)$ is known to attain a minimum (or maximum) within an interval (x_0, x_1) at x_m. The interval is successively subdivided at $x_2, x_3, \cdots, x_n$ so that x_n lies close to x_m within an user-specified tolerance. The strategy lies in mimimizing the total number of subdivisions n by diminishing the size of the bracketing interval optimally. This is done as follows (Press et al, 1986):

Generally, a minimum is said to be bracketed by a triplet of points (a, b, c) if $f(b)$ is less than both $f(a)$ and $f(c)$. a, b, c will be assumed variables in the present context as they can take on any values from x_0 to x_n. Say a point x_r has to be identified in (a, c). x_r would be optimum if it lies in the larger of the intervals $(a, b), (b, c)$ and be symmetrical with b about the midpoint of (a, c). This method also stipulates that it would be best if x_r is a fractional distance of 0.38197 from one end of the interval where it lies (Press et al, 1986). The bracket for the next subdivision will be either (a, b, x_r) or (b, x_r, c) depending upon whether $f(b)$ is greater than $f(x_r)$.

The fractions

$$0.38197 = \frac{3 - \sqrt{5}}{2}$$

$$0.61803 = \frac{\sqrt{5} - 1}{2}$$

are called the golden mean or golden section (Press et al, 1986). The method applies these fractions successively and every subdivided interval is a fraction 0.61803 of the previous interval. To initialize, (a, c) can be taken as (x_0, x_1) and b chosen within the interval based on the golden ratios. Further details of the golden section search algorithm can be found in Press et al, (1986).

If the fitted curve contains two sinusoids of different wave numbers, then LSSIN starts with the predominant sinusoid (to be specified) and identifies the wave number and amplitudes by the previous procedure. Then the

input data is splined and the evaluated component is subtracted to obtain the data for the other sinusoid. The wave number and amplitudes of this data are then evaluated similarly. A flow chart for the subroutine LSSIN is shown in Fig. (C.1), for the case of a single sinusoid. The source code is included in appendix A.

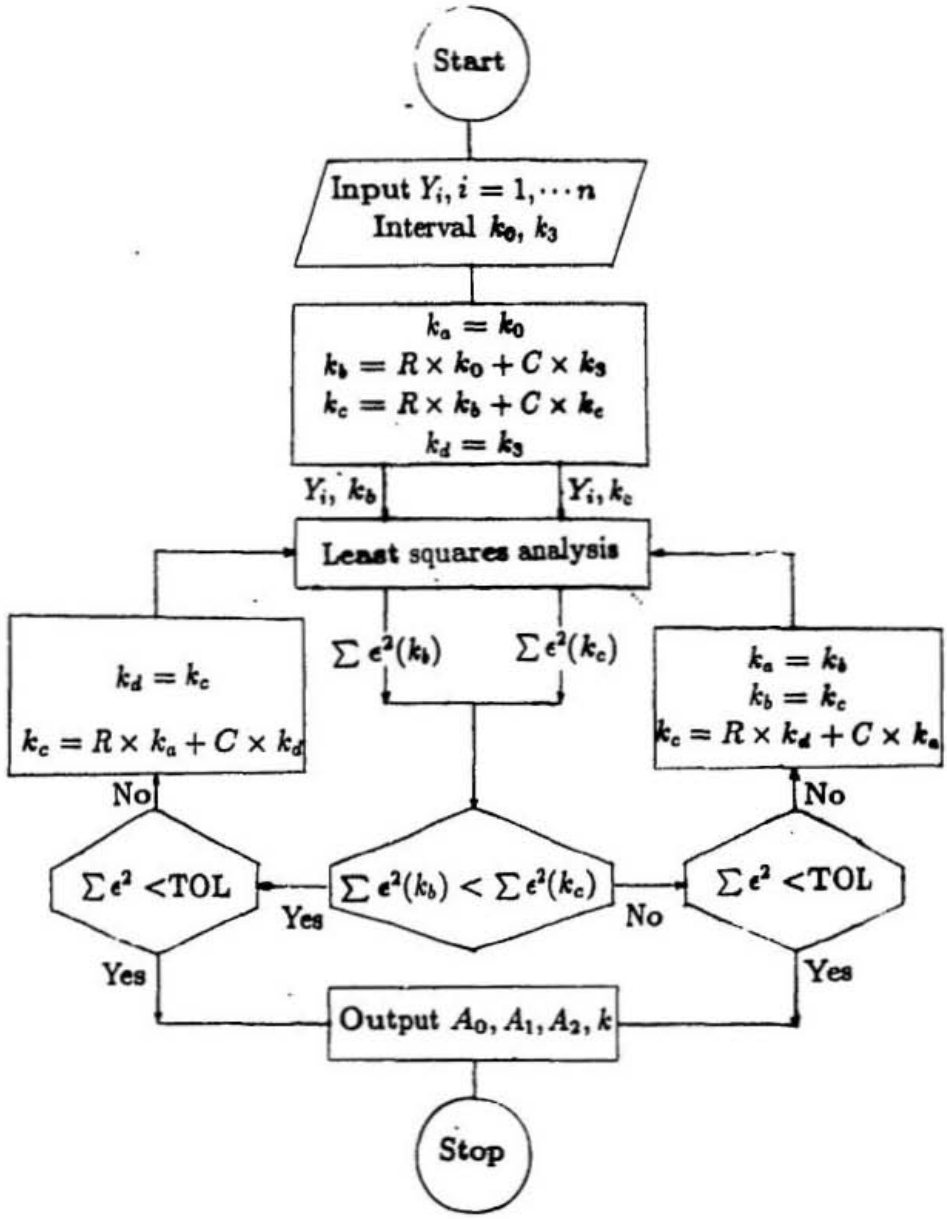

Figure (C.1) Flow chart for the subroutine LSSIN

Notes: R & C - Golden ratios; R = 0.61803, C = 0.38197.
$k_a - k_d$ - Dummy wave numbers
TOL - User-specified tolerance.

Appendix D

Harmonic components of $u|u|$

Let us consider a general function f made up of two sinusoids as

$$f = a\cos\theta + b\cos 2\theta \tag{D.1}$$

The requirement is to split $f|f|$ in a similar harmonic form. So let

$$f|f| = f_1\cos\theta + f_2\cos 2\theta \tag{D.2}$$

Using fourier series we can write

$$f_1 = \frac{1}{\pi}\int_0^{2\pi} f|f|\cos\theta \mathrm{d}\theta \tag{D.3}$$

$$f_2 = \frac{1}{\pi}\int_0^{2\pi} f|f|\cos 2\theta \mathrm{d}\theta \tag{D.4}$$

To evaluate these functions, we refer to Fig. (D.1) where the functions $a\cos\theta$ and f are plotted. At points θ_1 and θ_2, the function f changes sign. Using this information, the above integrals may be modified as

$$f_1 = \frac{1}{\pi}\int_0^{\theta_1} f^2\cos\theta \mathrm{d}\theta - \frac{1}{\pi}\int_{\theta_1}^{\theta_2} f^2\cos\theta \mathrm{d}\theta + \frac{1}{\pi}\int_{\theta_2}^{2\pi} f^2\cos\theta \mathrm{d}\theta \tag{D.5}$$

and an analogous expression for f_2. To identify the zero - crossing points of the function f, we readily note that due to symmetry about $\theta = \pi$, we have $\theta_2 = 2\pi - \theta_1$. To evaluate θ_1, we set

$$a\cos\theta_1 + b\cos 2\theta_1 = 0 \tag{D.6}$$

to get the quadratic equation

$$2b\cos^2\theta_1 + a\cos\theta_1 - b = 0$$

which can be solved to obtain

$$\cos\theta_1 = \frac{\sqrt{a^2 + 8b^2}}{4b} - \frac{a}{4b} \tag{D.7}$$

and

$$\theta_2 = 2\pi - \theta_1 \tag{D.8}$$

The indefinite integrals for f_1 and f_2 pose no complications. They can be evaluated as

$$\begin{aligned}\int (a\cos\theta + b\cos 2\theta)^2 \cos\theta \mathrm{d}\theta = \quad & \frac{ab\theta}{2} + \left(\frac{3a^2}{4} + \frac{b^2}{2}\right)\sin\theta \\ + \quad & \left(\frac{ab}{2}\right)\sin 2\theta + \left(\frac{a^2 + b^2}{12}\right)\sin 3\theta \\ + \quad & \left(\frac{ab}{8}\right)\sin 4\theta + \left(\frac{b^2}{20}\right)\sin 5\theta \end{aligned} \tag{D.9}$$

$$\int (a\cos\theta + b\cos 2\theta)^2 \cos 2\theta \mathrm{d}\theta = \frac{a^2\theta}{4} + (ab)\sin\theta$$

$$+ \left(\frac{a^2}{4} + \frac{3b^2}{8}\right)\sin 2\theta + \left(\frac{ab}{6}\right)\sin 3\theta$$

$$+ \left(\frac{a^2}{16}\right)\sin 4\theta + \left(\frac{ab}{10}\right)\sin 5\theta \quad \text{(D.10)}$$

Evaluating these integrals at θ_1 and θ_2 involves tedious trigonometry. Further, two simplifying assumptions need to be employed:

- Assuming $b << a$,

$$\sqrt{a^2 + 8b^2} \simeq a\left(1 + \frac{4b^2}{a^2}\right)$$

- Since θ_1 usually lies between $80^0 - 90\,\text{deg}$, we can relate $\cos^{-1}\theta$ to θ by a straight line as

$$\cos^{-1}\theta = \pi/2 - 1.007\theta$$

The results are quite sensitive to these assumptions, so their application should be delayed as much as possible. The desired results can be obtained as

$$f_1 = \frac{2.667}{\pi}a^2 + \frac{3.341}{\pi}b^2 \quad \text{(D.11)}$$

$$f_2 = \frac{4.461}{\pi} ab + \frac{0.336}{\pi} \frac{b^3}{a} \tag{D.12}$$

The last term in f_2 is very small compared to the first term when $b << a$. So it is not included in the present study.

The accuracy of the results can be tested by plotting $f|f|$ and $f_1 \cos\theta + f_2 \cos 2\theta$ together in Figs. (D.2) and (D.3) for different ratios of f_2 to f_1. The correlation can be observed to improve as this ratio increases in magnitude. The linearised function $2.667/\pi f_1^2 \cos\theta$ usually adopted in literature is also plotted in these graphs. The figures show that the proposed harmonization represents the actual function better, particularly in the regions around $\theta = 0, \pi/2$.

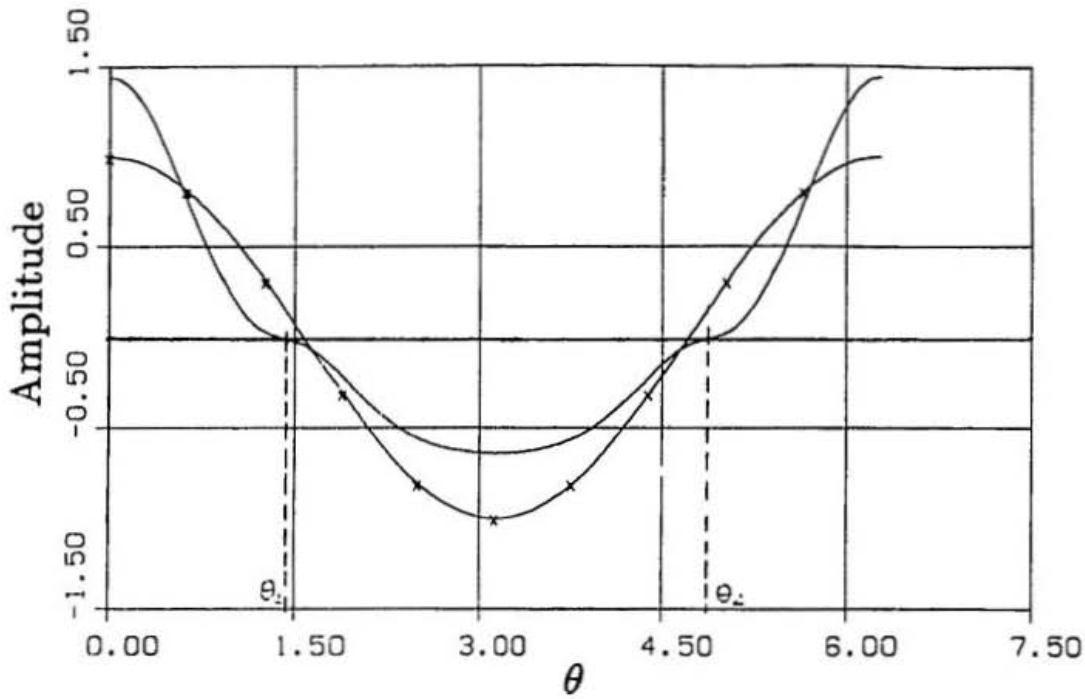

Figure (D.1) Cosine functions at $f_2 = 0.2f_1$.

—— $(f_1 \cos\theta + f_2 \cos 2\theta)|f_1 \cos\theta + f_2 \cos 2\theta|$

—×— $f_1 \cos\theta$

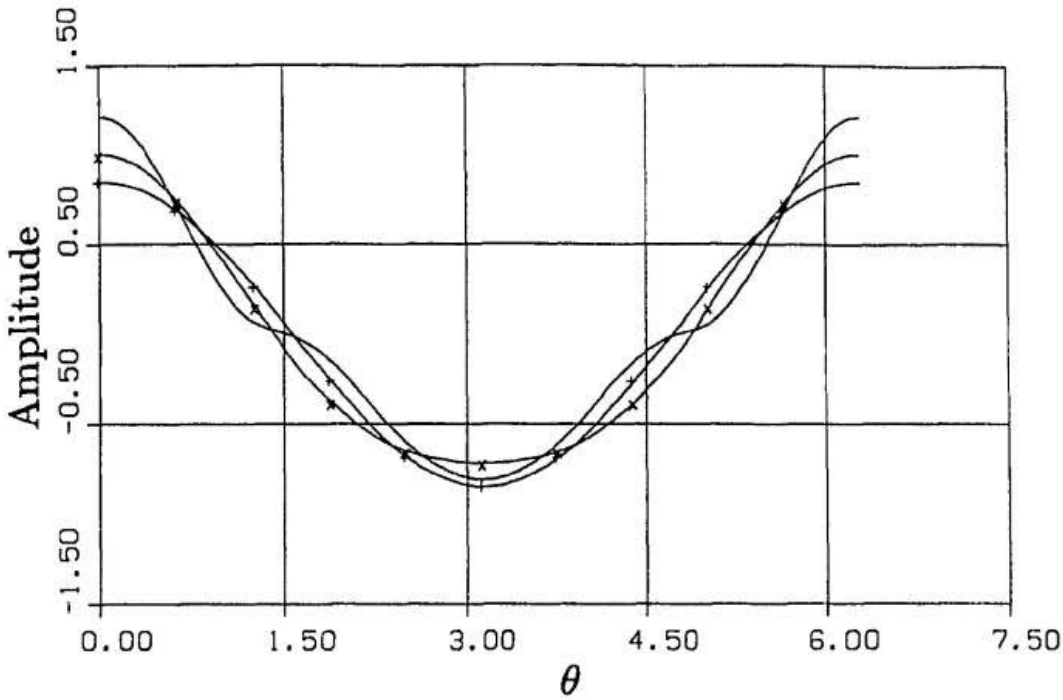

Figure (D.2) Harmonic components of $f|f|$; $f_2 = 0.1f_1$

——— $(f_1 \cos\theta + f_2 \cos 2\theta)|f_1 \cos\theta + f_2 \cos 2\theta|$

—×—×— $2.667/\pi f_1^2 \cos\theta + 3.341/\pi f_2^2 \cos 2\theta$

—+—+— $2.667/\pi f_1^2 \cos\theta$

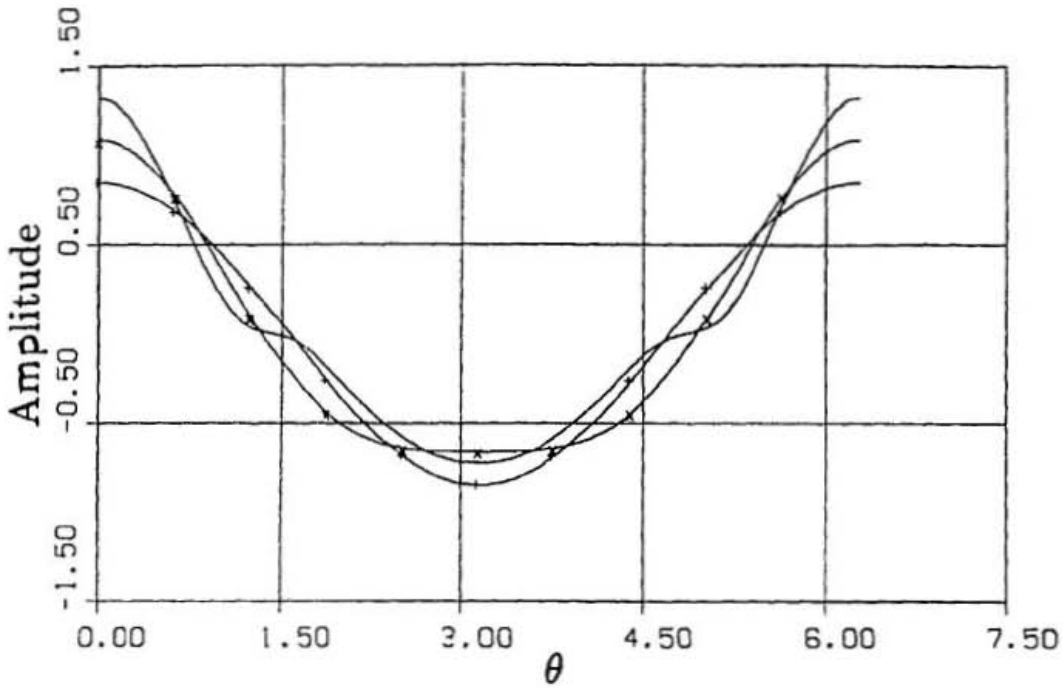

Figure (D.3) Harmonic components of $f|f|$; $f_2 = 0.15 f_1$

——— $(f_1 \cos\theta + f_2 \cos 2\theta)|f_1 \cos\theta + f_2 \cos 2\theta|$

—+—+— $2.667/\pi f_1^2 \cos\theta + 3.341/\pi f_2^2 \cos 2\theta$

——+—— $2.667/\pi f_1^2 \cos\theta$